DESIGN AND ANALYSIS OF X – BAND CAVITY MAGNETRON
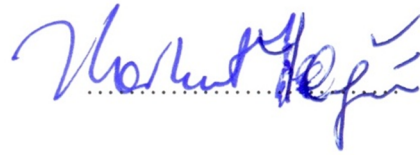
by
Türker İsenlik

Submitted to the Institute of Graduate Studies in
Science and Engineering in partial fulfillment of
the requirements for the degree of
Master of Science
in
Electrical and Electronics Engineering

Yeditepe University
2012

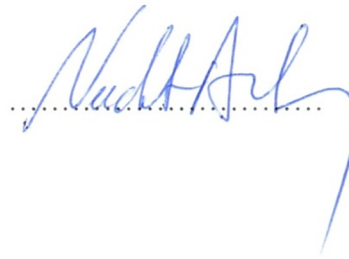DESIGN AND ANALYSIS OF X – BAND CAVITY MAGNETRON

APPROVED BY:

Assoc. Prof. Dr. Korkut Yeğin ....
(Supervisor)

Prof. Dr. Fuat Bayrakçeken ....

Prof. Dr. Necdet Aslan ....

DATE OF APPROVAL: 16./05./2012

ACKNOWLEDGEMENTS

First, I would like to express my gratitude to my supervisor Associate Prof. Dr. Korkut Yeğin for his advices, encouragement, technical and scientific support throughout the project development.

I would like to thank TUBITAK-BIDEB for financial support during my MSc. education.

I would like to thank my co-advisor Dr. İsa Araz who is currently director of KAMTAM, Cathode and Microwave Vacuum Tubes Research Center, for his technical and scientific support throughout the project development.

I would also like to thank Gökçen Kavaz. Her support and encouragement helped me to finish this project.

This work is dedicated to my dear parents and my friends for their encouragement, patience, support and love during the past years. It would be hard to finish my project without them.

ABSTRACT

DESIGN AND ANALYSIS OF X – BAND CAVITY MAGNETRON

Cavity magnetron as a high power microwave source has been around since the Second World War. It is mostly used in radars and communication satellites. Even though the theory of magnetron has been around for a long time, there is no straightforward design method to follow. Usually iterative techniques have been used and particle simulators are the first choice in the study and design of cavity magnetrons. In recent years, although MAGIC is very popular program, in this thesis, CST Particle Studio is used.

In a magnetron design, it is very important to start with accurately calculated parameters to ensure convergence to desired results and develop the design in a relatively short time. For this reason, a design method is derived and explained in detail in this thesis. The resulting expressions are used in the design of X band magnetron. Using eigenmode, tracking and PIC solver parts of CST Particle Studio, 3D computer model is formed and the effects of all primary design parameters are examined. In addition, simulations run with different program parameters to study the effects of modeling parameters on designed model.

Another important phenomenon in magnetron design is its noise. The noise generating mechanism has not been understood completely even though many studies have been devoted to this subject. On the other hand, the various experiments have been performed to reveal primary noise sources of a magnetron. According to these works, there exist several noise reduction techniques. These methods are separately modeled using CST Particle Studio and best noise reduction technique is chosen for particular magnetron geometry.
Thus, the contribution of this thesis is two-fold. First, the design of an X band cavity magnetron is detailed and the impacts of design parameters on the performance of an X-band magnetron are investigated. Then, the sources of noise in a magnetron are studied and noise reduction mechanisms are proposed and implemented on a hole-slot type eight cavity magnetron.

ÖZET

X BANT KAVİTE MAGNETRON TASARIMI VE ANALİZİ

Kavite magnetronlar, İkinci Dünya Savaşı'ndan bu yana mikrodalga frekanslarda yüksek güç gereksinimini sağlamak amacıyla kullanılmaktadır. Radar ve haberleşme uyduları başlıca kullanımalanlarıdır. Magnetron teorisi üzerine uzun zamandır çalışılmasına rağmen takip edilen belirlenmiş sabit bir tasarım metodu geliştirilememiştir. Tasarım sırasında genelikle iterative tekniklere yer verilir ve parçacık simulasyonu yapabilen programlar kullanılır. MAGIC bunlar içerisinde en yaygını olmasına rağmen, bu çalışmada CST Particle Studio kullanılmıştır.

Magnetron tasarımını görece kısa bir zamanda gerçekleştirebilmek ve istenilen sonuçlara yeterli hassasiyette ulaşabilmek için tasarımda kullanılan parametrelerin ilk değerlerinin doğru hesaplanması çok önemlidir. Bu nedenle, tasarım metodu geliştirilmiş ve çıkarılan metot açıkça anlatılmıştır. Belirlenen metot yardımıyla X frekans bandında çalışan magnetron tasarlanmıştır. CST Particle Studio'nun Eigenmode, Particle Tracking ve PIC solver kısımları kullanılarak yapının üç boyutlu modeli oluşturulmuş ve tüm tasarım parametrelerinin etkileri incelenmiştir. Ayrıca, simulasyonlar farklı program parametreleri ile de çalıştırılarak model üzerindeki etkileri gözlemlenmiştir.

Magnetron tasarımındaki bir diğer önemli konu da gürültü analizidir. Yıllardır yürütülen çalışmalara rağmen gürültü üreten mekanizma tamamen açıklanamamaktadır. Diğer yandan, gürültü kaynağını ortaya çıkarabilmek amacıyla bir çok deney gerçekleştirilmiştir. Yapılan bu çalışmalarda gürültü azaltma amacıyla çeşitli teknikler geliştirilmiştir. Bu metotların her biri CST Particle Studio ile modellenmiş, simule edilmiş ve sonuçları gözlemlenmiştir.

Yapılan çalışmalar sonucunda tezin katkısını iki ana başlık altında toplamak mümkündür. Öncelikle magnetron tasarımı detaylı bir şekilde açıklanmış, bu yapıdaki magnetron tasarımları için belirli bir tasarım yolu çıkarılmıştır. Ayrıca tasarım parametrelerinin magnetron performansını nasıl etkiledikleri de incelenmiştir. Ardından, magnetron

yapısında gürültüye neden olan mekanizma araştırılmış ve gürültü azaltma metotları açıklanmıştır. Bahsedilen teknikler tasarlanan sekiz kaviteli X frekans bandında çalışan magnetron yapısına CST Particle Studio yardımıyla uygulanmıştır.

TABLE OF CONTENTS

LIST OF FIGURES

LIST OF TABLES

1. INTRODUCTION

Rapid development of applications and systems related to microwave frequencies constantly increase the importance of microwave techniques. These techniques have been increasingly used in applications such as long distance communications, radar systems, heaters, defense and missile electronic systems, and space technologies. For all these devices and systems, high power microwave source is one of the most important parts of the system. As a power source, electron tubes have primary advantages over solid state devices that they are usually more efficient and can operate at higher temperature, hence go along with the production of high output power for relatively high frequencies [1].

Electron tubes can be classified into two general groups such as conventional vacuum tubes and microwave tubes. Microwave tubes perform the same functions of generation and amplification in the microwave portion of the frequency spectrum that vacuum tubes perform at lower frequencies. The conventional vacuum tubes, triodes, tetrodes, and pentodes, are still used as signal sources of low output power at low microwave frequencies. On the other hand, three characteristics of ordinary vacuum tubes become important as frequency increases; these are interelectrode capacitance, lead inductance and electron transit time which is the time required for electrons to travel from cathode to the plate. For extremely high frequency applications, standard electron tube construction becomes prohibitive.

In high frequency and high power systems such as radar systems, the primary signal sources are microwave tubes. Although there exist different types of tubes depending on their structure, or interaction mechanism between electrons and electromagnetic field, they have similar features about their operating principle. Microwave vacuum tubes typically consist of two or more electrodes enclosed in a glass, metal, or ceramic envelope. A cathode, which is a source of electrons, usually a metallic electrode that electrons emitted from thereby the methods such as thermionic emission, field emission, or secondary emission. Once the electrons are emitted, the movement of charged particles is controlled by the electromagnetic field. An electric field is supplied by an application of a voltage between the electrodes in the tube, and magnetic field can be established by a permanent

magnet outside the tube. By this interaction, it is intended to achieve that the DC energy stored in an external power supply can be converted to microwave energy at the output. This can be achieved by affecting the energy of electrons, for instance, as an electron is decelerated by the applied electromagnetic field, it loses its kinetic energy to the RF field. This obtained RF field is coupled out of the tube using coupling probes or waveguides. The determinant characteristics of the microwave tubes are their output powers, operating frequencies, efficiencies, bandwidth, noise and tuning range.

An exact analysis of a microwave tube would be very difficult. Two approaches may be used in analyzing the dynamic behavior of the electron beam: the earliest approach used Lagrangian approach and the other type is called the field or Eulerian approach. In the first one, the motion of an individual electron is studied, and in the second method, the electron beam is essentially treated as a charged fluid [2].

Microwave tubes can be classified into two groups depending on their different interaction mechanism between charged particles and the electromagnetic field: the microwave linear-beam tubes which are also called 'O' type tubes and the microwave crossed-field tubes which are also called 'M' type tubes. The linear beam tubes are tabulated as in Figure 1.1 [3].
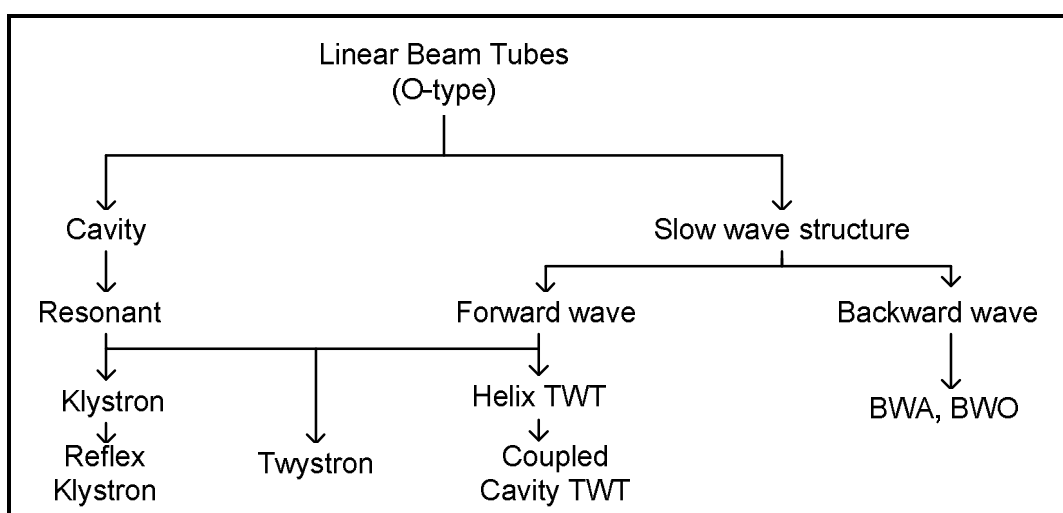
Figure 1.1. Linear beam tubes

The history of linear beam tubes began with the Heil oscillators in 1935 and the Varian brothers' klystron amplifier in 1939 [3]. The work was advanced by the space charge wave propagation theory of Hahn and Ramo in 1939 and continued with the invention of the helix-type traveling wave tube (TWT) by R. Kompfner in 1944 [3]. 'O' type tubes derive their name from the French TPO (tubes a propagation des antes).

A simple schematic of typical 'O' type tube is shown in Figure 1.2.
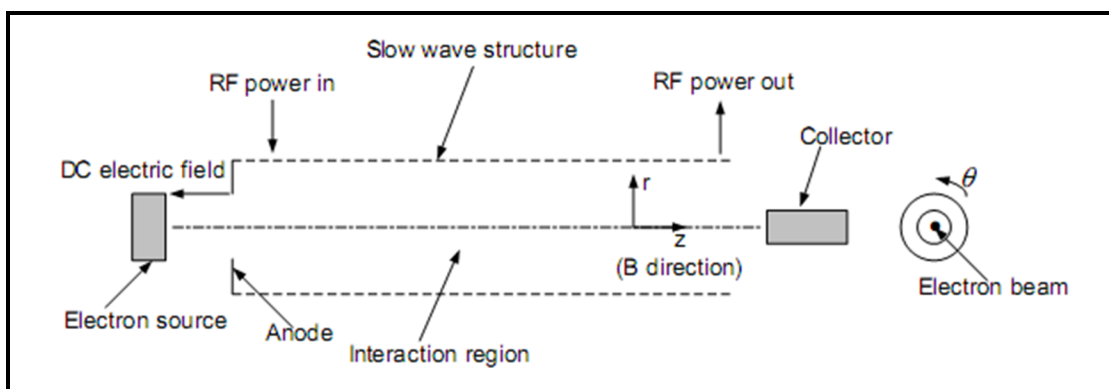
Figure 1.2. The schematic of a linear beam tube [4]

As it can be seen from the Figure 1.2, the interaction between electron beam and electromagnetic field is 2D. In this type of tube, the magnetic field is parallel to the longitudinal axis of the tube, and is used to hold the electron beam together as it travels the length of the tube. The general principle of operation of these tubes can be described as the electrons receive potential energy from the DC voltage before being arrived to interaction region and this energy is converted into kinetic energy. Then, in the interaction region, the acceleration or deceleration of the electrons by the electromagnetic field causes them bunched as they travel along the tube. These electrons induce current in the output, give up their kinetic energy to the RF fields and are collected by the collector [3].

The advent of the TWT started in 1933 by Haeff. He recognized the possibility of a traveling wave interaction between an electron beam and a nearby RF circuit. In 1940, Lindenblad was the first to describe helix traveling wave amplifiers that were similar to a helix traveling wave tube. He was the first to explain that a synchronous interaction between an electron beam and the RF wave on a helix. Finally, Kompfner built the first

traveling wave tube in early 1943 in England [5]. Kompfiner's experimental helix amplifier is shown in Figure 1.3.
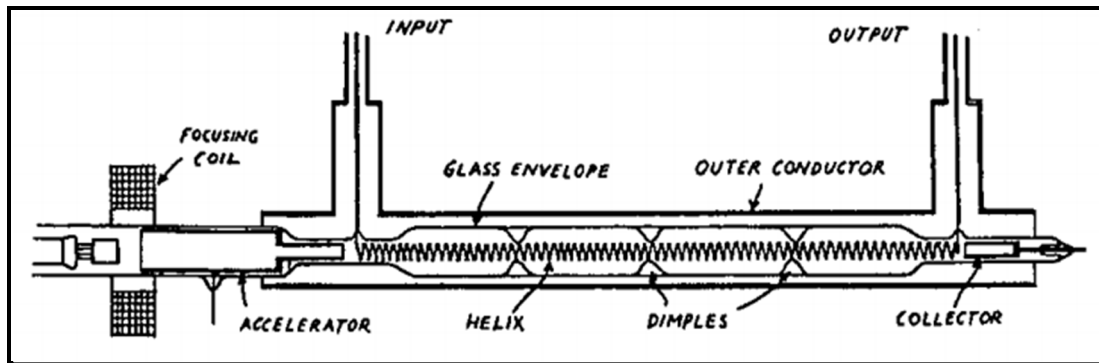
Figure 1.3. Kompfiner's experimental helix amplifier [5]

There are two types of TWTs: the helix TWT which is a relatively low power and broadband device, the coupled cavity TWT which is a relatively high power, but narrowband device. A typical schematic of a helix TWT is shown in Figure 1.4.
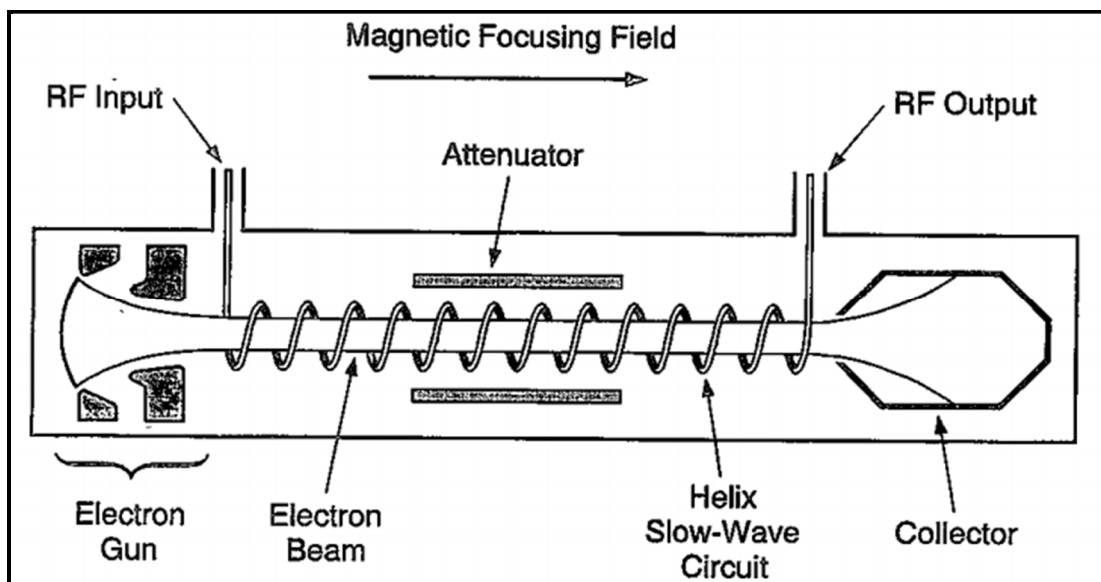
Figure 1.4. Traveling wave tube and the main elements [5]

The RF wave is coupled to the slow wave structure and the wave is slowed down so that it travels at nearly the same speed as the electron beam. Hence, the interaction between

electron beam and RF wave can be possible. The interaction forms electron bunches within the beam, and the beam current becomes modulated by the RF signal. The bunches react with the RF fields resulting in a net transfer of energy from beam to RF signal and consequent amplification. The amplified RF signal is coupled out at the end of the slow wave structure. The remaining energy of the electron beam is dissipated in the collector. Since there are no resonant structures involved, amplification is obtained over a wide bandwidth. The microwave crossed field tubes are tabulated as in Figure 1.5 [3].
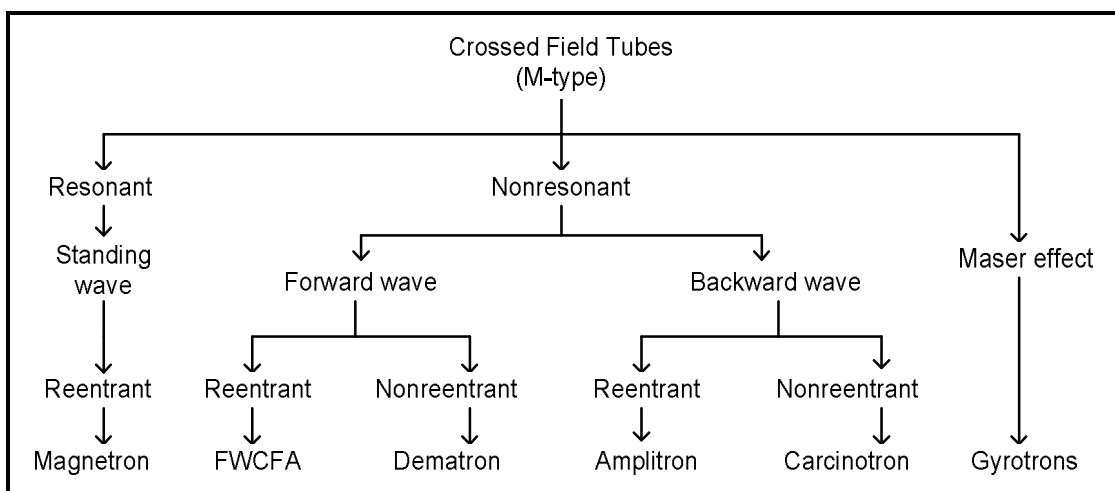
Figure 1.5. Crossed field tubes

Contrary to linear beam tubes, in crossed field tubes, dc magnetic field is perpendicular to the dc electric field and it plays an important role in the RF interaction process. They are also called 'M' type tubes which derive their name from the French TPOM (tubes a propagation des ondes a champs magnetique: tubes for propagation of waves in a magnetic field) [3]. In a crossed field tube, the electrons emitted from the cathode are accelerated by the electric field and gain velocity, and their path is bent by the magnetic field.

Magnetron is a microwave oscillator and a crossed field device ('M' type tube). It can be considered as a diode with a magnetic field parallel to the axis. There is a cylindrical cathode and a coaxial anode, which contains several resonant cavities. In order to understand the theory and the importance of the magnetron, it can be helpful if there is knowledge about the history and development of the device. The history of magnetron can be followed in Figure 1.6.
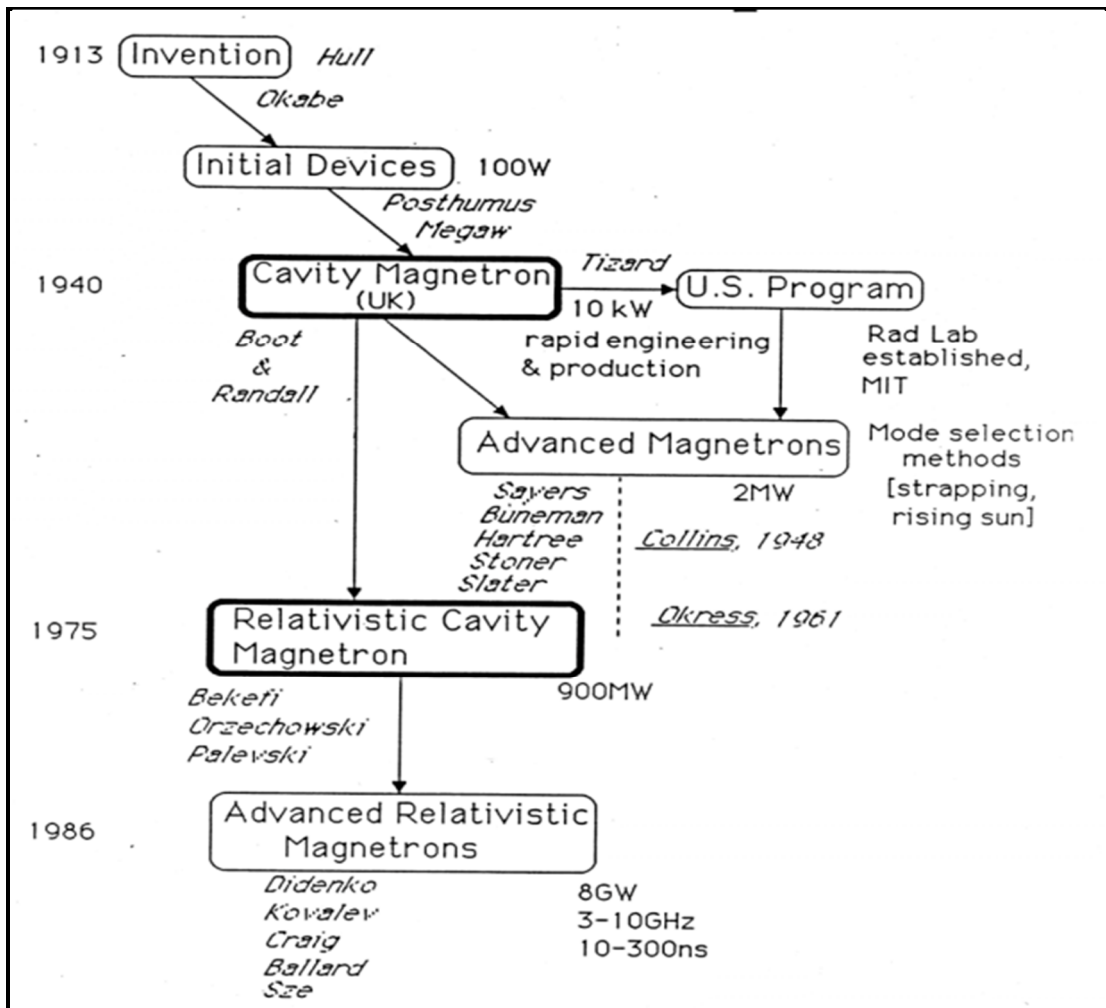
Figure 1.6. The history of the magnetron [6]

The origin of a magnetron theory and development of their operation goes to 1913 when Arthur Hull first investigated, then in 1921, the first magnetron was demonstrated to produce radio frequency oscillations by Hull at the General Electric Laboratories in Schenectady, New York [7]. By 1925 Elder at General Electric was able to produce an output of 8 kW at 30 kHz with an efficiency of 69% [7]. In 1935, Posthomus first described and built a cavity type magnetron oscillator, he explained its operation as being due to an interaction between the tangential components of a traveling RF wave rotating with a velocity equal that of the average velocity of electrons results in conversion of electron energy to amplification of the RF wave [5]. He also demonstrated that, if traveling wave conditions fulfilled which means the electron cloud rotated about the cathode in synchronism with the RF field, then the efficiency can be grown up. Early types of

magnetrons only operated in UHF region and their efficiency were relatively low. The structure schematic of early magnetrons is shown in Figure 1.7.
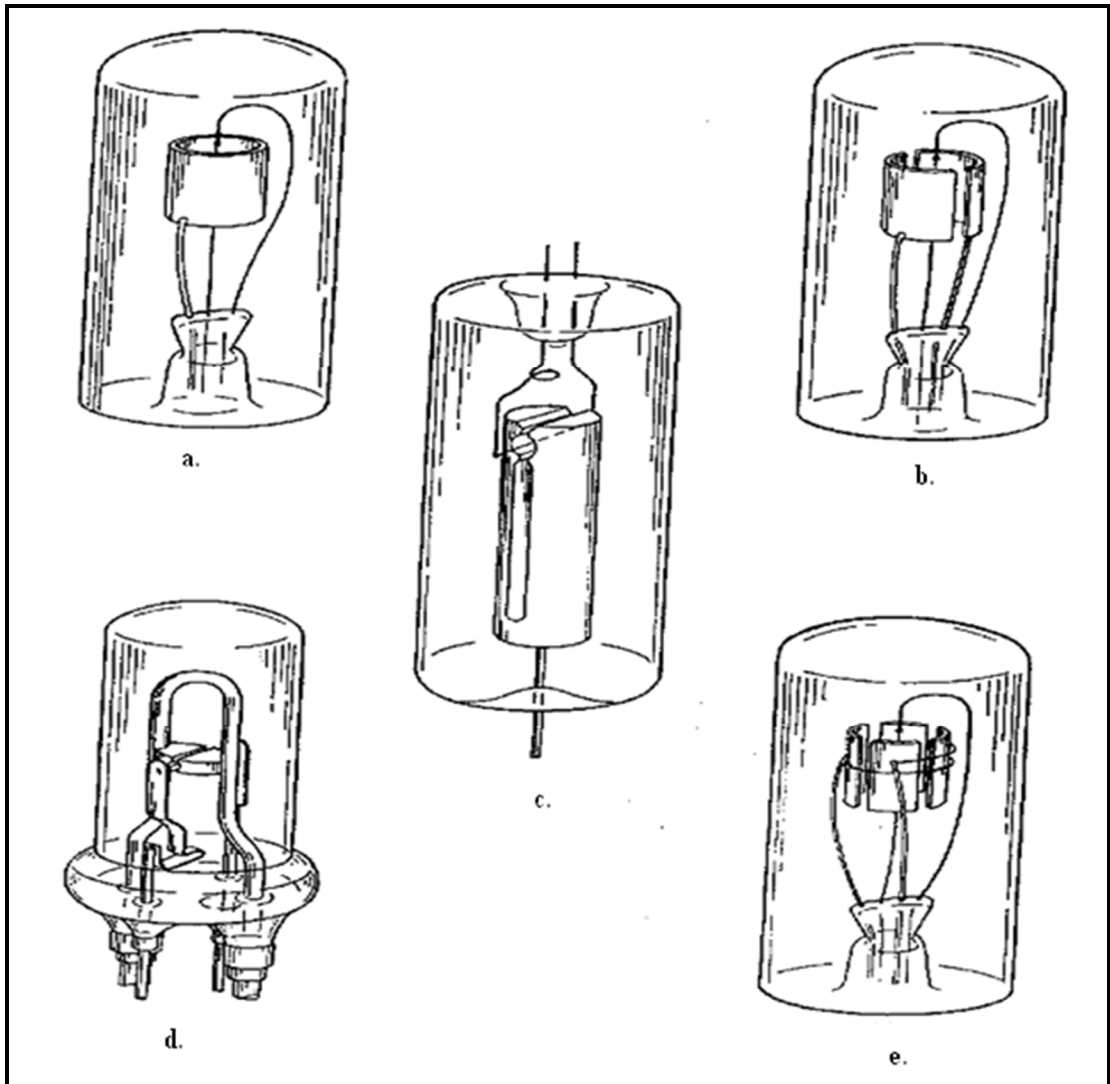
Figure 1.7. Structure of early magnetrons, a. original Hull diode, b. split anode, c. split anode with internal resonator, d. improved split anode, e. four segment anode [8]

In 1934, four-cavity magnetron developed by A.L. Samuel at the Bell Telephone Laboratories. As it can be seen from Figure 1.8, the anode is a part of the vacuum envelope, since the magnetic field had to be provided by a solenoid only low magnetic field could be applied.
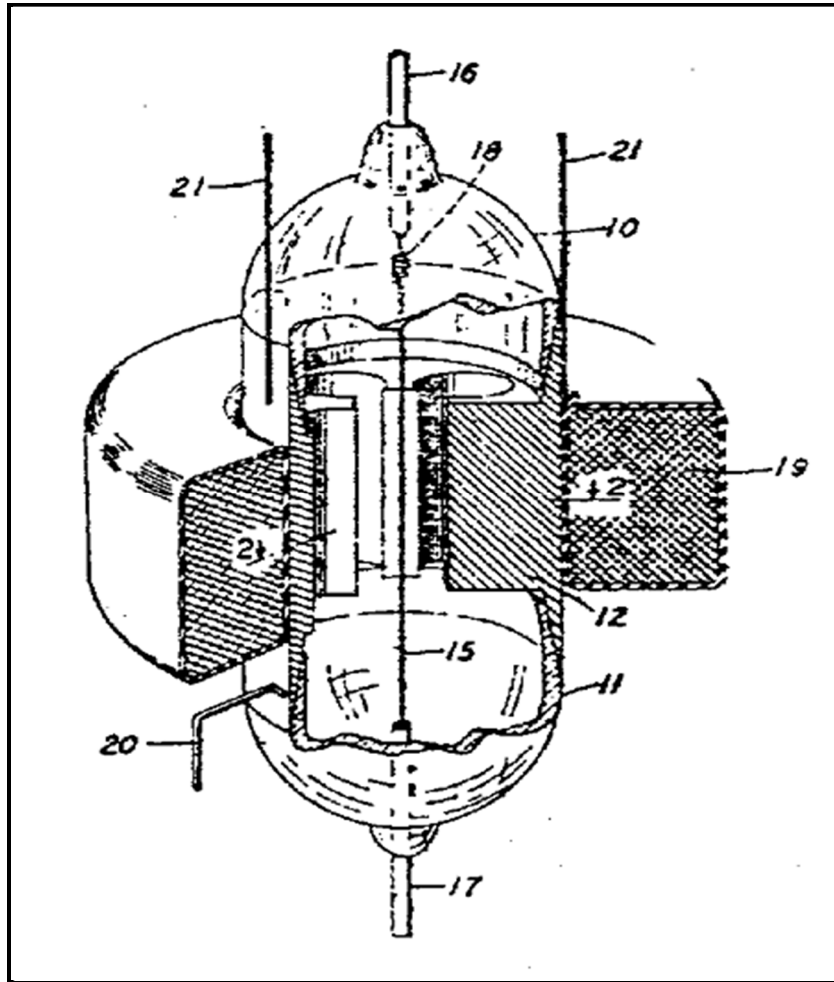
Figure 1.8. Four-cavity magnetron [7]

During the World War II, an urgent need for high power microwave generators for radar transmitters led to the rapid development of the magnetron to its present state. The first successful multicavity magnetron was developed in Russia by Aleksereff and Malearoff in 1936-1937, operating at a wavelength of approximately 9 cm was able to produce about 300 W continuous microwave powers with efficiency of about 20% [9]. Figure 1.9 shows the schematic of four-cavity version of this device, the anode was made of a solid copper block which was water cooled.
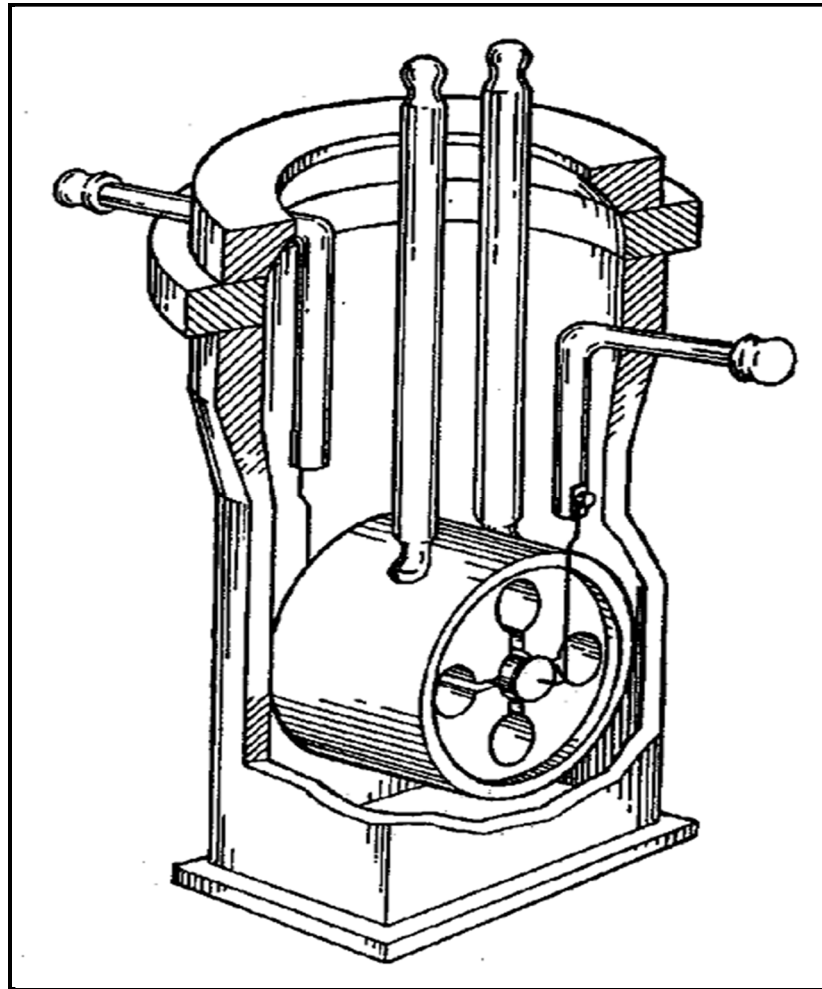
Figure 1.9. The multicavity magnetron developed by Aleksereff and Malearoff [8]

In late 1939, Boot and Randall designed the multicavity magnetron with an external anode contrary to earlier designs where the anode was within a glass envelope. By this design, the magnet gap could be reduced and cooling the anode was easier [7]. They also study the type of cavity resonator, the number of cavities and the form of the output circuit. In 1940, the first experimental results of the tube which had six cavities in the anode block established such that the magnetron was able to produce 400 W of continuous power at a length of 9.8 cm. Such properties of this design as the anode being part of the vacuum envelope and the output coupling loop inside a cavity let the high-power cavity magnetron possible. This development was the essential part of the development of microwave radar systems. In addition to these developments, the Japan Radio Company had developed an 8-cavity, water cooled magnetron at a wavelength of 10 cm with a continuous power of 500

W. The first experimental magnetron of Boot and Randall's magnetron is shown in Figure 1.10 and Figure 1.11.
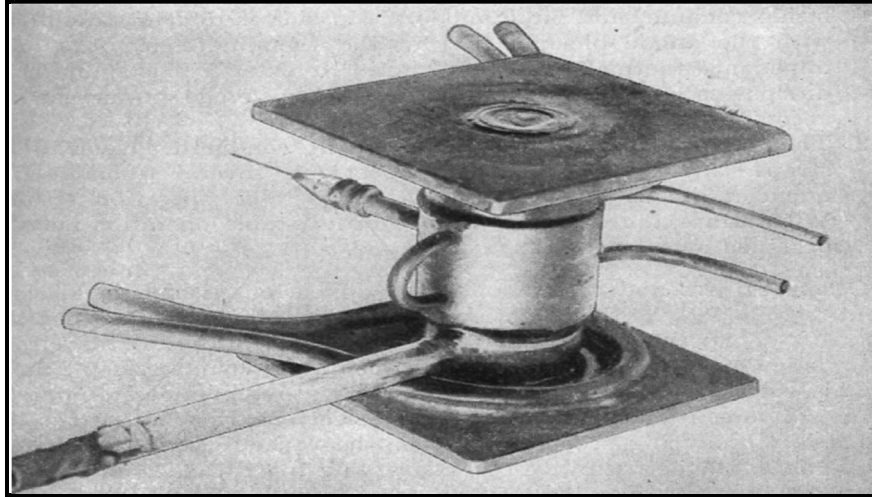
Figure 1.10. Randall and Boot's first experimental magnetron [8]
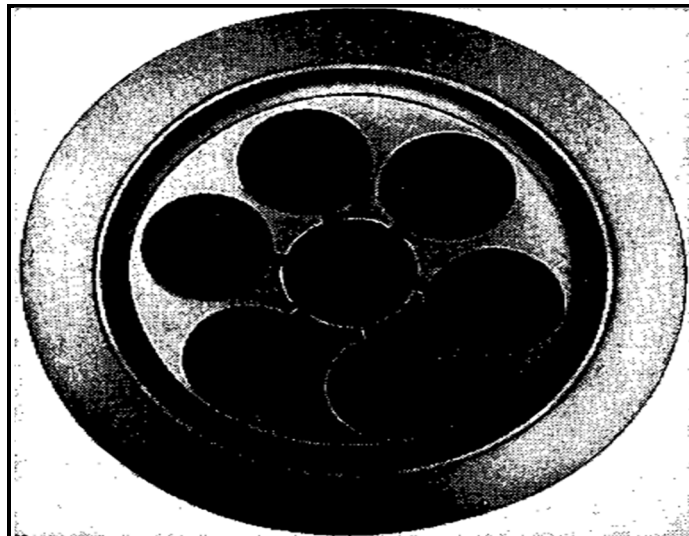
Figure 1.11. Anode block of Randall and Boot's first experimental magnetron [8]

After design of Randall and Boot's magnetron, the General Electric Company (GEC) started to design and manufacture the sealed-off versions of this design. Air cooled tubes emerged contrary to water cooled. The leader of GEC laboratories made two important changes to the original Randall and Boot's design: the first one was to pulse the tube at very high voltages, and the second one was to increase the diameter of the cathode and to

use oxide-coated cathodes. By August 1940, the first of a revised design with 8 cavities rather than 6 was tested and it produced 10 kW. The figure of this design is shown in Figure 1.12.
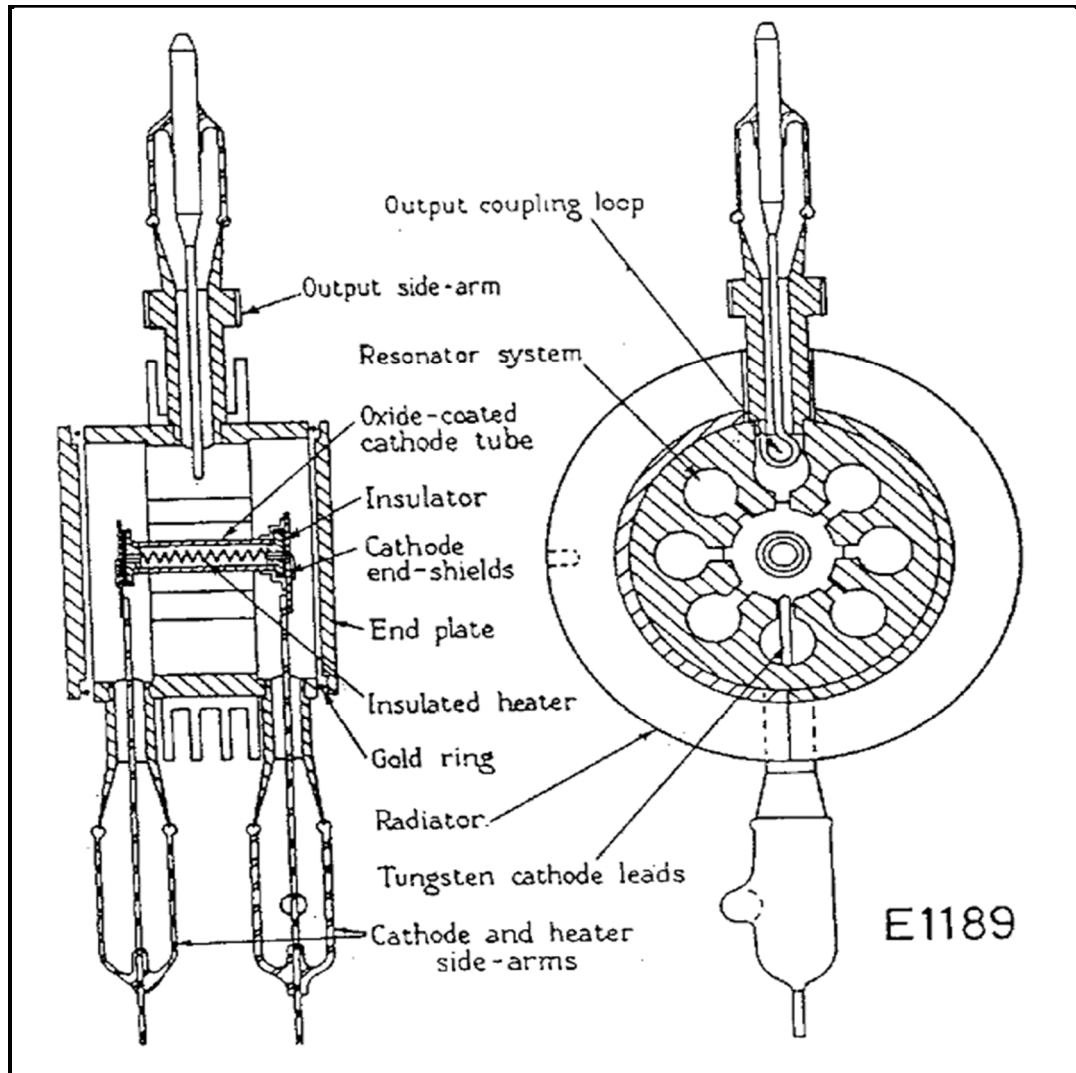
Figure 1.12. An eight cavity magnetron [7]

In addition, in September 1941, John Sayers found that increased frequency separation could be achieved by interconnecting alternate segments which are called "strap". The measurements showed a considerable increase in magnetron efficiency, i.e. unstrapped tube had an efficiency of 12 percent, but the strapped tube was 55 percent efficient with improved stability [7]. After the study of conventional magnetrons, in order to produce much more power, the relativistic magnetrons were suggested. Starting from 1970s,

relativistic cavity magnetrons have been constantly investigated. The first relativistic magnetron design was developed by Bekefi, Orzechowski, and Palevski. The output microwave power was about 900 MW [10], whereas the conventional magnetrons generate about 10 MW power. When the magnetrons produced continuous wave power output, the heating problem appeared at cathode due to back bombardment. In order to solve this problem and also to produce more power, the pulsed magnetron design was developed. The general parameters of conventional and relativistic magnetrons are given in comparison in Table 1.1 [6].

Table 1.1. General operating parameters for conventional and relativistic magnetrons

Parameter	Conventional Magnetrons	Relativistic Magnetrons
Voltage	≤100 kV	≥500 kV
Current	~100 A	≥5-10 kA
Cathode process	Thermionic and secondary emission	Explosive emission
Pulse duration	≥ 1 ms	≤ 100 ns
Rise time	≤ 200 kV/ms	~ 100 kV/ns
Power	≤ 10 MW	≥ 1GW
Efficiency	~50-90 %	~20-40 %
Tunable range	~5 %	~30 %

The rising sun and strapping techniques which are used in conventional magnetrons for good mode selection, cannot be applied to relativistic magnetrons due to high field stress that would cause arcing and field emission. Conventional and relativistic magnetrons are pictured in Figure 1.13. The relativistic magnetron is briefly discussed in detail in section 2.2.4.
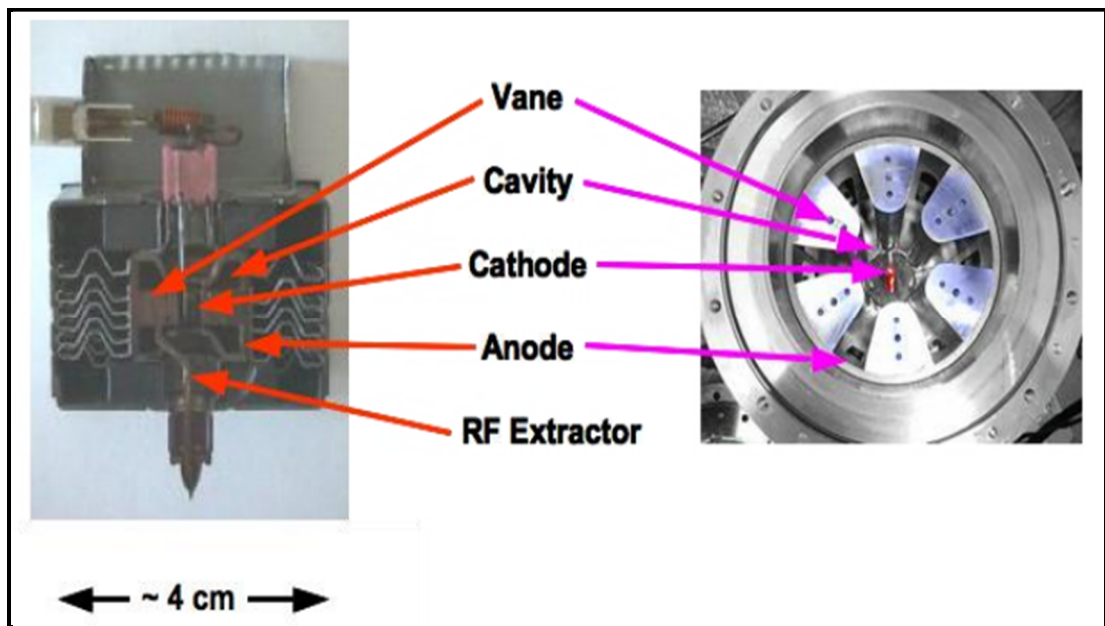
Figure 1.13. The cut through of a conventional magnetron used in a microwave oven is at the left hand side, and the relativistic magnetron from the University of Michigan's is at the right hand side [11]

2. OPERATING PRINCIPLE OF MAGNETRONS

In this chapter, operating principles of cavity resonators, especially cylindrical ones are given. The various types of magnetrons and the theory of these magnetrons will be further investigated and analyzed in detail.

2.1. CYLINDRICAL CAVITY RESONATORS

A cavity resonator is a metallic enclosure that confines the electromagnetic energy. The stored electric and magnetic energies inside the cavity determine its equivalent inductance and capacitance. The energy dissipated by the finite conductivity of the cavity walls determines its equivalent resistance [3]. There are types of cavity resonators such as rectangular cavity resonator and cylindrical cavity resonator which are termed by cavity shapes. The resonant cavities have many advantages and for this reason they are used at microwave frequencies. They have a very high Q which give a narrow bandwidth and allow very accurate tuning. The shape and size of cavities determine the resonant frequencies, in general the smaller the cavity the higher the resonant frequency.

A cylindrical cavity resonator can be constructed from a section of circular waveguide at both ends [12]. Since the dominant circular waveguide mode, which is the resonant mode having the lowest frequency, is the TE_{11} mode, the dominant cylindrical cavity mode is TE_{111} mode. The dominant TM mode is TM_{110} mode. The resonant frequencies for the TE_{nml} and TM_{nml} circular cavity modes are derived as:

The geometry of cylindrical cavity is given in Figure 2.1.
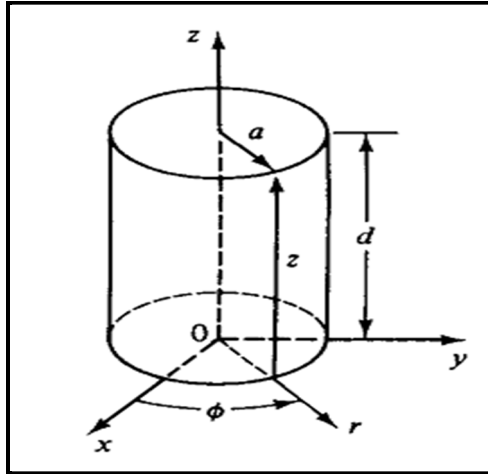
Figure 2.1. The geometry of cylindrical cavity [3]

The wave function in cylindrical cavity should satisfy Maxwell's equations subject to the boundary conditions. The transverse electric fields (E_r, E_ϕ) of the TE_{nm}, or TM_{nm} circular waveguide mode can be written as [12]

$$\overrightarrow{E_t}(r,\phi,z) = \vec{e}(r,\phi)\left[A^+ e^{-j\beta_{nm}z} + A^- e^{j\beta_{nm}z}\right] \qquad (2.1)$$

where, $\vec{e}(r,\phi)$ represents the transverse variation of the mode, A^+ and are A^- arbitrary amplitudes of the forward and backward travelling waves. The propagation constants are

$$\beta_{nm} = \sqrt{k^2 - \left(\frac{p'_{nm}}{a}\right)^2} \qquad (2.2)$$

for TE_{nm} mode and

$$\beta_{nm} = \sqrt{k^2 - \left(\frac{p_{nm}}{a}\right)^2} \qquad (2.3)$$

for TM_{nm} mode.

where $k = \omega\sqrt{\mu\varepsilon}$, μ is a permeability, ε is a permittivity and p_{nm}, p'_{nm} are the mth roots of J_n Bessel functions of first kind and the derivative of Bessel function with respect to its argument respectively.

According to boundary conditions $\overrightarrow{E_t} = 0$ at $z = 0$ and $z = d$

$$A^+ = A^- \tag{2.4}$$

and

$$A^+ \sin\beta_{nm}d = 0 \tag{2.5}$$

are found. This means that

$$\beta_{nm}d = l\pi \tag{2.6}$$

for $l = 0,1,2,\dots$

Thus, the resonant frequencies of TE$_{nml}$ and TM$_{nml}$ are obtained

$$f_{nml} = \frac{c}{2\pi\sqrt{\mu_r\varepsilon_r}}\sqrt{\left(\frac{p'_{nm}}{a}\right)^2 + \left(\frac{l\pi}{d}\right)^2} \tag{2.7}$$

for TE$_{nml}$ mode and

$$f_{nml} = \frac{c}{2\pi\sqrt{\mu_r\varepsilon_r}}\sqrt{\left(\frac{p_{nm}}{a}\right)^2 + \left(\frac{l\pi}{d}\right)^2} \tag{2.8}$$

for TM$_{nml}$ mode.

2.2. MAGNETRON

Magnetron is a high power microwave source that can be classified as a diode which has usually cylindrical shape. It is mostly used in radars and communication satellites; also it is used for consumer electronic industry such as microwave oven. As it is mentioned in the first part, the theory of magnetron and its beginning of development history goes to very past years, the first quarter of 20th century. Hull invented the magnetron in 1921 and the theory has been developed since this date.

All magnetrons have anode and cathode parts which can be in different forms, operated in a dc magnetic field normal to a dc electric field. The electrons emitted from the cathode are influenced by these crossed electric and magnetic fields which result a curved electron path. The development of magnetron theory also follows the evolution of geometry of early type magnetrons, are shown in Figure 2.2. Hull's first magnetron is represented in Figure 2.2.a. Okabe developed the split anode magnetron in 1929 is shown in Figure 2.2.b., and the development of the split anode magnetron by dividing the anode into more segments indicated in Figure 2.2.c. In all these magnetrons, the anode structures are connected to outer oscillation circuits, on the other hand, Figure 2.2. d. shows the resonant cavity magnetron, which the resonant cavities replaced outer oscillation circuits developed by Randall and Boot [13]. They discovered that the output power can be increased with this change.
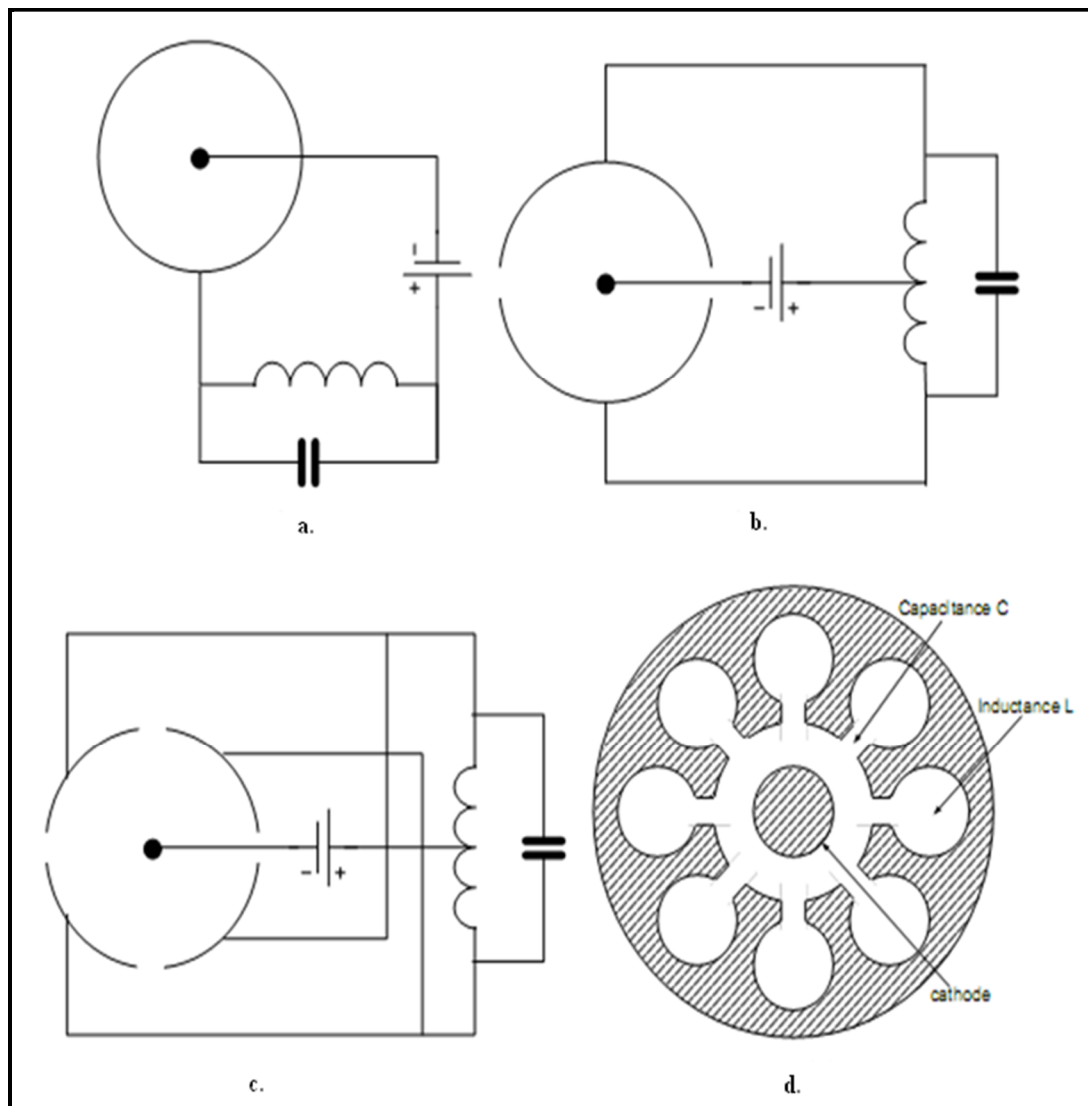
Figure 2.2. a. Cylindrical anode magnetron, b. Split anode magnetron, c. Multi-segment magnetron, d. Resonant cavity magnetron [4]

The magnetrons classified into two groups according to their operating principle:

- Negative resistance oscillation magnetron (Habann type magnetron)
- Electron transit time oscillation magnetron (resonant cavity magnetron)

2.2.1. The Negative Resistance Oscillation Magnetron

This type of magnetron uses a static negative resistance between two anode segments [3]. The general construction of negative resistance magnetrons is similar to the cyclotron

frequency magnetrons except that the anode has two halves which are at different RF potentials as shown in Figure 2.3.
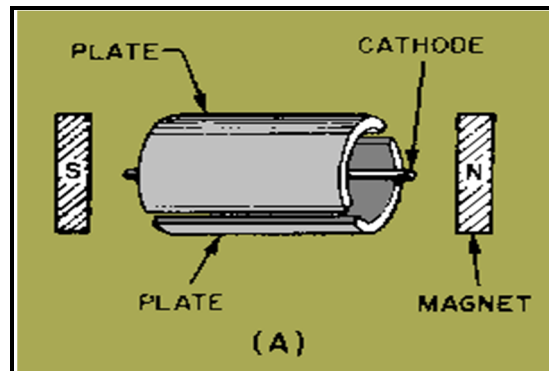
Figure 2.3. The general shape of negative resistance oscillation magnetron [14]

If an applied magnetic field to a split anode magnetron is greatly increased over what is required for the cyclotron frequency magnetrons, this type of oscillation occurs. Figure 2.2.b. also represents this type of magnetron. The Figure 2.4 is a typical split anode magnetron developed by Philips [15].
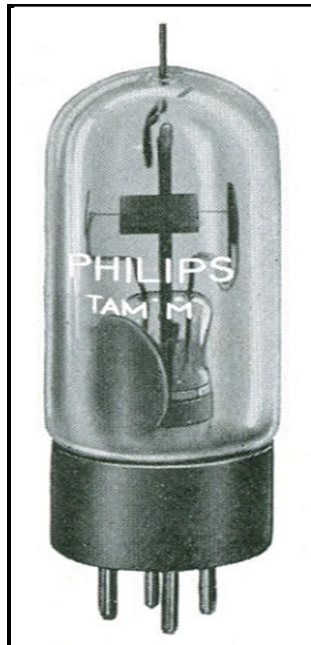
Figure 2.4. Philips split anode magnetron

Under the influence of electromagnetic field, emitted electron from the cathode points toward the more negative potential plate. The path of electron can be seen in Figure 2.5.
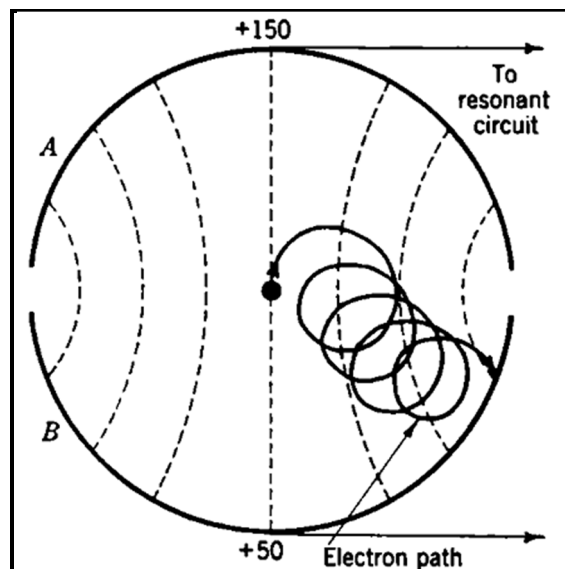
Figure 2.5. The trajectory of an electron in a negative resistance oscillation magnetron. Two anode plates with different potentials, 150 Volts and 50 Volts [8]

Because of the fact that only few electrons reach the higher potential plate and most of the electrons strike the more negative part of the anode, more current induced in lower potential plate which is the explanation of negative resistance oscillation. By the help of resonant circuit located between the plates, the oscillated signal can be obtained. Since required magnetic field for negative oscillation magnetrons is much greater than for cyclotron frequency oscillation magnetrons, the length of the tube is limited to keep the magnet at reasonable dimensions. These types of magnetrons are capable of operating at 100 cm wavelength and output powers of 100 Watts with an efficiency of 25 percent [16].

2.2.2. The Resonant Cavity Magnetron

The design of high performance magnetron with high electrical and thermal conductivity features in a cylindrical symmetry device with a high frequency output circuit could be capable of giving a relatively large anode current and high power [17]. This type of magnetron operation depends on the electron transit time oscillation. Although electron beam and RF field interaction inside a magnetron is very complicated, a simplified electron motion in a planar and cylindrical diode is investigated under the influence of applied electric and magnetic fields before explanation of the resonant cavity magnetron operation.

2.2.2.1. Electron Motion in an Electromagnetic Field inside a Planar Diode
The motion of electron beam is assumed to be in a uniform electromagnetic field since the solution of the inhomogeneous differential equations in a non-uniform field is extremely difficult to obtain and cannot be determined exactly. On the other hand, fortunately, there are uniform electric and magnetic fields in magnetrons for the electron-field interaction.

In an applied electromagnetic field, the motion of electrons depends on the orientation of the two fields, electric and magnetic field. For instance, if the magnetic field is in the same direction with the electric field, the magnetic field exerts no force on the electron. On the other hand, if the magnetic field is applied at right angle to the electric field, which is our case, a magnetic force is also exerted on the electron beam. This type of field is called a crossed field. This is demonstrated in Figure 2.6.
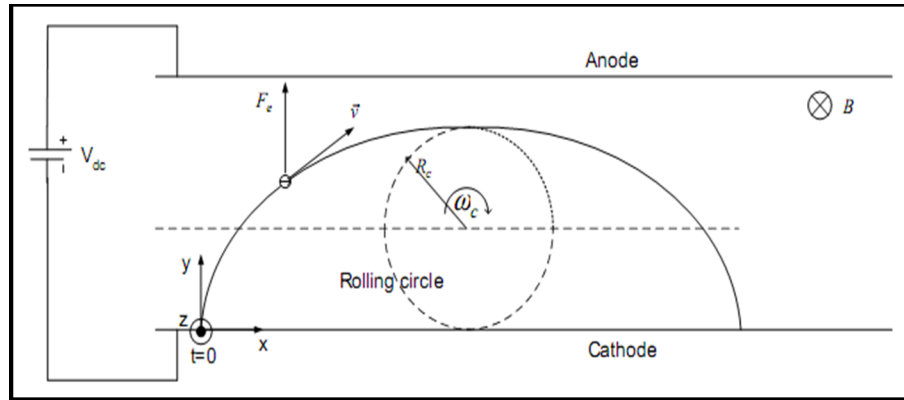
Figure 2.6. The electron trajectory in a crossed field planar diode [4]

As it can be seen from the Figure 2.6, there are two infinitely large plane electrodes, anode and cathode, with potential difference of V_{dc}. Since the distance between two electrodes d, the electric vector field between the electrodes is $\vec{E} = E(-\vec{a}_y) = (V_{dc}/d)(-\vec{a}_y)$. A uniform magnetic field is applied as $\vec{B_0} = (B_0)(-\vec{a}_z)$ perpendicular to the electric field. The motion of electron emitted from the cathode under the influence of electric and magnetic field is described by Lorentz force equation. We can represent the velocity of an electron as, $\vec{v} = v_x \vec{a}_x + v_y \vec{a}_y = \frac{dx}{dt}\vec{a}_x + \frac{dy}{dt}\vec{a}_y$ where $\vec{a}_x$ and $\vec{a}_y$ are the unit vectors in a direction x and y, respectively. The electric and magnetic force are written as follows;

$$\vec{F_e} = q\vec{E} = (-e)\vec{E} = (-e)E(-\vec{a}_y) = (e)E(\vec{a}_y) \tag{2.9}$$

$$\vec{F_m} = q(\vec{v} \times \vec{B}) = e(-B_0\frac{dx}{dt}\vec{a}_y + B_0\frac{dy}{dt}\vec{a}_x) \tag{2.10}$$

where, $\frac{dx}{dt}$ and $\frac{dy}{dt}$ are the horizontal components of the electron velocity in the Cartesian coordinate system. Then, the following equation can be written,

$$\vec{F} = m\vec{a} = \vec{F_e} + \vec{F_m} = e(E\vec{a}_y - \vec{B_0}\frac{dx}{dt}\vec{a}_y + \vec{B_0}\frac{dy}{dt}\vec{a}_x) \tag{2.11}$$

If the acceleration vector is divided into components such that, $\vec{a} = \frac{d^2x}{dt^2}\vec{a}_x + \frac{d^2y}{dt^2}\vec{a}_y$, equation 2.11 can be rewritten as

$$\left(m\frac{d^2y}{dt^2}\right)\vec{a}_y = (eE - eB_0\frac{dx}{dt})\vec{a}_y \qquad (2.12)$$

$$\left(m\frac{d^2x}{dt^2}\right)\vec{a}_x = (eB_0\frac{dy}{dt})\vec{a}_x \qquad (2.13)$$

The solutions of the above differential equations are easily obtained and it can be seen that the trajectory of an electron is a cycloid.

$$x = A_1\sin(\omega_c t + \phi) + A_2 t + x_0 \qquad (2.14)$$

$$y = A_1\cos(\omega_c t + \phi) + y_0 \qquad (2.15)$$

where, A_1, A_2, x_0 and y_0 are all constants, that can be determined by the initial conditions, and $\omega_c = eB_0/m$ is the angular frequency. Considering the following simple initial conditions;

$$x|_{t=0} = y|_{t=0} = \frac{dx}{dt}\Big|_{t=0} = \frac{dy}{dt}\Big|_{t=0} = 0 \qquad (2.16)$$

The equation 2.7 and equation 2.8 become as

$$x = \frac{-m}{e}\frac{E}{B_0^2}sin\omega_c t + \frac{E}{B_0}t \qquad (2.17)$$

$$y = \frac{-m}{e}\frac{E}{B_0^2}cos\omega_c t + \frac{m}{e}\frac{E}{B_0^2} \qquad (2.18)$$

These equations show that with above initial conditions, the trajectory of an electron is like a point on a circle rolling along the cathode surface as shown in Figure 2.6 with an angular frequency $\omega_c = eB_0/m$ and a cyclotron period $T = 2\pi/\omega_c$. The radius of the rolling circle is found as

$$R_c = \frac{y_{max}}{2} = \frac{y(\frac{T}{2})}{2} = \frac{mE}{eB_0^2} \tag{2.19}$$

The maximum distance an electron travels in one period T, is

$$x(T) = 2\pi R_c = 2\pi \frac{mE}{eB_0^2} \tag{2.20}$$

As it can be easily seen from the equation 2.12, the radius of the trajectory of an electron will be varied with a magnetic field B_0 for a given electric field E. The situation that an electron just touch the anode, in other words, tangential to the anode plate, which is also called a cut-off condition, when $y_{max} = d$, the magnetic field, B_c is determined using the equation 2.19,

$$B_c = \sqrt{\frac{2mE}{ed}} = \frac{1}{d}\sqrt{\frac{2m}{e}V_{dc}} \tag{2.21}$$

Also this condition can be expressed in terms of cut-off voltage for a given magnetic field, B_0 such that

$$V_c = \frac{d^2 eB_0^2}{2m} \tag{2.22}$$

The trajectories of electron can be represented as in Figure 2.7. If there exists only an electric field, which means absence of magnetic field, electron moves as Curve 1, if the magnetic field is smaller than the cut-off magnetic field value B_c, electron movement is like Curve 2, if an applied magnetic field $B = B_c$, the electron just touch the anode plate, and the electron orbit is like Curve 3, as a last, if the magnetic field is larger than the cut-off value B_c, the electron moves as Curve 4.
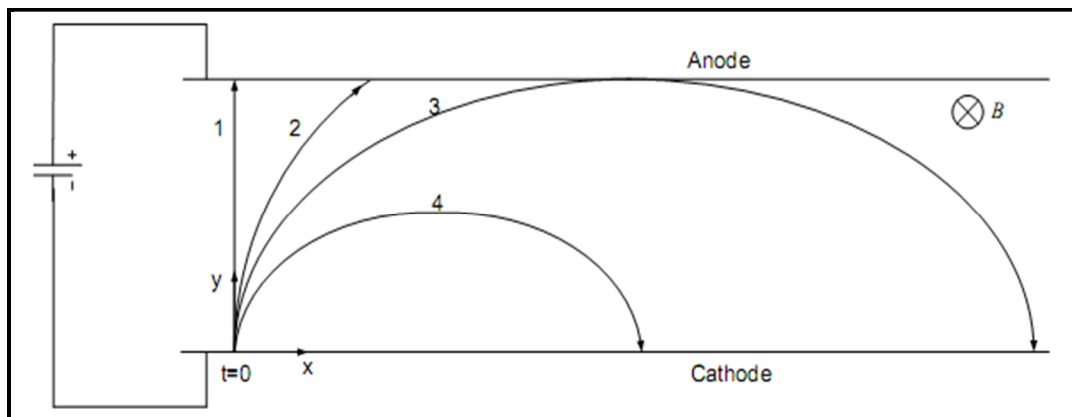
Figure 2.7. The electron trajectories in a crossed field planar diode for different magnetic fields [4]

As a last stage, if there is a an AC field in an interaction space between the cathode and anode, when the magnetic field is larger than the cut-off value, B_c, the electron does not go through the anode plate directly. Depending on emission time from the cathode, electron will be accelerated or decelerated. This situation is represented in Figure 2.8.
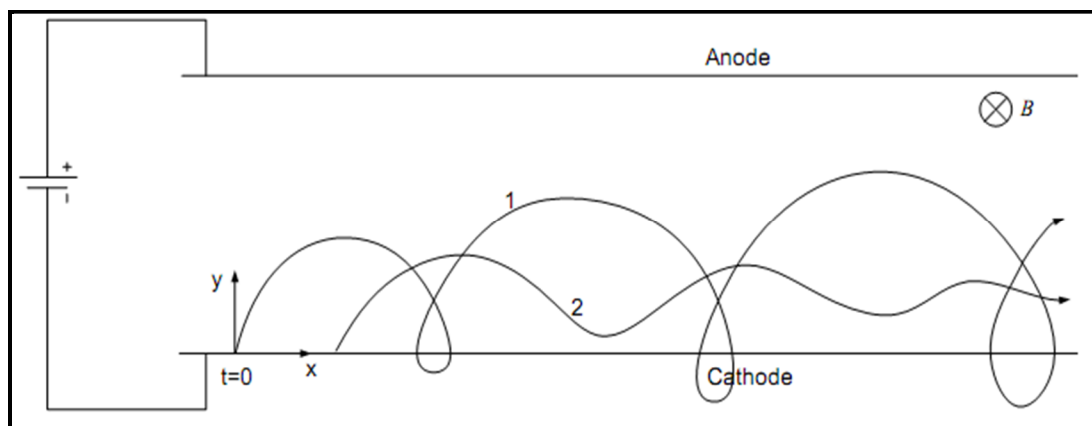
Figure 2.8. The trajectory of electrons when an AC field is applied [4]

Curve 1 demonstrates the situation that an electron is accelerated by the AC field, it moves back to the cathode plate quickly, the additional energy of an electron comes from the AC field, thus they will not affect or amplify the AC field. When an electron is decelerated by the AC field, the trajectory of an electron is like a Curve 2, the energy lost by the electron is gained by the AC field, and thus this electron causes to amplify the AC field.

2.2.2.2. Electron Motion in an Electromagnetic Field inside a Cylindrical Diode

Figure 2.9 represents the geometry of the cylindrical diode, with a cathode radius a, anode radius b. The potential difference V_0 is applied between the cathode and anode plates. The magnetic field B is parallel to the axis of the diode, into the page, and perpendicular to the electric field.
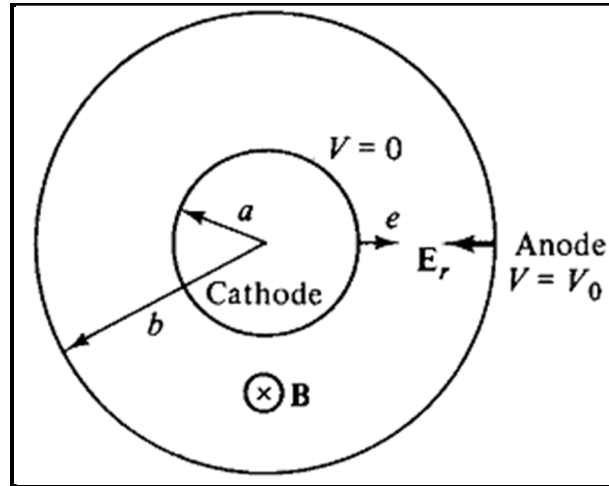
Figure 2.9. The geometry of the cylindrical diode [3]

The analysis of an electron motion inside a cylindrical diode is made as similar way in previous section. The differential equations should be rewritten in cylindrical coordinates. The velocity and acceleration vectors can be written according to Figure 2.1 respectively,

$$\vec{v} = \frac{dr}{dt}\vec{a_r} + r\frac{d\phi}{dt}\vec{a_\phi} + \frac{dz}{dt}\vec{a_z} \qquad (2.23)$$

$$\vec{a} = \left(\frac{d^2r}{dt^2} - r\left(\frac{d\phi}{dt}\right)^2\right)\vec{a_r} + \frac{1}{r}\frac{d}{dt}\left(r^2\frac{d\phi}{dt}\right)\vec{a_\phi} + \frac{d^2z}{dt^2}\vec{a_z} \qquad (2.24)$$

where, $\vec{a_r}$, $\vec{a_\phi}$ and $\vec{a_z}$ are unit vectors in cylindrical coordinates. Using the equations 2.23 and 2.24, the kinetic equations of the electron 2.12 and 2.13, are written as

$$eE - eBr\frac{d\phi}{dt} = m\left(\frac{d^2r}{dt^2} - r\left(\frac{d\phi}{dt}\right)^2\right) \qquad (2.25)$$

$$eB\frac{dr}{dt} = m\frac{1}{r}\frac{d}{dt}\left(r^2\frac{d\phi}{dt}\right) \tag{2.26}$$

By considering the initial condition, $\frac{d\phi}{dt}\big|_{r=a} = 0$ from the equation 2.26, the angular velocity of the electron can be obtained that

$$\omega_0 = \frac{d\phi}{dt} = \frac{\omega_c}{2}\left(1 - \frac{a^2}{r^2}\right) \tag{2.27}$$

where, $\omega_c = eB_0/m$ is a cyclotron frequency of an electron. For the electron just grazing the electron, the conditions $r = b$, $V = V_0$, $\frac{dr}{dt}\big|_{r=b} = 0$ and since the electron leaves the cathode with zero velocity, the kinetic energy equation is written as

$$\frac{1}{2}mv_b^2 = eV_0 \tag{2.28}$$

where, $v_b = b\frac{d\phi}{dt}$ is the angular velocity. Using the equations 2.27 and 2.28, the cut-off voltage and magnetic field are obtained as follows

$$V_{oc} = \frac{e}{8m}B^2b^2\left(1 - \frac{a^2}{b^2}\right)^2 \tag{2.29}$$

$$B_c = \frac{(8V_0\,m/e)^{1/2}}{b(1 - a^2/b^2)} \tag{2.30}$$

These equations mean that, for a given magnetic field B, if $V_0 < V_{oc}$, the electrons will not reach the anode, otherwise, it will strike the anode plate. Conversely, for a given V_0, if $B > B_c$, the electron misses the anode, otherwise, it reaches the anode. These are represented in Figure 2.10. Curve 1 for the absence of magnetic field, Curve 2 represents the trajectory for an electron in a magnetic field $B < B_c$, Curve 3 is a representation of cut-off condition, $B = B_c$ as a last, for $B > B_c$, the electron moves in a way as Curve 4.
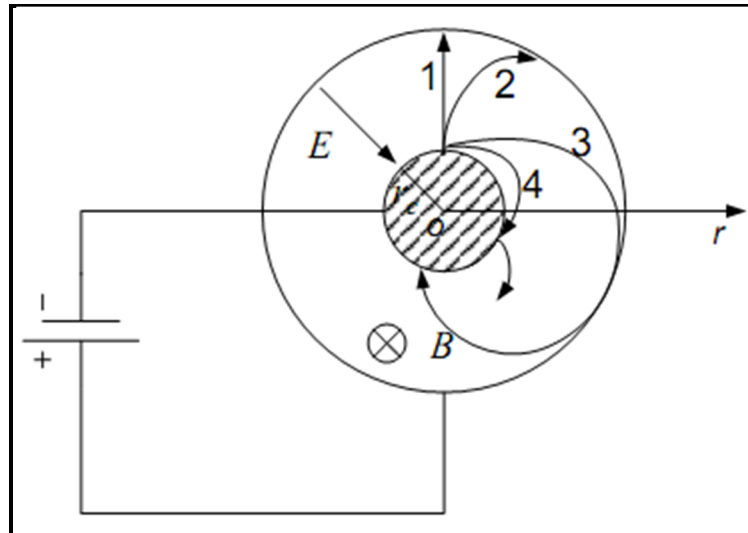
Figure 2.10. The electron trajectories in a crossed field cylindrical diode for different magnetic fields [4]

Until now, the principle of electron transit time oscillation has been expressed, and anymore, the theory of resonant cavity magnetron will be explained.

2.2.2.3. The Theory of Resonant Cavity Magnetron

At the time World War II, by the need of high power and wavelengths of 10 cm or less magnetrons, this type of magnetron was found and from this time it has been developed for more output power, more stable, low noise and high frequency operation. The following features of resonant cavity magnetron make it very important and effective, a large diameter oxide coated cathode can be used which cause to stable operation and large emitting area; the anode block is part of the vacuum envelope which eases the heat dissipation; the separate resonators are coupled by conducting elements to cause the efficiency increase [8].

This type of magnetron is composed of coupled resonators surrounding a cylindrical cathode and it is designed to convert DC input power to RF output power. This conversion is a result of interaction between electron beam and RF field in a place between the cylindrical cathode and the anode block which is called the interaction space. In this mentioned geometry, the cathode is maintained at a negative potential, while the anode block is at ground potential to create a potential difference between cathode and anode

blocks. A constant and uniform magnetic field is applied in this interaction space in a direction parallel to the axis of the tube, which is also perpendicular to the electric field. This magnetic field is provided by an electromagnet or permanent magnet with pole faces external to the magnetron [8]. The anode block consists of number of resonators which open into the interaction space. Output power is extracted from one resonator by coupling loop. All these described components and parts can also be seen in Figure 2.11.
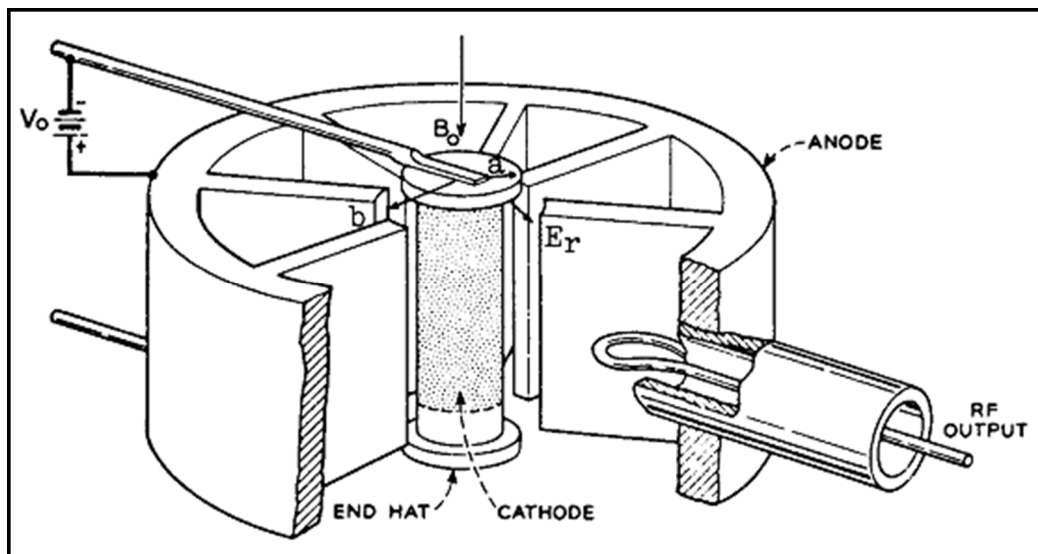
Figure 2.11. The schematic of a typical cylindrical magnetron (vane type) [3]

The resonant system design is a very important part of the magnetron design, since the operating voltage, frequency (wavelength), interaction between the electron beam and RF field are all determined by the dimensions and shapes of the resonant system. Also the resonant system is responsible to make the operation of the magnetron as stable as possible.

Now, the all required definitions, theorems and subjects about the resonant cavity magnetrons are explained in detail to understand the theory and operating principle clearly.

2.2.2.4. Electrical Equivalent Circuit

In order to explain the RF oscillation in a magnetron and to define the mode concept, eight-cavity hole and slot magnetron is considered as an example. Figure 2.12

demonstrates the structure of the eight-cavity hole and slot magnetron and equivalent circuit model.
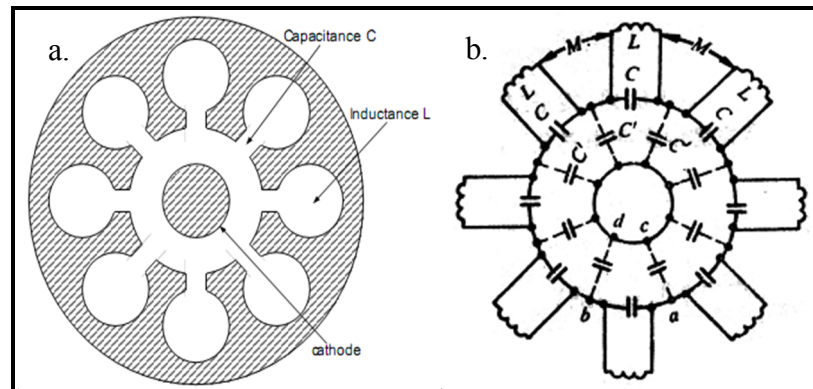
Figure 2.12. a. The cross section of an eight cavity hole and slot magnetron, b. Equivalent circuit model of eight cavity hole and slot magnetron [4]

As shown in Figure 2.12.a, the cavity consists of a cylindrical hole in the anode block and a slot which connects the cavity to the interaction space of a magnetron. These cavities replace resonant circuits and the equivalent circuit can be modeled as Figure 2.12.b. The parallel sides of the slot form the plates of a capacitor, while the walls of the hole behave as an inductor. Thus, the hole and slot structure form a resonant LC circuit. 'L' and 'C' represent inductance and capacitance of individual cavities, whereas 'C'' is the capacitance between the individual anode block and the cathode. 'M' demonstrates the magnetic coupling due to magnetic flux in one individual cavity to adjacent cavity. All of these are also valid in other types of magnetron such as vane, rising sun and slot. Figure 2.13 is a representation of vane type magnetron cavity.
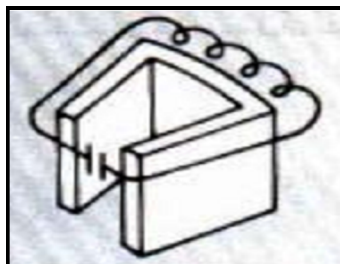
Figure 2.13. The individual cavity of vane type magnetron [18]

The oscillation frequency of individual cavity resonators is $\omega_0 = 1/\sqrt{LC}$ and LC tanks of each cavity are connected in series. Since the distance between the cavities are same and symmetrically located, the phase difference between each cavity is the same. This phase difference is a very important phenomenon in magnetron operation which determines the operating modes. This concept can be explained as follows;

The oscillating voltage between the anode vanes in one cavity can be written as

$$V_1 = V_m \sin(\omega_0 t) \tag{2.31}$$

Then, in the adjacent cavity, the oscillating voltage is,

$$V_2 = V_m \sin(\omega_0 t - \varphi) \tag{2.32}$$

where, V_m is the amplitude of the RF voltage and φ is the phase difference between the adjacent cavities. If it is continued like that, for an eight cavity magnetron, the oscillating voltage for the last cavity becomes,

$$V_8 = V_m \sin(\omega_0 t - 7\varphi) \tag{2.33}$$

Since the magnetron is a closed circuit, $V_9 = V_m \sin(\omega_0 t - 8\varphi)$ become equal to $V_1 = V_m \sin(\omega_0 t)$ leads to

$$8\varphi = 2\pi n \tag{2.34}$$

where, $n = 0, \pm1, \pm2, \dots$.

If this result is generalized for N cavity magnetron, the equation 2.34 becomes as

$$N\varphi = 2\pi n \tag{2.35}$$

or,

$$\varphi = \frac{2\pi n}{N} \qquad (2.36)$$

From an equation 2.36, it is obviously seen that there exists more than one mode that can satisfy the same phase difference. The modes corresponding to $n = 0, 1, 2, ...$ and $n = 0, -1, -2, ...$ are pairs of degenerate modes which are called doublets. If all the resonators are identical and the structure is perfectly symmetrical, the frequencies of these degenerate modes are equal. Thus the total important modes in an N cavity magnetron correspond to $n = 1$ to $n = N/2$. It can be easily seen that for $n = N/2$, the phase difference become as $\varphi = \pi$, which is also result of $n = 0$, corresponds to a condition of zero charge distribution on every anode segments, thus this mode does not exist. This non-degenerate characteristic of the $n = N/2$ mode which is also called $\pi - mode$, is an important feature. In actual magnetrons, they do not have perfect symmetrical structure, and these asymmetries cause the fact that the doublets have slightly different frequencies. This situation increases the importance of $\pi - mode$. When the magnetron is operated in desired mode, $\pi - mode$, the electric field and charge disposition can be illustrated as in Figure 2.14. The phase of a, b, and c differs progressively by $\pi/2$. The magnetic fields shown in Figure 2.14.b., are produced by the currents flowing around the inside of the cavities.
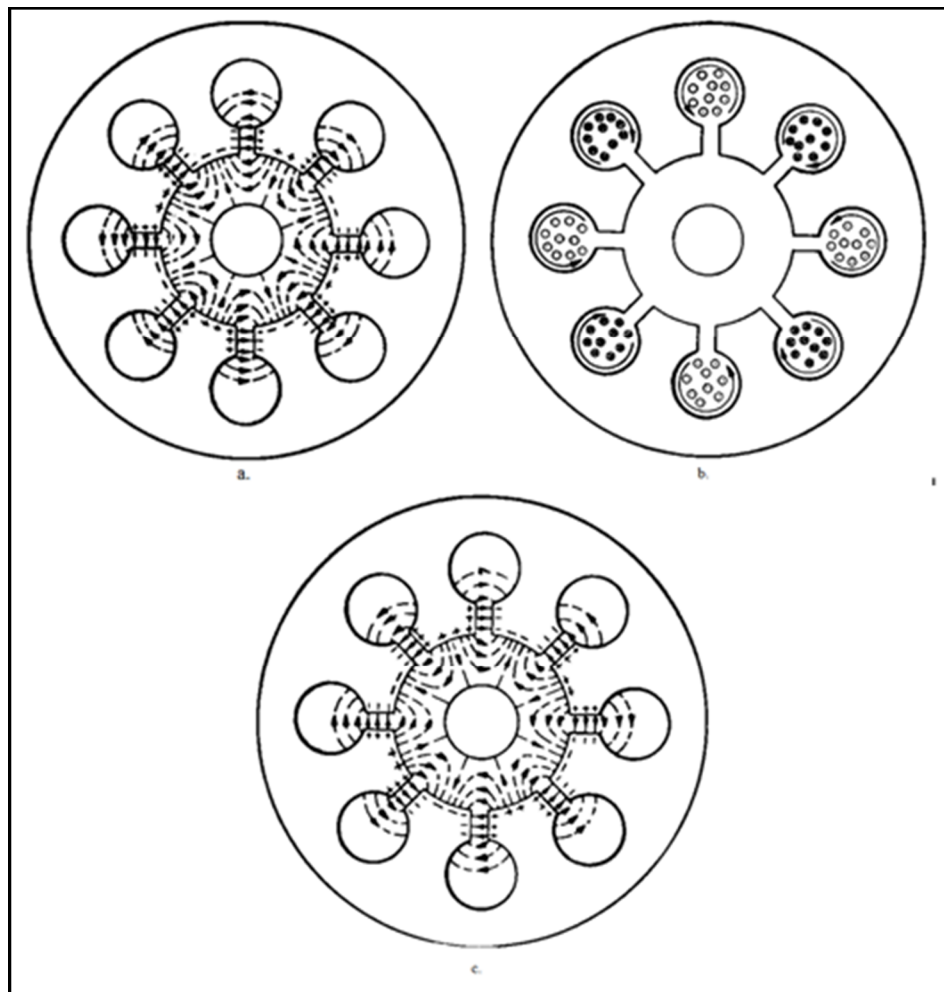
Figure 2.14. a. The electric field and charges in an oscillating eight cavity hole-slot magnetron in $\pi - mode$, b. The currents and magnetic field in mentioned magnetron, c. The formed electric field and charges after a one half period of case a [8]

For an eight cavity magnetron, the possible important modes are n=1, 2, 3, and 4, the phase differences between adjacent resonators corresponding to these modes are $\pi/4$, $\pi/2$, $3\pi/4$, π. Charge and electric field distribution for these four modes are illustrated in Figure 2.15.

The field and charge distribution of various modes are different and thus, the effective capacitance and inductances are different which results the existence of different resonant frequencies for each mode. Unfortunately, the difference in frequencies of each mode which is also called mode separation is not as good as it is desired for many times. The separation should be approximately 5-20 percent between the desired mode and the nearest

frequency to it [8]. On the other hand, for instance, in an eight cavity magnetron, the frequency separation is only 1-2 percent [19]. Also except the $\pi - mode$, each modes have a close doublet which causes a problem that the two components of a doublet have nearly same frequencies. In addition, the magnetron has more stable, higher output power and higher efficiency in a $\pi - mode$ operation. For these reasons, the $\pi - mode$ is usually selected as an operating mode in a magnetron.
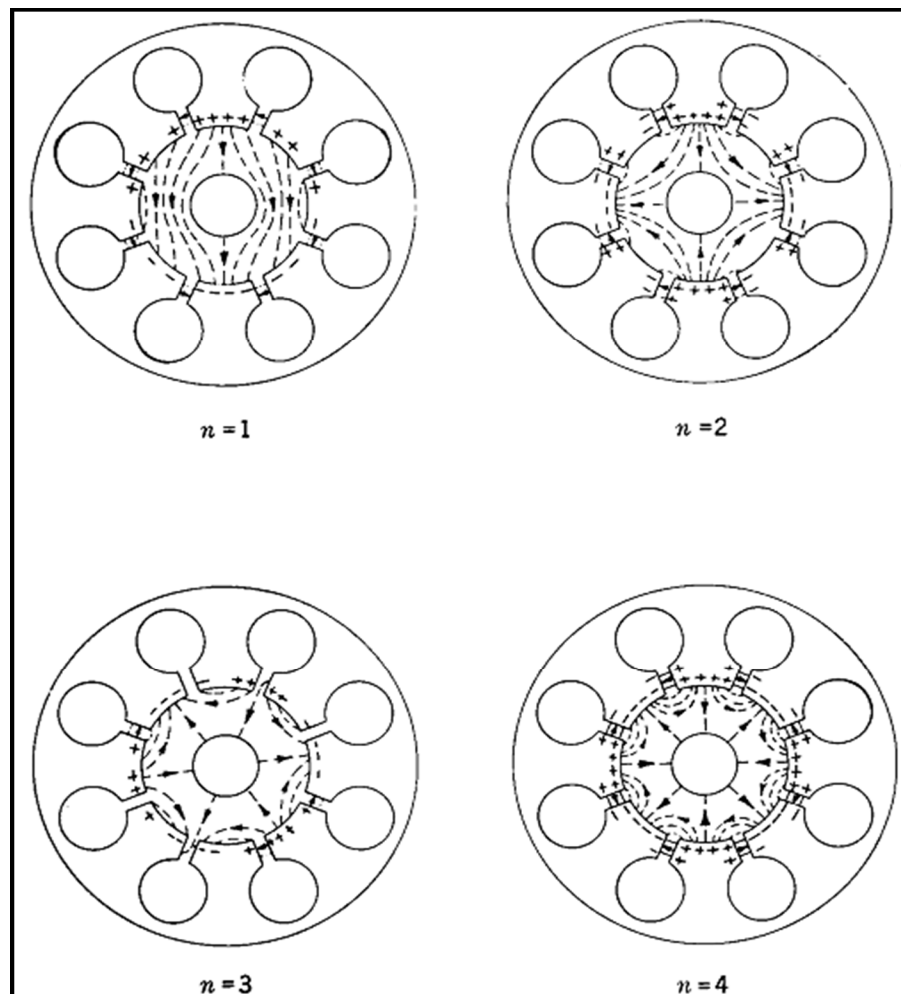
Figure 2.15. The charge and field distribution for an eight cavity magnetron for different four modes [8]

If the frequency difference between the $\pi - mode$ and other modes is not as good as it is desired, the frequency jumping appears which causes the low efficiency and instability. In order to overcome this problem, several methods have been developed; one of them is adding strap.

2.2.2.5. DC Voltage - Magnetic Field Relationship (The Hartree and Hull Conditions)

In a magnetron, the actual source of the RF field is emitted electrons from the cathode. The movement of the electrons in the interaction space determines the output power and efficiency. The path and trajectory of an electron is determined by a constant magnetic and electric fields. The magnetic field is applied parallel to the axis of the cathode, a constant radial electric field results from the applied DC potential difference between the anode and cathode. There exists also a varying electric field extending into the interaction space from charges concentrated near the ends of the anode block segments. The movement of an electron is determined by the Lorentz force as it is explained in section 2.2.2.1 and 2.2.2.2. Figure 2.16 illustrates the path of an electron under the influence of different strength applied magnetic fields.
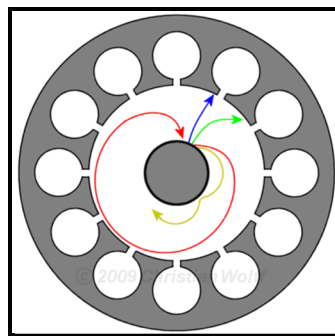
Figure 2.16. The path of an electron under the influence of different magnetic field strengths [20]

The electrons are emitted from the cathode which is a source of them and some emitted electrons are used to transfer energy and amplify the RF field, whereas the residual electrons strike the anode block. In order to maintain a regular electron movement, there should be a potential difference between the anode and cathode blocks. This potential difference is provided by a DC voltage source. The DC voltage causes an electric field between plates and it affects emitted electrons. The required DC voltage which has an extremely important role in a magnetron operation is first obtained by Hull in 1921. In section 2.2.2.2, when an electron motion inside a cylindrical diode is analyzed, for an electron just graze the anode block, the cut off voltage is found

$$V_{oc} = \frac{e}{8m} B^2 b^2 (1 - \frac{a^2}{b^2})^2 \qquad (2.37)$$

where, V_o is the cut off anode voltage, B is a cut off constant magnetic field, a is a cathode radius and b is an anode radius. If an applied anode voltage is smaller than V_{oc}, in the absence of RF field, the electron cannot reach the anode. This voltage, V_{oc}, is called Hull voltage. If the trajectory of electrons are entitled as follows; when an electron just graze the anode ($B = B_c$), it is called "cut off regime", when an electron strike the anode ($B < B_c$), it is called "before cut off regime" and when an electron returns to the cathode instead of reaching the anode ($B > B_c$), it is called "after cut off regime", the Hull parabola can be shown in Figure 2.17.
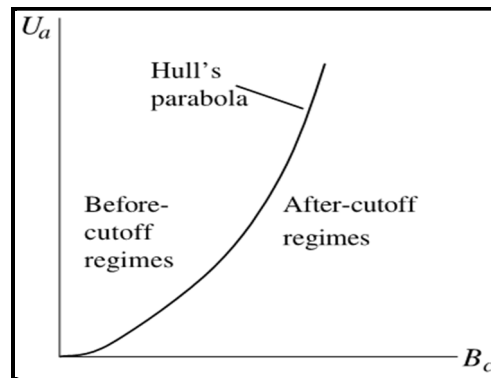
Figure 2.17. The Hull parabola, where U_a is an anode voltage [19]

After the voltages in a region above the Hull parabola, although there exists an emission from the cathode and the electrons reach the anode, unfortunately, the RF field cannot be occurred due to fact that the electrons emitted below the cut off voltage oscillate and the oscillation frequency appears, conversely, at the voltages above the cut off voltage, there does not exist an oscillation. Since, for higher voltages, the electrons already strike the anode plate until they complete their trajectory. Thus, the energy of electrons cannot be coupled to RF field, and all energy is transferred to anode.

If the resonant frequency of mode n is ω, the period of travelling wave which is the time to travel around the anode become

$$\frac{n2\pi}{\omega} \tag{2.38}$$

If it is called $T = 2\pi/\omega$, the rotating frequency is

$$\Omega = \frac{2\pi}{nT} = \frac{\omega}{n} \tag{2.39}$$

In order to be the electron beam in an interaction space between anode and cathode plates, the magnetron should be operated below the cut off or Hull voltage. The condition for starting oscillation is that the electrons should rotate synchronously with the RF field which means the angular frequency of electron should equal to the rotating frequency of the travelling wave. Let the angular frequency of an electron be Ω_e, then,

$$\Omega_e = \Omega = \frac{\omega}{n} \tag{2.40}$$

By considering this condition, the threshold voltage which is also called Buneman-Hartree voltage for RF oscillation to start in a magnetron is found as

$$V_{th} = \frac{B}{2}\Omega_e(b^2 - a^2) - \frac{b^2}{2}\Omega_e{}^2\frac{m}{e} \tag{2.41}$$

For the detailed derivation, the reference [19] can be examined. When the anode voltage is applied above this threshold voltage, oscillations can begin. By considering the conditions and equations 2.29 and 2.33 together, the operation region of a magnetron is determined. It is shown in Figure 2.18.
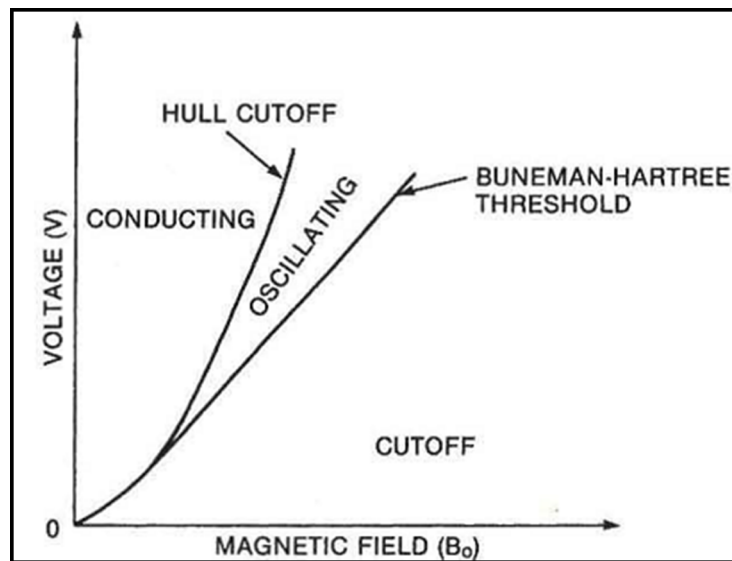
Figure 2.18. The magnetron operating curves and oscillating region [21]

For an eight cavity magnetron, as an example, this region can be seen in Figure 2.19. According to equations 2.37 and 2.41, as it is shown in Figure 2.19, the lines do not intersect; the threshold line is only tangent to the Hull parabola. Below the Hartree voltage line and above the Hull parabola, magnetrons cannot operate. The reason why above voltages cannot operate is explained before. If the anode voltage is smaller than this threshold voltage, the required DC voltage cannot be obtained and the electrons cannot move in synchronism with rotating RF field. As it is seen from the figure, $\pi - mode$ has the lowest Hartree voltage. In practice, the anode voltage is set below the$\pi - 1$ mode line which corresponds to n=3 in Figure 2.19.
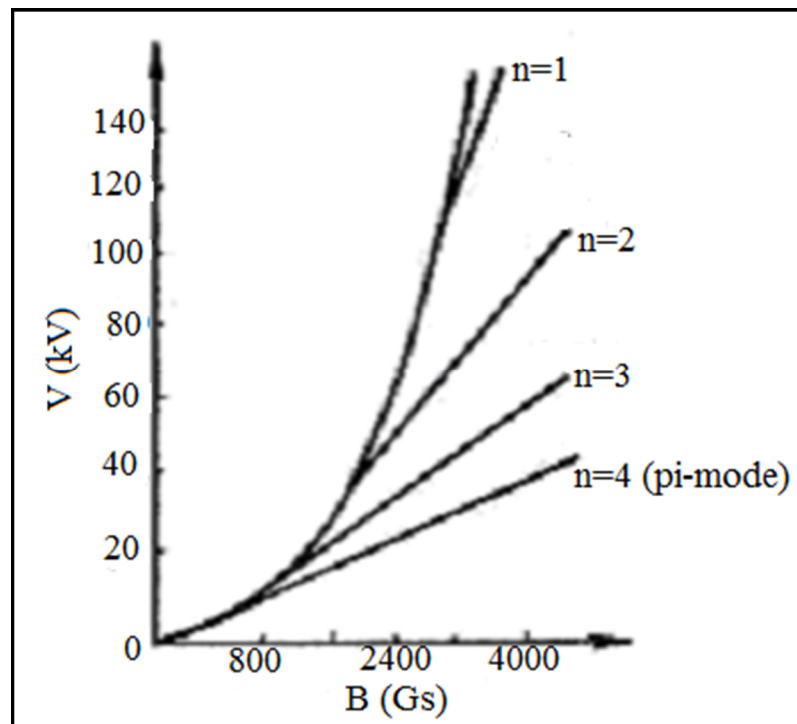
Figure 2.19. The Hartree-Hull diagram of an eight cavity magnetron [8]

In magnetrons, the transfer of electron energy to RF field with zero anode current is not possible. This situation can be illustrated in Figure 2.20. The dashed line is an ideal case; however, the real characteristic is shown by solid curve in Figure 2.20.a.
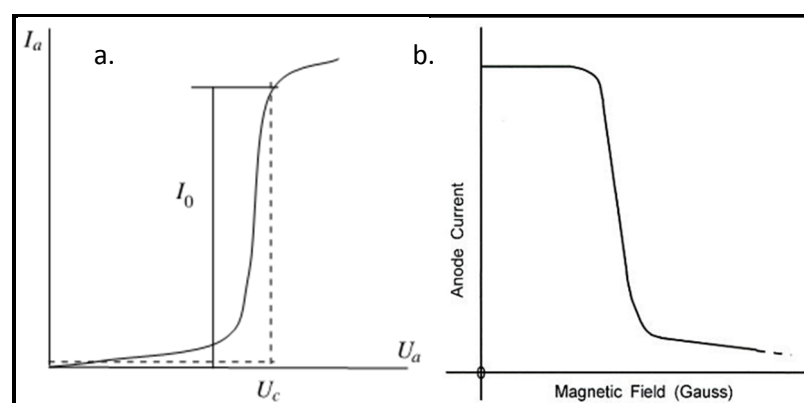
Figure 2.20. a. Voltage-current characteristic of a magnetron, where U_c is cut off Hull voltage, I_a is an anode current; b. Magnetic field-current characteristic of a magnetron [19, 22]

2.2.2.6. RF field and Electron Beam Interaction

The movement of electrons under the influence of electromagnetic fields in a resonant cavity magnetron is similar to that in a cylindrical diode. In order to understand the interaction of the RF field and electron beam clearly, first the velocity modulation can be explained. An electron can be accelerated or decelerated by an applied field. There are two cases should be considered. First, when an electron travels in an opposite direction with an electric field as shown in Figure 2.21.a, the velocity of an electron increases due to fact that the negatively charged electron are attracted to the positively charged plate.
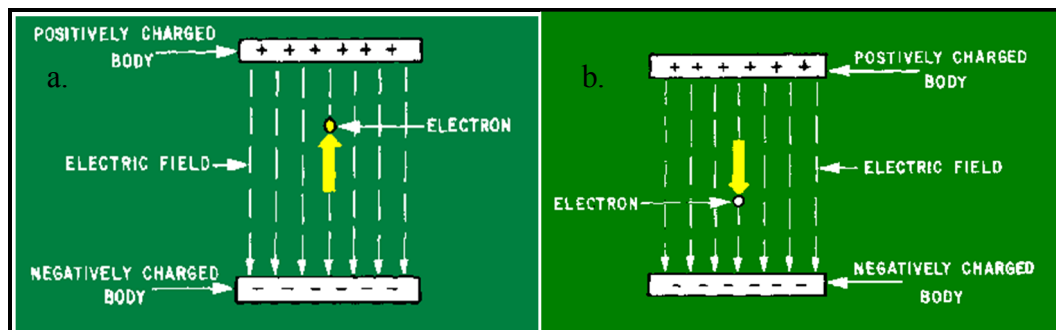
Figure 2.21. a. The direction of an electron is against the lines of electrostatic force, b. An electron travels in the same direction with the electrostatic lines of force [23]

As the velocity of an electron increases, the energy of an electron also increases. The important point is that this additional energy acquired from the electrostatic field. Thus, it is clear that, if an electron travels in an opposite direction to electric field lines, there is an energy transfer from the field to an electron and velocity of an electron increases.

On the contrary, if an electron travels in the same direction with the electric field lines as shown in Figure 2.21.b, the velocity of an electron decreases, thus, the energy is also reduced, and this lost energy is gained by the field. These changes in electron velocity cause to produce electron bunch. Eventually, the variation in the electron beam velocity is defined as velocity modulation.

Now, the interaction mechanism between the RF field and electron beam can be discussed. As it is mentioned before, the emitted electrons from the cathode travel towards the anode in an interaction space under the influence of DC electric field and magnetic field in a

curved trajectory. The RF field distribution of $\pi - mode$ and the possible electron trajectories are shown in Figure 2.22.
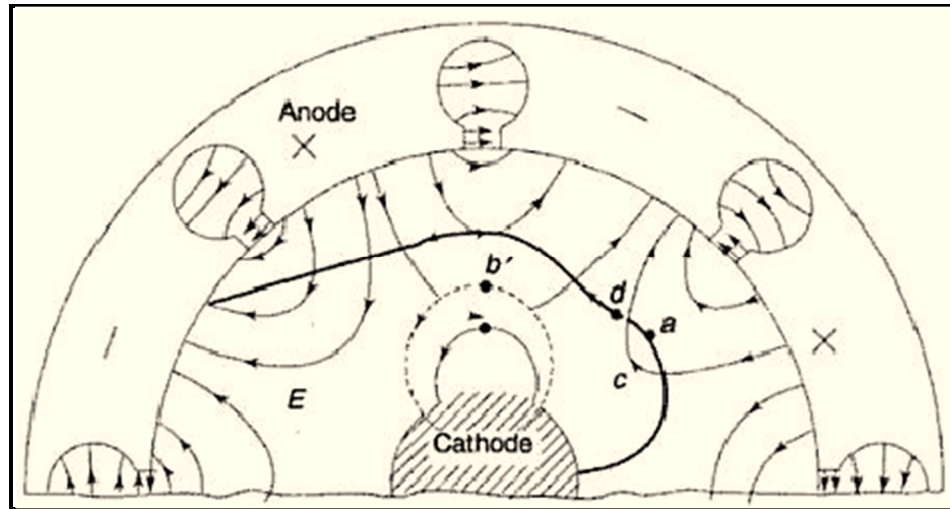
Figure 2.22. The electron trajectories under the influence of fields in $\pi - mode$ oscillating magnetron [24]

When the magnetic field exceeds the cut off value, the electrons try to return the cathode in the absence of the RF field. Because of the effects of electric field shown in Figure 2.22 by relatively thin arrows, electron 'a' is in the decelerating electric field which causes the electron is retarded. An applied magnetic field on the retarded electron 'a' according to Lorentz magnetic force equation $\vec{F} = q(\vec{v} \times \vec{B})$, reduces, since the velocity of an electron is decreased by the field. By adjusting the DC anode voltage and magnetic field, it can be achieved that the electron 'a' takes approximately one half cycle of the RF oscillations of the cavities from one slot position to the adjacent resonator. Thus, an electron 'a' is always in a retarding field and according to velocity modulation, it delivers the energy to the RF field until it finally strikes the anode block. On the other hand, an electron 'b' is an accelerating field and it will turn back to the cathode. Since it strikes the cathode and remains in the interaction space for a much shorter time, it will not contribute energy to the RF field, in fact, according to velocity modulation principle, it will take small energy from the RF field. Furthermore, returned electron 'b' causes heating loss in the cathode plate. The electrons 'c' and 'd' shown in Figure 2.22, are also in decelerating RF field, however, their movement under the influence of fields such that the electron 'c' moves faster than an

electron 'a' and the electron 'd' travels in a velocity slower than an electron 'a' in order to form bunch around an electron 'a'. These electrons from 'c' to 'd' forms an electron cloud which is called spokes. This phenomenon is called phase focusing. Figure 2.23 shows the electron spokes in an eight cavity magnetron.
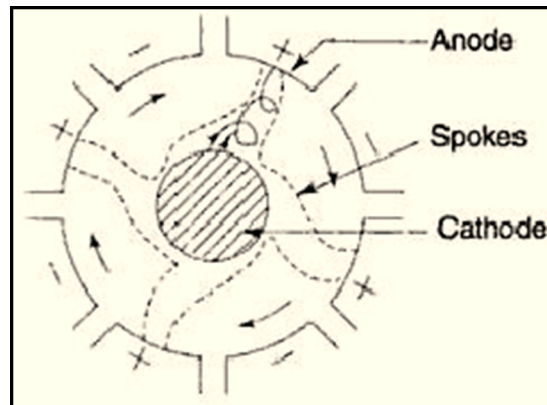
Figure 2.23. The electron spokes of an eight cavity magnetron operating in $\pi - mode$ [24]

The number of spokes is determined by the operating mode. For $\pi - mode$ oscillations, electron spokes have angular velocity equal to two anode poles per cycle. For eight cavity magnetron this number is four as shown in Figure 2.23. The electrons within the spokes continue to give up the energy to the RF field until they strike the anode.

2.2.3. The Type of Anode Blocks in Resonant Cavity Magnetrons

The resonant cavity magnetrons are also classified according to their anode block shapes as shown in Figure 2.24.
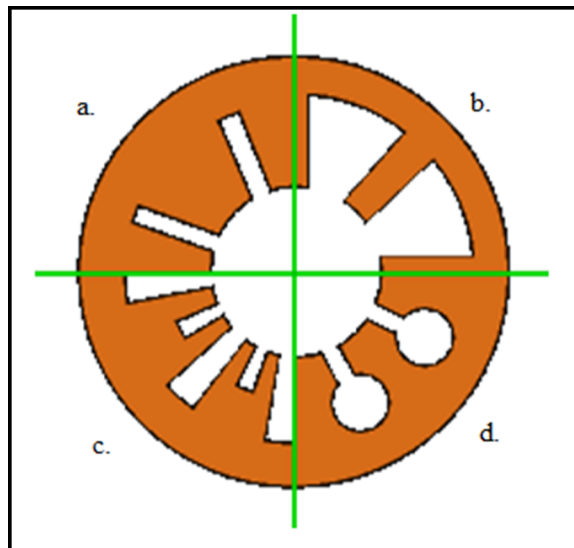
Figure 2.24. The general schematic of four different cavities; a. slot-type, b. vane-type, c. rising-sun type, d. hole and slot type [20]

In four different types, more used cavities are hole-slot, vane, and rising sun magnetrons. These three of them are explained below.

2.2.3.1. Hole-Slot Type Magnetron

Hole and slot type magnetrons are the first cavity magnetrons. The cavities of these type magnetrons consist union of a circle and a rectangle. The cross section of an eight cavity magnetron is shown in Figure 2.25.
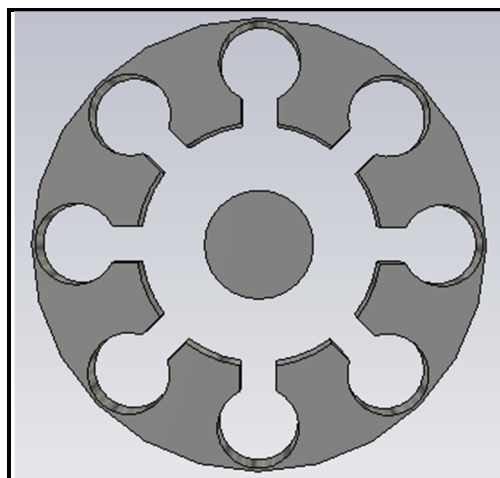
Figure 2.25. The general schematic of an eight cavity hole and slot magnetron

2.2.3.2. *Vane Type Magnetron*

The cavities of these magnetrons consist of one type structures. As being in other cavity types, they are used to adjust the resonant frequency. The general schematic is illustrated in Figure 2.26.
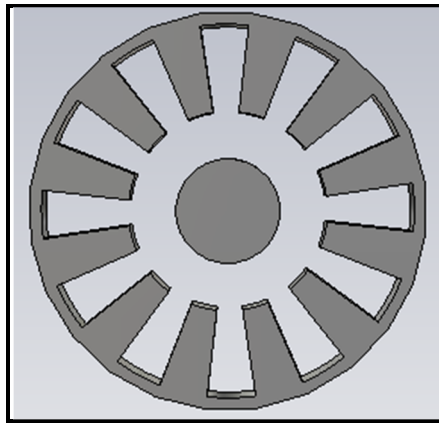
Figure 2.26.The cross section of a twelve cavity vane type magnetron

2.2.3.3. *Rising-Sun Type Magnetron*

The rising sun anode structure consists of two resonating systems, small and large cavities. The cross section view is shown in Figure 2.27. In this figure, the waveguide is also shown which is used as the output structure to transfer the amplified RF field to the out of the magnetron.
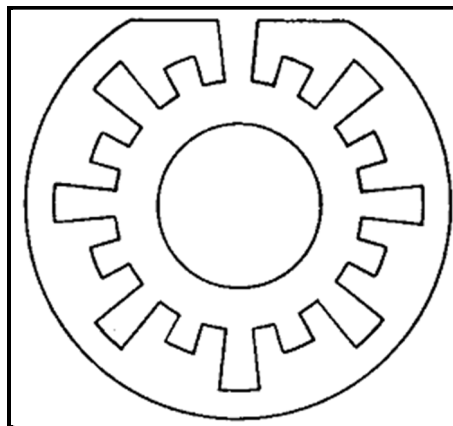
Figure 2.27. The rising sun type magnetron geometry [25]

Rising sun resonators are generally used for relatively high frequencies, above 10 GHz. Because the dimensions of resonators become smaller when the operating frequency increases, and the fabrication of strapped structure become difficult mechanically. In addition, their small spacing results in large copper losses which cause a decrease in magnetron efficiencies. Therefore, like these high frequencies, rising sun type anode structures are used for mode separation instead of strapping. Furthermore, the other advantage of the rising sun design is its effectiveness when a large number of cavities are needed.

The operating principle for mode separation in a rising sun anode structure is based on the influence of different size cavities on the frequencies. The two different size resonators have different resonant frequencies, and the resonant frequency of a magnetron is obtained between those frequencies of small and large cavities. The RF voltage across the large cavities is larger than that across the small cavities, thus, the RF fields extending from the segments into the interaction space are not uniform. However, fortunately, these non-uniform fields are nearly as efficient as uniform fields. Desired mode separation can be achieved by adjusting the ratio of the frequencies of the large and small cavities. There exists a net circulating RF current around the entire anode. The RF currents in the large cavities exceed those in the small cavities and since the large cavity currents are in the same direction, the net circulating current arises. This situation is illustrated in Figure 2.28. The direction of this current is shown by dotted arrow.
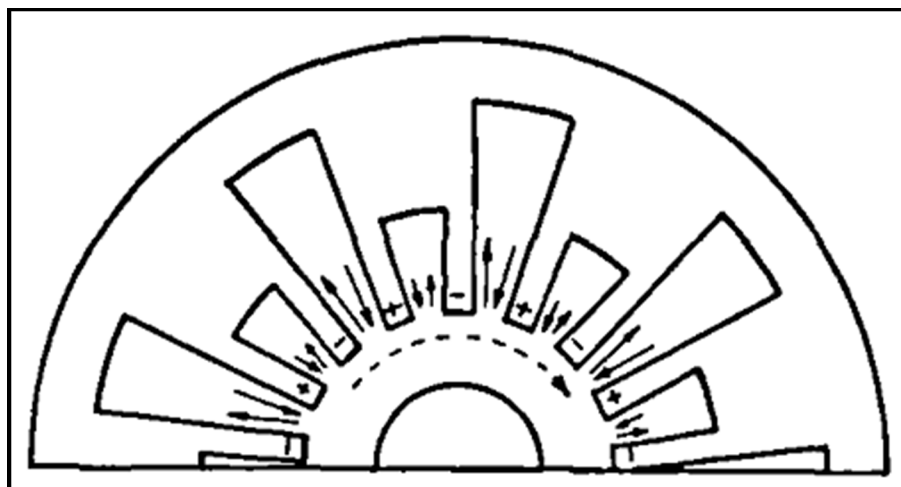
Figure 2.28.The circulating RF current in a rising sun magnetron [8]

2.2.4. The Relativistic Magnetron

Relativistic magnetrons were developed after the invention of cavity magnetrons for the applications of much higher voltages obtained by conventional magnetrons and explosive emission cathodes. The relativistic magnetron is a high current extension of the conventional magnetrons due to fact that using the explosive emission cathodes overcomes the current limitations related to cathode emission and space charge. Thus, the current and output power increases.

The first relativistic magnetron was developed by Orzechowski and Bekefi in 1976 [10] and the six vane A6 relativistic magnetron explored by Palevsky and Bekefi [26]. This first relativistic magnetron is operated at a frequency three GHz with a potential 360 kV, a magnetic field eight kG and a field emission current of 35 kA, which gave a 1.7 GW output power with a 35 percent efficiency and 30 ns pulse duration [19]. In order to increase the pulse duration of a relativistic magnetron is increasing the volume of the device by increasing the number of resonators which also optimize the output power [25]. There is one more advantage of the relativistic magnetron compared to conventional ones; large number of resonators can be used. Since in conventional magnetrons, increasing the number of resonators decreases the mode separation. Furthermore, the magnetron with the pin cathode was able to exhibit better mode stability than the cylindrical velvet cathodes at lower peak microwave power [27]. The operating frequencies of relativistic magnetrons extended from the S-band to the X-band in 1980 and to the L-band in 1991 [6]. Figure 2.29 illustrates the Bekefi relativistic magnetron.
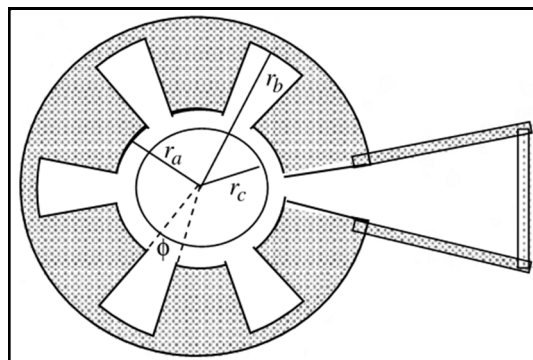
Figure 2.29. The geometry of Bekefi relativistic magnetron [19]

Table 2.1. The characteristic dimensions of several relativistic magnetrons [27]

Magnetron	r_c	r_a	r_b	L	φ	frequency	N
A6	1.58	2.11	4.11	7.2	20	2.34	6
B6	1.58	2.11	4.11	3.81	20	2.34	6
D6	1.83	2.46	4.83	8.42	20	1.98	6
J6	1.69	2.22	3.82	7.2	18	2.81	6

In Table 2.1, dimensions of some relativistic magnetrons are given, where, the lengths are in cm, angle is in degree and frequency is in GHz. Hull and Hartree conditions for relativistic magnetrons is given as [19]

$$B_c = \frac{2}{\sqrt{(e/m)}(1 - {r_c}^2/{r_a^2})r_a}\sqrt{2V_a + \frac{(e/m)V_a^2}{c^2}} \qquad (2.42)$$

It is the cut off magnetic field value. The non-relativistic approximation of the Hull parabola given in equation 2.37 can be used for $V_a < 300$ kV, whereas the equation is valid for $V_a > 5$MV [19]. Hartree voltage equation for the relativistic magnetron is given as

$$V_{th} = \frac{B}{2}\Omega_e(b^2 - a^2) - c^2(1 - \sqrt{1 - \left(\frac{r_a\Omega_e}{c}\right)^2 \frac{m}{e}}) \qquad (2.43)$$

The maximum efficiency is taken near the Hartree straight line as being in conventional magnetrons. The relativistic magnetrons efficiency (10-40 percent) is lower than that of the conventional magnetrons (80-90 percent). The efficiency can be increased by an axial diffraction output and transparent cathode [28].

3. THE DESIGN AND ANALYSIS OF AN X BAND MAGNETRON: HOLE-SLOT TYPE

The operating principle of magnetron was mentioned in chapter two. In this chapter, further information is given about magnetron design. Primary design parameters, the method of magnetron design, the requirements for design and simulation are all explained in detail. According to these instructions, X band hole-slot type resonant cavity magnetron is designed. 3D modeling of a designed magnetron is performed. The effects of design parameters and computer model parameters are investigated. The steps of modeling and simulation results are presented.

3.1. THE DESIGN OF MAGNETRON

Although it is widespread use in industry since World War II, its physical and electrical characteristics are very complicated to fit an algebraic model. There are various parameters that affect the performance directly. In the first part, these parameters are described to develop procedures of magnetron design.

3.1.1. The Principles of Design

The cathode, the resonant system, the interaction space and the magnetic circuit are four principal parts of magnetron and the design of magnetron is formed by considering the design of these components. On the other hand, these four parts are not independent from each other that the design of one part cannot be realized independently. The design procedure and design parameters are described clearly in [8]. The parameters that indicate the requirements for the magnetron design are called primary design parameters; frequency, pulse-power output, voltage, efficiency, pulse duration and average power input, heater power, tuning requirements, frequency stability and weight [8]. These express the relationship between the magnetron components. In general, to achieve the design over-all magnetron, the requirements to consider are these primary design parameters and the consistency between the designs of four parts of the structure.

The first step of magnetron design might be a design of the interaction space. If the primary design parameters are known and the interaction space is designed, then the rest of the components will be determined. The requirements for the interaction space design are voltage, current, wavelength, shape factors and relative operating point. The shape factors N, σ, μ are the parameters that determine the structure of the interaction space. Here,

- N: The number of resonators (oscillators).
- σ: The ratio of cathode radius to anode radius (r_c / r_a).
- μ: The ratio of the space thickness between vanes to total length of vane thickness and space thickness (w / d) that can be seen from the Figure 3.1.
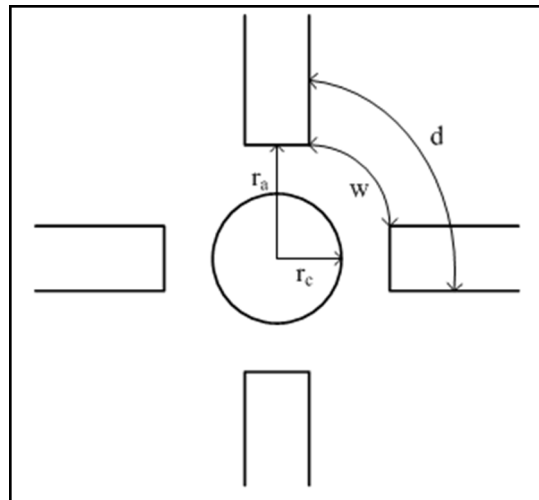
Figure 3.1. The cross section of interaction space of a magnetron

The parameters to determine the nature of electronic orbits are called relative operating point: b, i, g. These are the dimensionless variables that will be found by the following expressions [8];

$$b = \frac{B}{B_1} \tag{3.1}$$

$$i = \frac{I}{i_1} \tag{3.2}$$

$$g = \frac{G_L}{G_1} \tag{3.3}$$

where, B is a magnetic field, I is a current, G_L is a slot conductance and the scale factors, B_1, i_1, G_1 are defined as;

$$B_1 = 2\left(\frac{m}{e}\right)\left(\frac{2\pi c}{n\lambda}\right)\frac{1}{\left[1 - \left(\frac{r_c}{r_a}\right)^2\right]} = \frac{2.12}{(n\lambda)\left[1 - \left(\frac{r_c}{r_a}\right)^2\right]}Tesla \tag{3.4}$$

$$i_1 = \frac{2\pi a_1}{\left[1 - \left(\frac{r_c}{r_a}\right)^2\right]\left(\frac{r_c}{r_a} + 1\right)}\left(\frac{m}{e}\right)\left(\frac{2\pi c}{n\lambda}\right)^3 r_a^2 \varepsilon_0 h = \frac{8440 a_1}{\left[1 - \left(\frac{r_c}{r_a}\right)^2\right]\left(\frac{r_c}{r_a} + 1\right)}\left(\frac{2\pi r_a}{n\lambda}\right)^3 \frac{h}{r_a} A \tag{3.5}$$

$$G_1 = \frac{i_1}{V_1} \quad 1/\Omega \tag{3.6}$$

and

$$V_1 = \frac{1}{2}\left(\frac{m}{e}\right)(\frac{2\pi c}{n\lambda})^2 r_a^2 = 253000(\frac{2\pi r_a}{n\lambda})^2 \quad V \tag{3.7}$$

a_1 is a function of r_a/r_c and is shown in Figure 3.2 [8]. n is chosen as N/2 that corresponds to $\pi - mode$.
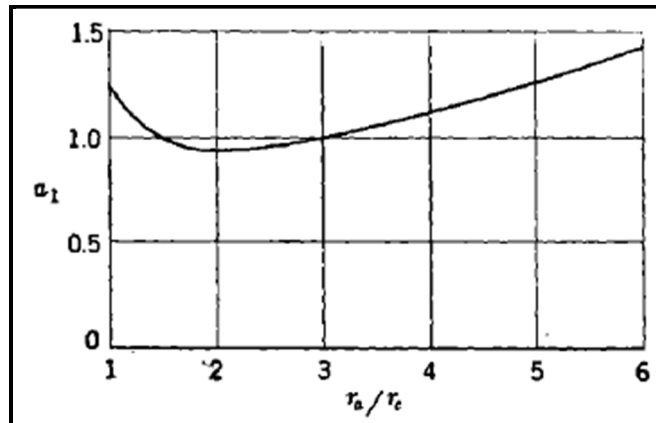
Figure 3.2.The variation of a_1 as a function of r_a/r_c [8]

If the primary design parameters, shape factors and relative operating point are known, then it is possible to design interaction space of the magnetron. For the interpretation of the performance of "family of magnetron", the helpful charts are used. The magnetrons which have geometrically similar interaction space cross sections and resonant systems made up of equivalent resonators are called family of magnetrons [8]. There are two diagrams that are used to interpret the performance and behavior of a magnetron. The "performance charts" show the relationship between susceptance H, current I, voltage V, power P, and wavelength λ for constant load. On the other hand, the "Rieke diagram" shows the relationship among conductance G, magnetic field B, power P, voltage V and wavelength λ for constant current I. Here, H and I are related with the input section, G and B with the output section and P, V and λ are the observed quantities [29]. By choosing the shape factors N, σ, μ and the parameters related to the relative operating points b, i, the other required design parameters g, v, p are determined from one of the performance charts. "v" and "p" are dimensionless parameters defined as

$$v = \frac{V}{V_1} \tag{3.8}$$

$$p = \frac{P}{P_1} \tag{3.9}$$

$$P_1 = i_1 v_1 \tag{3.10}$$

V and P are voltage and power respectively, V_1 and P_1 are characteristic scale factors. The design of interaction space permits determination of the parameters electronic efficiency η_e, slot conductance G_L, slot width w, anode height h, anode radius r_a, cathode radius r_c, cathode current density J, magnetic field B, which are called secondary design parameters. Consequently, using the following equations [8], the secondary design parameters are found in terms of V, I, λ, the shape factors N, σ, μ, the relative operating points b, i, g. These equations are obtained using the equations 1 to 9;

$$B = b \frac{42400}{\lambda N (1 - \sigma^2)} \tag{3.11}$$

$$h = 2.39\lambda \left(\frac{v}{V}\right) \left(\frac{I}{i}\right) N \frac{(1-\sigma^2)^2(1+\frac{1}{\sigma})}{a_1} \tag{3.12}$$

$$r_a = \lambda \frac{N}{6320} \sqrt{\frac{V}{v}} \tag{3.13}$$

$$G_L = g \left(\frac{v}{V}\right) \left(\frac{I}{i}\right) \tag{3.14}$$

$$r_c = \lambda \frac{N}{6320} \sqrt{\frac{V}{v}} \sigma \tag{3.15}$$

$$w = \frac{\mu\lambda}{1010} \sqrt{\frac{V}{v}} \tag{3.16}$$

$$J = 420 \frac{i}{\lambda^2} \sqrt{\frac{V}{v}} \frac{1}{N^2\lambda} \frac{a_1}{(1-\sigma^2)^2(1+\frac{1}{\sigma})} \tag{3.17}$$

$$\eta_e = \frac{p_1}{i_1 v_1} \tag{3.18}$$

Further information and some useful graphics are given about the parameters that can help the design of a magnetron in reference [8]. They are obtained from the experiments and are used to choose the initial parameters for the first assumptions. The determination of secondary design parameters provides the design of the remaining parts of the magnetron which are resonant system, cathode and magnetic circuit. Hence, the overall magnetron design is completed. The general design procedure of magnetron is presented in Figure 3.3 [8].
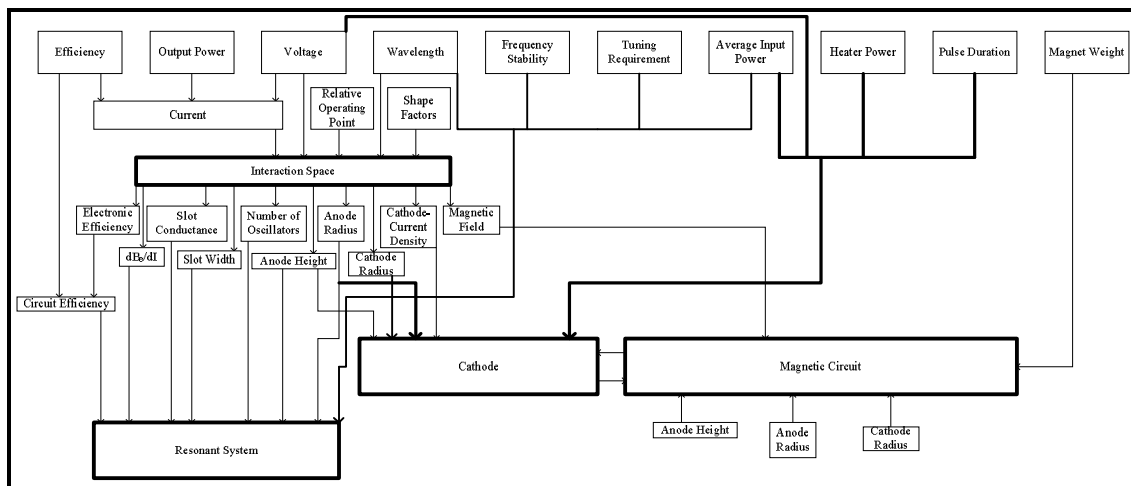
Figure 3.3. The analysis of general design procedure of magnetron

Since the number of equations do not equal to the number of unknown parameters, some of the variables must be chosen and fixed with initial values, and then the other parameters should be found by the design equations. Here, one way of design procedures is expressed, in this explained way, the primary design parameters are fixed, shape factors and the relative operating point are assumed and the other parameters are determined according to design equations. The other methods are mentioned in [8]. The assumptions are mostly based on the previous experience. If computed parameters are not consistent the other aspects of the design and if one is not acquired desired solution, then the initial assumptions are changed instead of the new values. Since developed equations depend on assumptions and theoretical ideal cases like infinitely long resonators, it can be made some minor corrections after the design and simulations to improve the results.

There are some limitations on the size about the main parts of structure such as anode height, number of resonators, anode diameter, and the ratio w/d, etc. There are suggested values that can keep the operation of a magnetron more stable. For instance, if the number of resonators increases, the range of other parameters that can be used decreases or the structure height is usually kept less than 0.8λ. The important points about both design and development of a magnetron are given in [29 - 32].

The dimensions of the magnetron structure and all design parameters is given about the typical X band magnetrons, such as BM50, 2J41, 2J42, 725A, 4J50, 4J52 can be examined in [8].

3.1.2. The Design of an X Band Magnetron

In this part, according to design rules and taking into consideration all desired specifications, X band hole slot type resonant cavity magnetron is designed. The design and dimension parameters about cathode, interaction space, anode and magnets are determined. Meanwhile the structure material of cathode is very important in terms of design and realization. It should be designed to have satisfactory long life and have high durability against very high temperatures, back bombardments. There are various types of cathodes in terms of used materials in composites. Since the experimental validation is not performed, the cathode block structure is assumed to have sufficient strength and the design of material structure is neglected. On the other hand, this subject was examined in literature and different types of cathodes are used to improve the magnetron performance [6, 8, 31, 33 - 37].

The design parameters can be specified according to their related parts of magnetron as follows:

The cathode part;

- The length (h) and radius (r_c) of the cathode block.
- Cathode voltage (V_c).

Interaction space;

- Voltage (V_{app}) between anode and cathode blocks.
- The distance between cathode and anode blocks (r_{an_ir}-r_c).
- Applied magnetic field (B_{app}) orthogonal to electric field.

The anode part;

- The length (h) and the inner (r_{an_ir}) and outer (r_{an_or}) radiuses of anode block.
- The length ($slot_l$) and width ($slot_w$) of the slot.
- The number of resonators (N).
- Hole radius (r_{hole}).
- Anode voltage (V_a).

Magnetic circuit;

- Applied magnetic field (B_{app}).

Generic design procedure is expressed step by step. Meanwhile, it should not be forgotten that all calculations are approximate; many assumptions are required to use equations and inequalities. These calculations just provide useful insight and help to start by reasonable values in very complicated magnetron design. Appropriate particle simulator programs, computer codes should be used to determine final values of parameters.

Step 1: First, the operating frequency and desired output power should be specified. According to given specifications, required number of resonators can be estimated, hence, n=N/2 is fixed and non-degenerate mode is determined.

Step 2: As a second part, for a given resonant frequency, the shape parameters, cathode radius, inner anode radius, the length of anode (cathode) block, hole radius, slot width and slot length are determined according to inequalities and further information [8].

$$\frac{r_c}{r_{an\_ir}} \le 0.5 \qquad (3.19)$$

and

$$\frac{r_c}{r_{an\_ir}} \approx \frac{N-4}{N+4} \qquad (3.20)$$

and

$$h \leq 0.8\lambda \tag{3.21}$$

First, r_c is chosen and fixed according to previous experiences, then using (3.19), (3.20) and (3.21), the other parameters are obtained.

If desired efficiency is also given in step 1, then the following equations about the anode radius should also be kept in mind. On the other hand, in this case, output voltage is also required to know, the synchronous voltage related to the phase velocity is given as [38]

$$V_{out} = \frac{1}{2\eta} v_p^2 \tag{3.22}$$

where, v_p is the phase velocity and defined as

$$v_p = \frac{\omega}{\beta} \tag{3.23}$$

and,

$$\beta = \frac{\pi}{L} \tag{3.24}$$

where, L is the distance between cavities and it is found as

$$L = \frac{2\pi r_{an\_ir}}{2n} \tag{3.25}$$

Hence, anode inner radius can be found from given parameters; frequency, number of resonators, efficiency and voltage using the following equation

$$r_{an\_ir} = \frac{n}{\omega} \sqrt{2\eta V_{out}} \tag{3.26}$$

Then, using (3.19), (3.20) and (3.21), r_c and h are determined. There are no formulas or equations directly related to the other shape parameters, hole radius, slot width and length.

On the other hand, Figure 3.4 can be taken into consideration, where λ_r^1 indicates that fringing fields have been neglected.
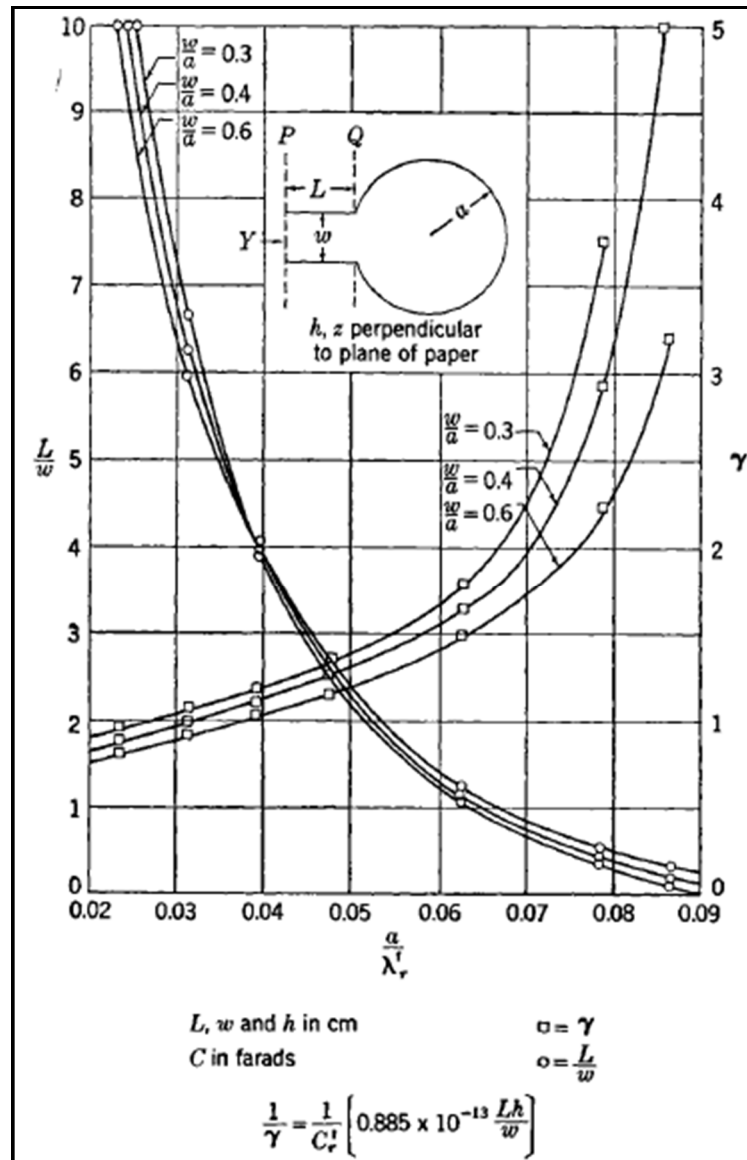
Figure 3.4. Design parameter curves for hole – slot type resonators [8]

Moreover, there are known information about these parameters such that the radius of hole affects the resonant frequency directly, when it is increased, then the operation frequency decreases, slot length is inversely proportional to the resonant frequency. In addition, the ratio $\mu = w/d$ according to Figure 3.1, is approximately chosen 0.25~0.3.

Step 3: The next step is to find required magnetic field and the potential difference between anode and cathode blocks. Using the following equations, the equation related with cut off magnetic field is obtained

$$\Omega = \frac{\omega}{n} = \frac{2\pi f}{n} \tag{3.27}$$

where, Ω is an angular velocity of an electron. It was also found in chapter 2 and it can be written as

$$\Omega = \omega_0 = \frac{\omega_c}{2}\left(1 - \frac{r_c^2}{r_{an\_ir}^2}\right) \tag{3.28}$$

Here, ω_c is a cyclotron angular frequency and it is defined as

$$\omega_c = \frac{e}{m}B_0 \tag{3.29}$$

where, e is an electron charge value equals -1.602177x10^{-19} C, m unit mass value of an electron, 9.10939x10^{-31} kg, and B_0 is cut off static magnetic field in unit Tesla. Combining the equations (3.27), (3.28), (3.29), the following relation is obtained,

$$\frac{\omega}{n} = \frac{2\pi f}{n} = \frac{e}{2m}B_0\left(1 - \frac{r_c^2}{r_{an\_ir}^2}\right) \tag{3.30}$$

The equation (3.30) can be rewritten as

$$B_0 = \frac{4\pi f m}{ne}\frac{1}{\left(1 - \frac{r_c^2}{r_{an\_ir}^2}\right)} \tag{3.31}$$

Hence, unknown variable B_0 is found. As it is explained in chapter 1, required potential difference between the anode and cathode blocks should be in an interval which the boundaries are determined by Hartree voltage and Hull – cut off voltage values. This

interval determines the magnetron operation region. The Hartree and Hull cut off voltage equations are rewritten respectively as below

$$V_t = \frac{r_{an\_ir}^2}{2}\left(1 - \frac{r_c^2}{r_{an\_ir}^2}\right)\frac{\omega}{n}B_{app} - \frac{r_{an_{ir}}^2}{2}\frac{m}{e}\left(\frac{\omega}{n}\right)^2 \tag{3.32}$$

and

$$V_0 = \frac{e}{8m}r_{an_{ir}}^2\left(1 - \frac{r_c^2}{r_{an\_ir}^2}\right)B_0^2 \tag{3.33}$$

Using the equation (3.33), Hull cut off voltage can be determined easily. The equation (3.32) can be rewritten in other form as

$$V_t = \left(2\frac{B_{app}}{B_0} - 1\right)V_0 \tag{3.34}$$

where, B_{app} is an applied magnetic field which is chosen less than cut off static magnetic field, B_0. After determination of Hull cut off and Hartree voltages, required voltage value, V_{app}, must be chosen in an interval,

$$V_t < V_{app} < V_0 \tag{3.35}$$

It should be noted that, the choice of B_{app} changes Hartree voltage value, which also affects operation region.

Step 4: The last step is computer modeling of magnetron. After determination of design parameters, appropriate computer programs should be used to simulate designed magnetron. Since the calculations using the equations are approximate, particle simulators are necessary to find the exact values of parameters and to understand real performance. If required, the parameter values can be changed according to simulation results, hence the desired specifications are obtained.

Now, design procedure explained above is applied in order. The operating frequency of the magnetron, $f = 10$ GHz, is specified which is in X band, $8 - 12$ GHz. It is the only known parameter to start design for the beginning. The number of resonator is chosen N=8, so the non-degenerate mode, $\pi - mode$, becomes n=N/2=4. As it is known, the magnetron operation is based on the cathode emitted electron motion in the interaction space under the influence of orthogonal electric and magnetic fields for a desired specific frequency. Some of the design parameters described above as V_{app}, B_{app}, r_c, r_{an_ir}, n and resonant frequency, f, are all dependent to each other. For this reason, it is required to choose some of these, and then the rest can be found by formulas and inequalities mentioned above.

We start the design by choosing the radius of cathode as $r_c = 0.14\lambda$, where$\lambda = c/f$ is a wavelength. According to inequalities (3.19), (3.20), $r_{an\_ir} = 0.3\lambda$ is found and the length of anode block is chosen as $h = 0.58\lambda$. The next step is to find the magnetic field and the potential difference between anode and cathode blocks. Using related equation (3.31), $B_0 = 0.228325\,T$ is found. The operation region is also determined by obtaining Hartree and Hull cut off voltages. Using an equation (3.33), $V_0 = 56.81$ is found, then if applied magnetic field value, $B_{app} = 0.21$, is taken, using an equation (3.34), Hartree threshold voltage, $V_t = 47.69$ kV is obtained. By considering the inequality (3.35), $V_{app} = 48$kV is determined. In order to get exact values, various simulations are performed. After simulations, the rest of the dimensions of the magnetron structure are obtained as $h = 0.58\lambda$, $r_{hole} = 0.12\lambda$, $slot_l = 0.07\lambda$, and $slot_w = 0.1\lambda$. Hence, an X band resonant cavity magnetron dimensions are determined and the design is achieved.

3.2. 3D MODELING OF X BAND MAGNETRON

Computer modeling of magnetron structure is very important and necessary to design and characterize the behavior of a device. It is required for detailed analysis of principle of operation and to see the performance of designed structure. Using the computer programs, various simulations are performed to study and design the magnetron [38 - 48].

In general, the magnetron is difficult to model relative to o-type devices due to facts that the electromagnetic field and the electron cloud interaction is at least two-dimensional, and

also depending on the interaction process, the geometry and analysis of such devices requires large memory.

In this report, CST Particle Studio is used for all required simulation work. CST Particle Studio is a part of the CST Studio Suite. It is dedicated for the 3D simulation of the electromagnetic fields interacting with charged particles. It is based on the Finite Integration Technique (FIT) and for the simulation of charged particle interaction with electromagnetic fields, PIC codes are used [49].

The interaction between charge particles and electromagnetic fields to obtain behavior of particle trajectories and to provide current and charge densities are determined by the technique called particle in cell (PIC). The algorithm scheme of PIC is illustrated in Figure 3.5 [50, 51].
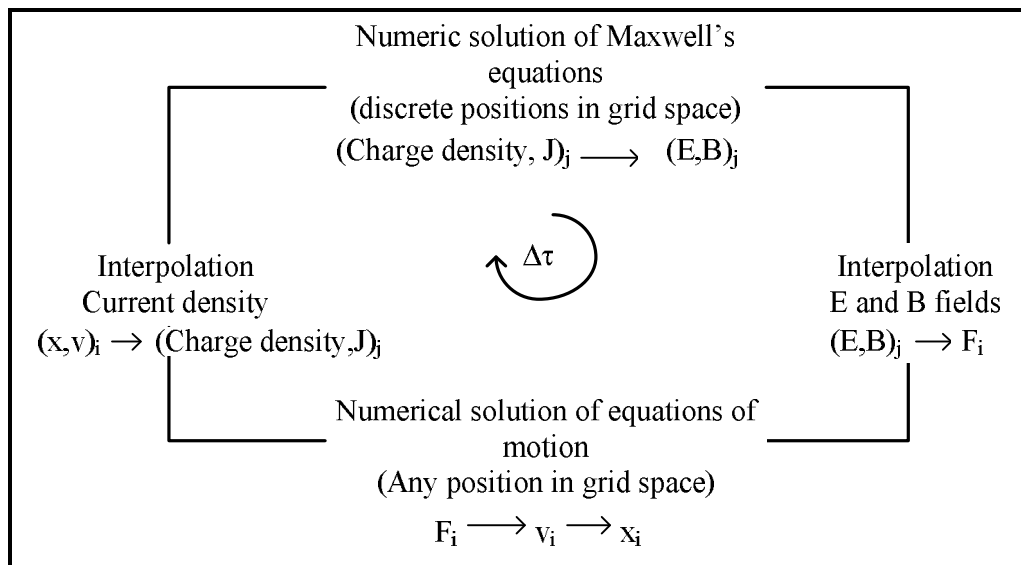

Figure 3.5. The scheme of PIC algorithm

Using relativistic equation of motion, Lorentz force and Maxwell's equations, this cycle is rounded. The electromagnetic fields will only be obtained at discrete positions in grid space, whereas the particle quantities can be determined any position.

In our simulation works, the explosive emission model is used. It depends on the electric field by the way that if the electric field strength near the cathode is greater than a user specified threshold breakdown field, electron emission will start. This process is irreversible that if it is started once, then it could not stop by the threshold again [52].

Simulation of a designed magnetron using CST Particle Studio is achieved in a three steps which are

- Eigenmode solver section,
- Particle Tracking solver section
- PIC solver section

3.2.1. Eigenmode Solver Section

In the first part, using eigenmode solver, the resonant frequencies (modes) and their electromagnetic field patterns are calculated [53]. For this solver, there are two methods called Advanced Krylov Subspace (AKS) and Jacobi-Davidson method (JDM) [54]. AKS solver calculates the resonant modes in a determined frequency interval, whereas for the JDM solver, there is no limit as in AKS solver, which causes the increment in solver time with the number of modes to calculate.

For much more accurate structure models, Perfect Boundary Approximation (PBA) method is utilized for meshing [55]. Using the classical hexahedral staircase mesh, the structure becomes robust and appears as Figure 3.6 and Figure 3.7. On the other hand, mesh types as PBA and FPBA (Fast PBA), the structure is modeled with improved performance and robustness which increase the accuracy. This model is seen in Figure 3.8 and Figure 3.9.
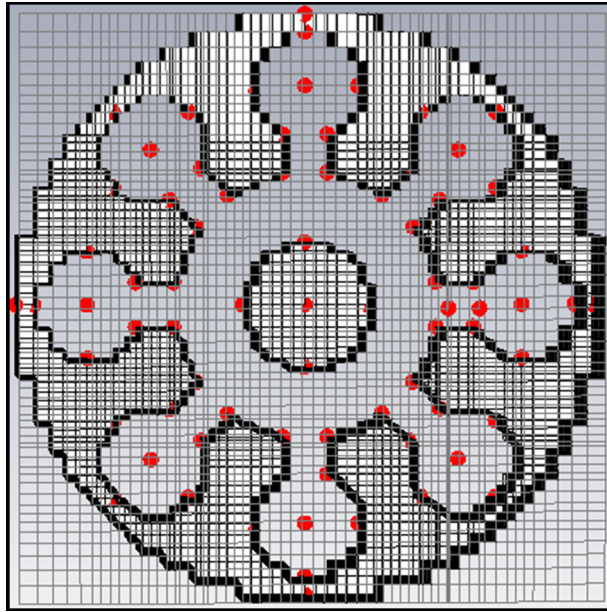
Figure 3.6. The cross section of magnetron in xy plane with staircase mesh
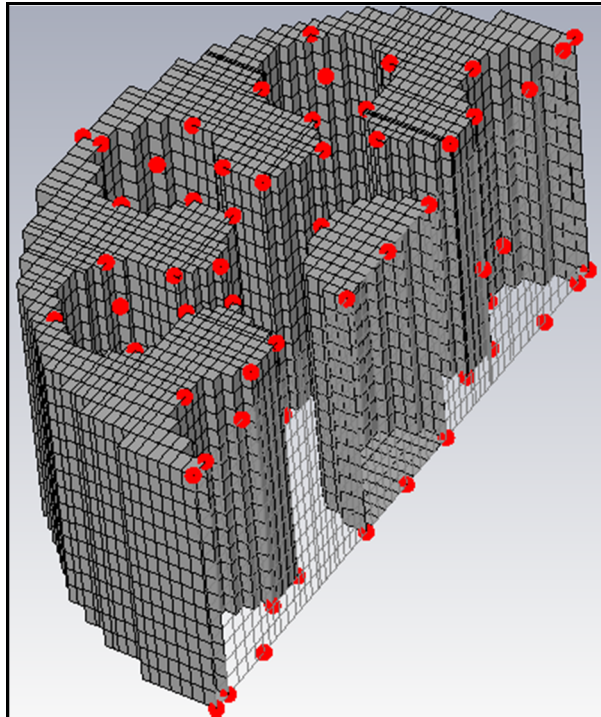
Figure 3.7. The cross section of magnetron in xz plane with staircase mesh
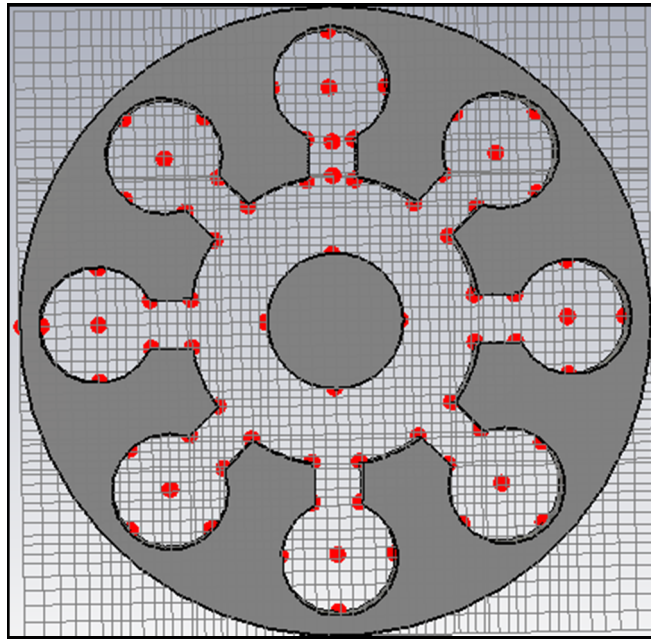
Figure 3.8. The cross section of magnetron in xy plane with FPBA mesh
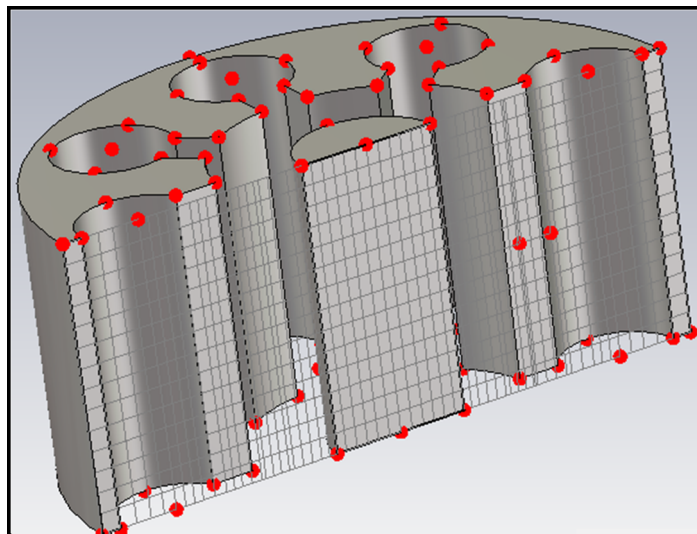
Figure 3.9. The cross section of magnetron in xz plane with FPBA mesh

Since the dimensions of structure was determined in previous part 3.1.2, magnetron construction is easily built to complete the first part of simulation: Eigen mode part. The purpose of this part is to find the exact dimensions of the structure to ensure the magnetron operates at $\pi-mode$. For this, the resonant modes and the electromagnetic field patterns are observed using both AKS and JDM solver methods. The dimensions, $h = 0.58\lambda$,

$r_{hole} = 0.12\lambda$, $slot_l = 0.07\lambda$, and $slot_w = 0.1\lambda$, those cannot be found using formulas or equations directly, are determined by these simulations. To start the eigenmode simulation, PEC surface is removed, remained part is filled by vacuum, and background material is selected as PEC, hence the electromagnetic field patterns can be observed in created vacuum space. The boundaries are chosen as tangential electric field becomes zero, $E_t = 0$. First AKS solver method is used and there exists 6 modes in determined frequency range, 8 – 12 GHz. The electromagnetic field patterns, surface currents and electromagnetic energy densities are observed as

Figure 3.10. 3D E – field pattern of mode 1 for a designed 8 cavity hole slot magnetron.
The resonant frequency is 8.597 GHz

Figure 3.11. 3D H – field pattern of mode 1 for a designed 8 cavity hole slot magnetron. The resonant frequency is 8.597 GHz
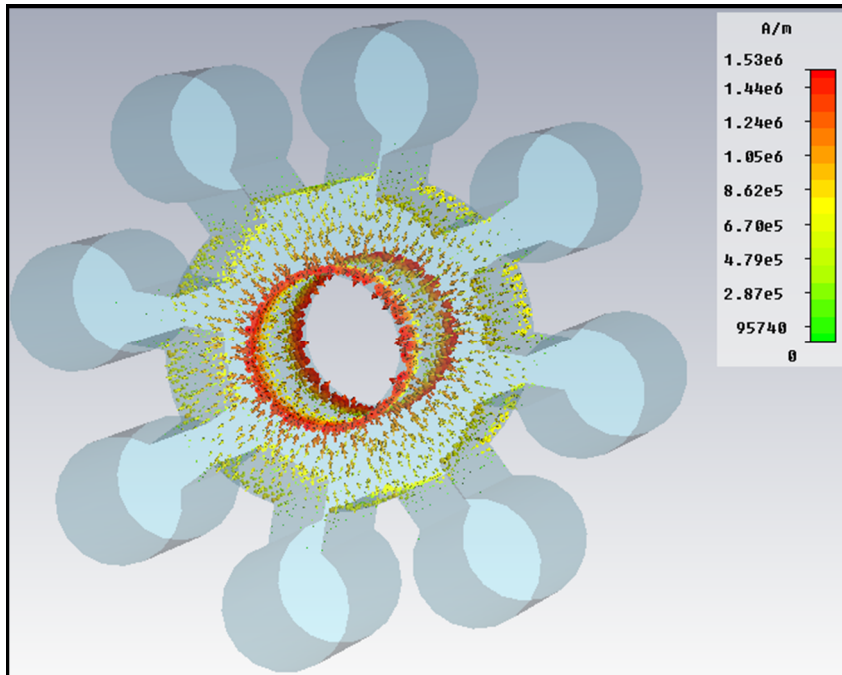
Figure 3.12. 3D surface current pattern of mode 1 for a designed 8 cavity hole slot magnetron. The resonant frequency is 8.597 GHz

Figure 3.13. 3D electric energy density pattern of mode 1 for a designed 8 cavity hole slot magnetron. The resonant frequency is 8.597 GHz

Figure 3.14. 3D magnetic energy density pattern of mode 1 for a designed 8 cavity hole slot magnetron. The resonant frequency is 8.597 GHz

As it is seen from Figure 3.10 – 3.14, electric, magnetic field distributions and current densities do not behave as expected from oscillating magnetron in $\pi - mode$ for a frequency 8.597 GHz. Although desired frequency is an interval 8 – 12 GHz, the calculations for the design equations are done for a specific frequency $f = 10$ GHz. Therefore, we investigate the behavior of magnetron about this frequency $f = 10$GHz. There are found resonant modes apart from this mode, which also contains $\pi - mode$. The electric patterns of these modes except $\pi - mode$ are shown is Figure 3.15 to Figure 3.18.
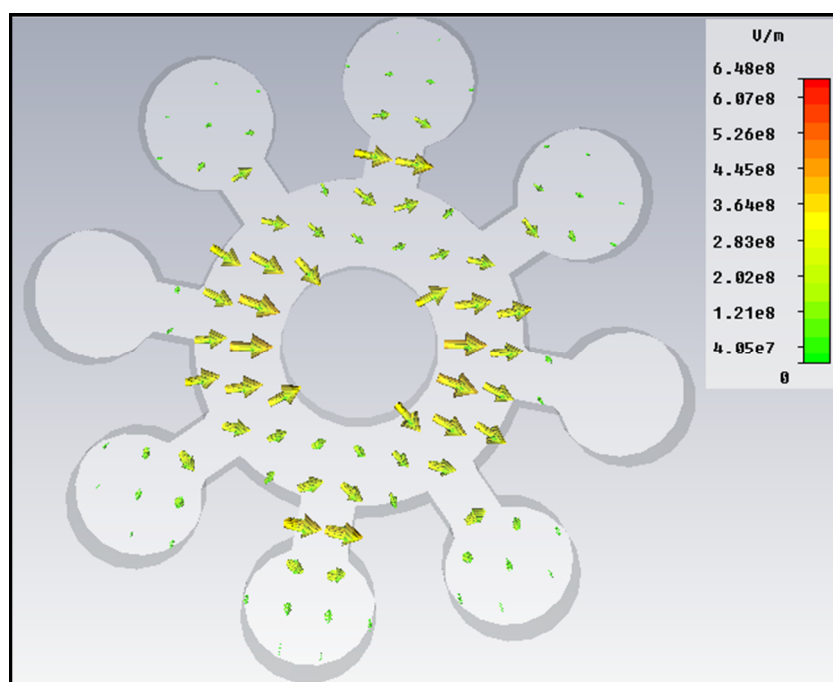
Figure 3.15. 3D E – field pattern of mode 2 for a designed 8 cavity hole slot magnetron. The resonant frequency is 9.329 GHz
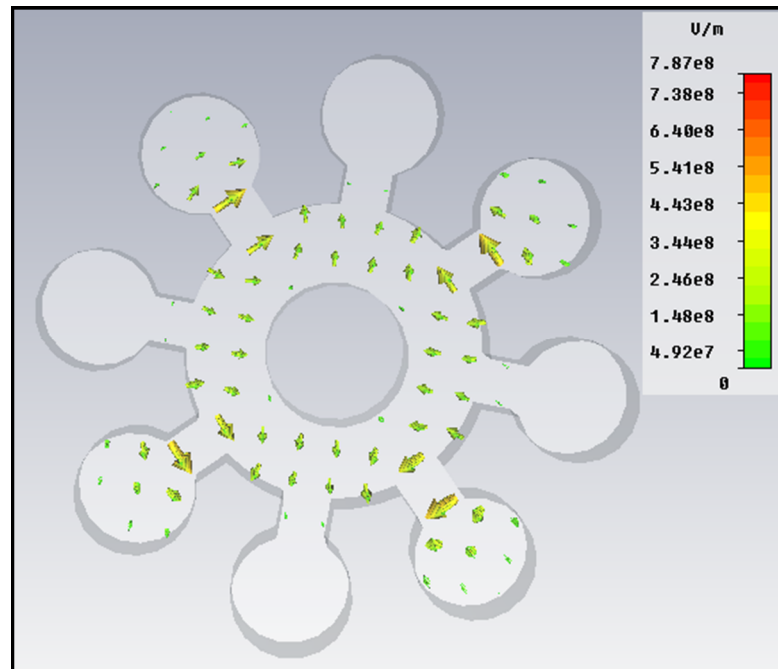
Figure 3.16. 3D E – field pattern of mode 3 for a designed 8 cavity hole slot magnetron.
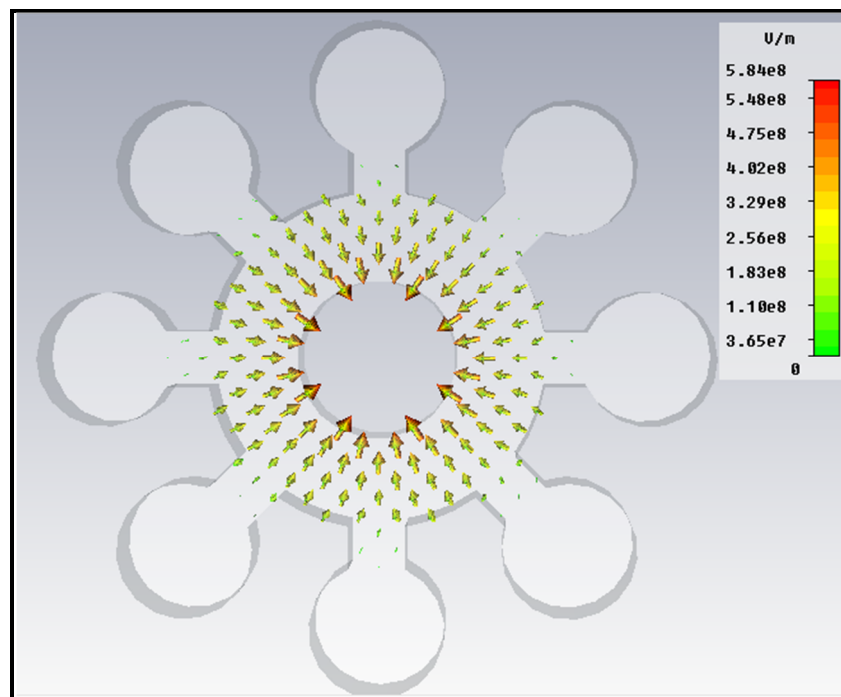The resonant frequency is 9.885 GHz
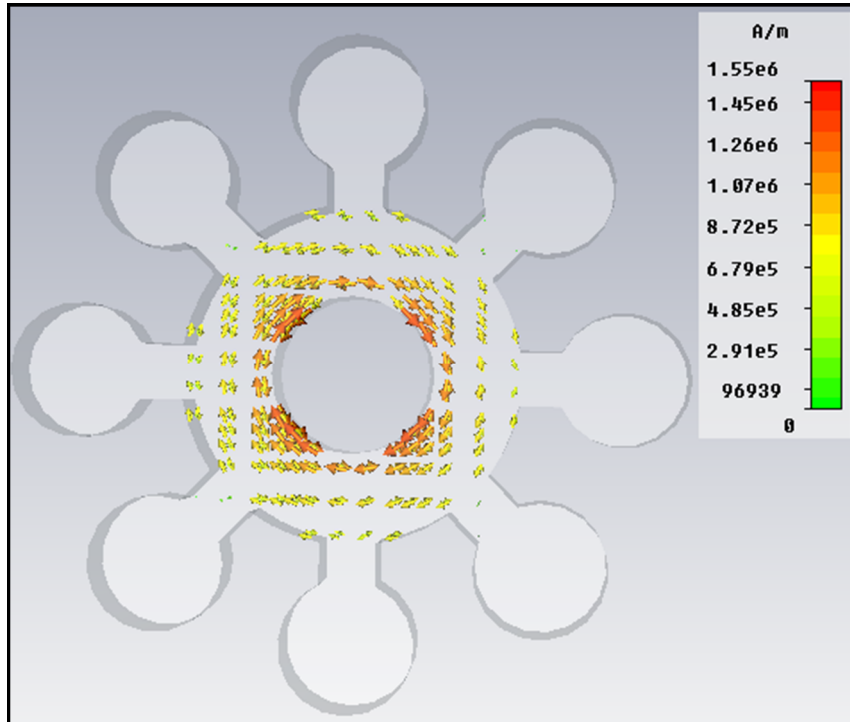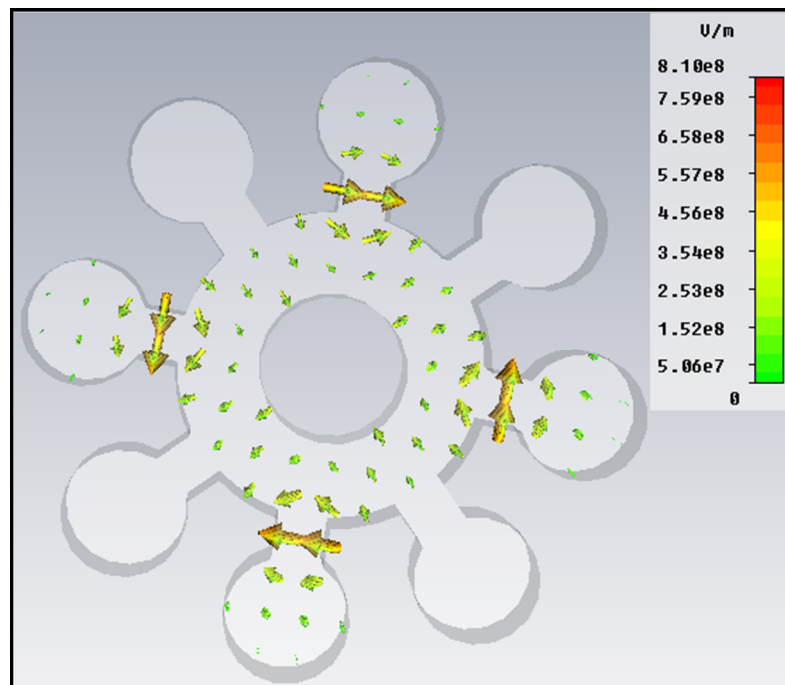

Figure 3.17. 3D E – field pattern of mode 4 for a designed 8 cavity hole slot magnetron.
The resonant frequency is 9.905 GHz
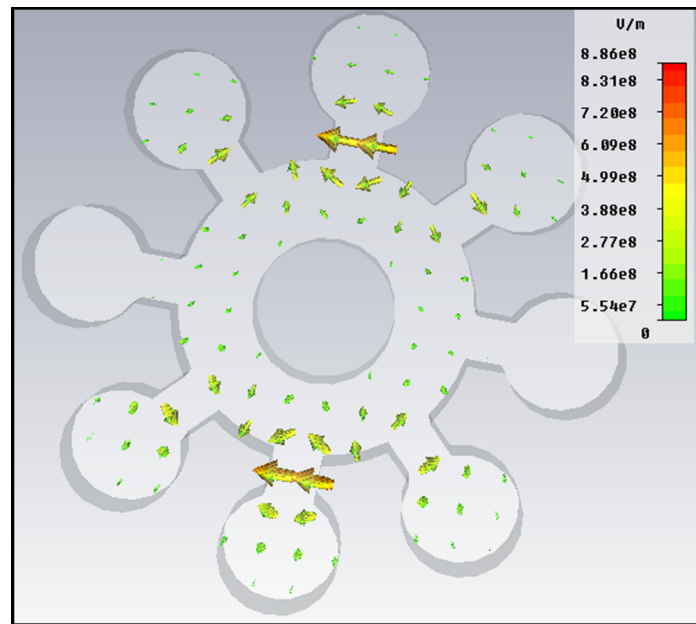
Figure 3.18. 3D E – field pattern of mode 5 for a designed 8 cavity hole slot magnetron. The resonant frequency is 10.074 GHz

This desired mode is appeared at a frequency $f = 10.118$ GHz which appears change in frequency as 0.118 GHz from the calculated one. The electromagnetic field patterns, surface current and energy densities for this frequency are figured as

Figure 3.19. 3D E – field pattern of mode 6 ($\pi - mode$) for a designed 8 cavity hole slot magnetron. The resonant frequency is 10.118 GHz

Figure 3.20. 3D H – field pattern of mode 6 ($\pi - mode$) for a designed 8 cavity hole slot
magnetron. The resonant frequency is 10.188 GHz
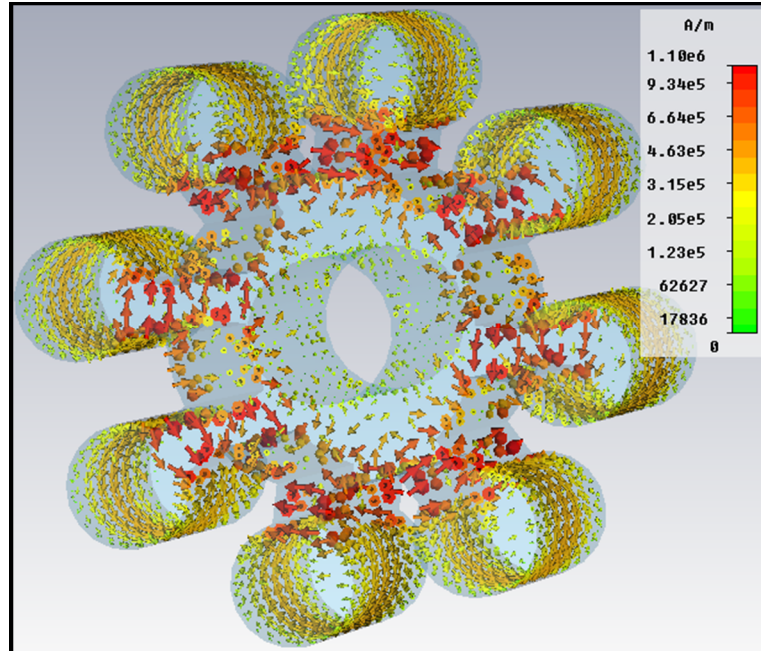
Figure 3.21. 3D surface current pattern of mode 6 ($\pi - mode$) for a designed 8 cavity hole
slot magnetron. The resonant frequency is 10.188 GHz
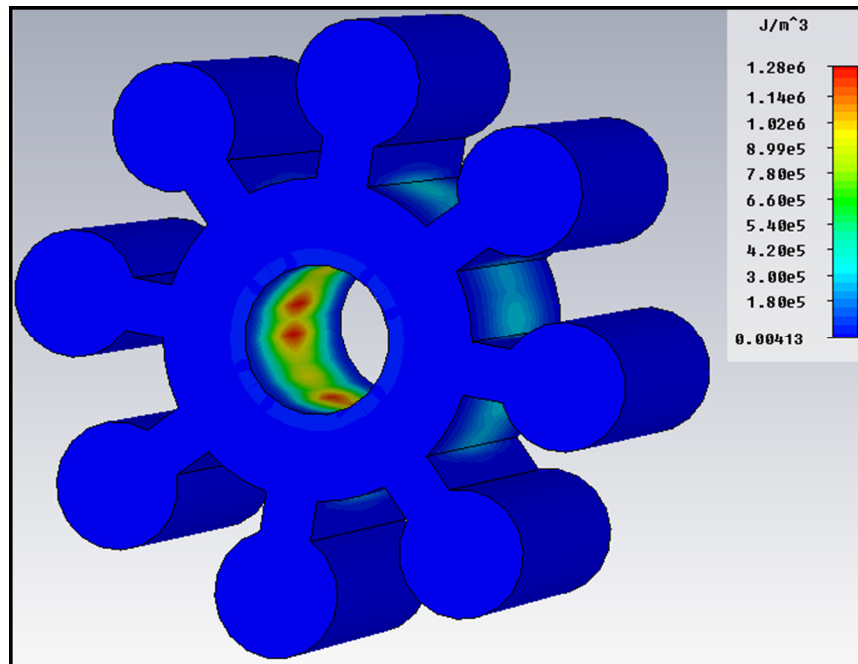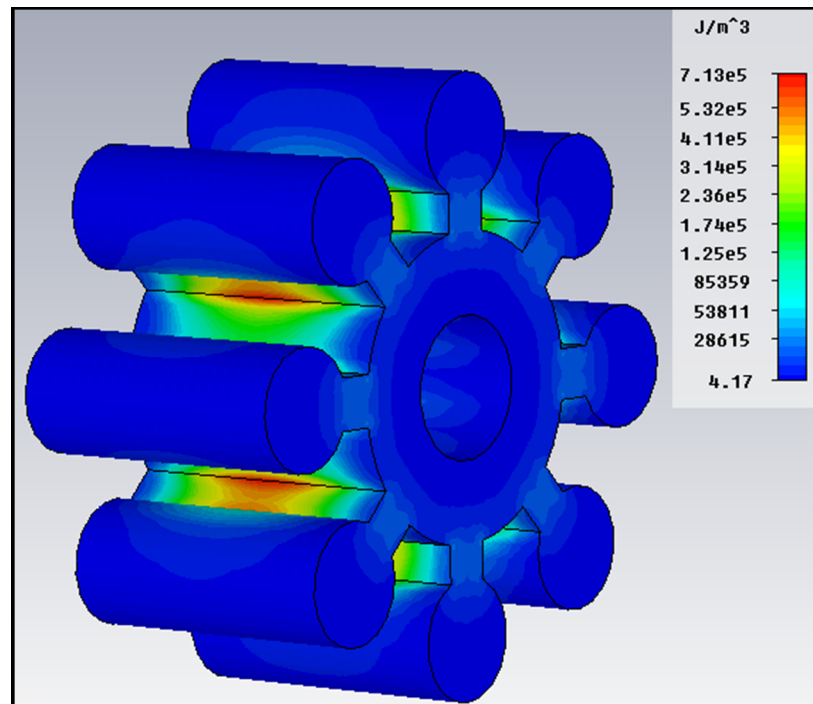
Figure 3.22. 3D electric energy density pattern of mode 6 ($\pi - mode$) for a designed 8 cavity hole slot magnetron. The resonant frequency is 10.188 GHz
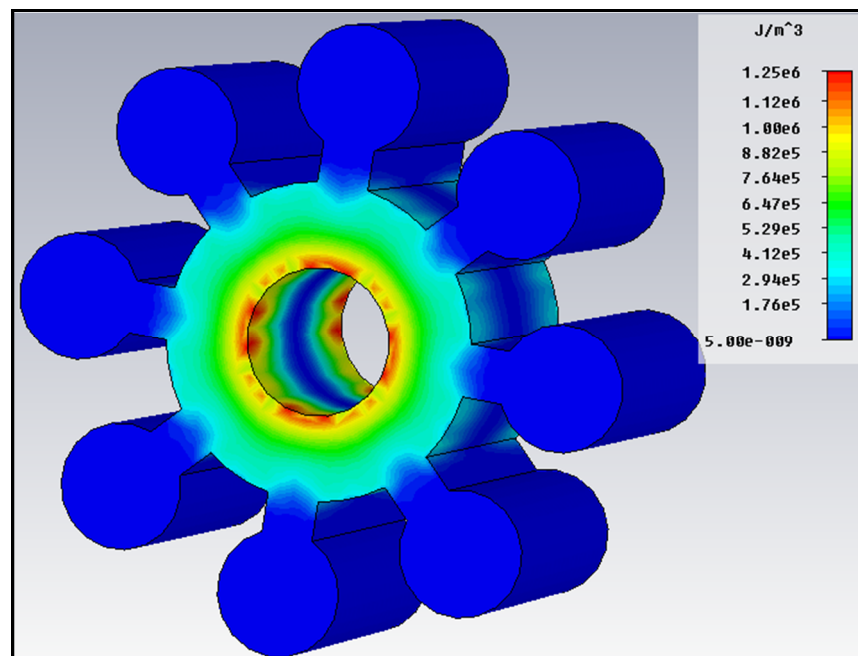

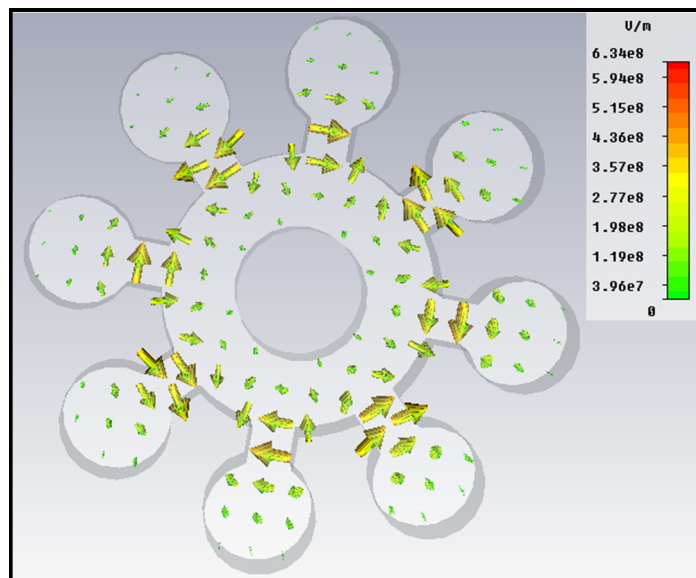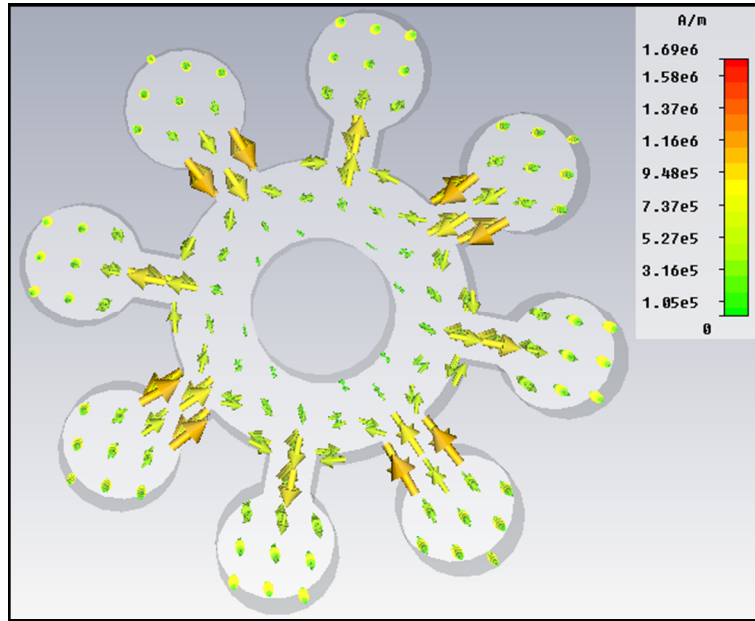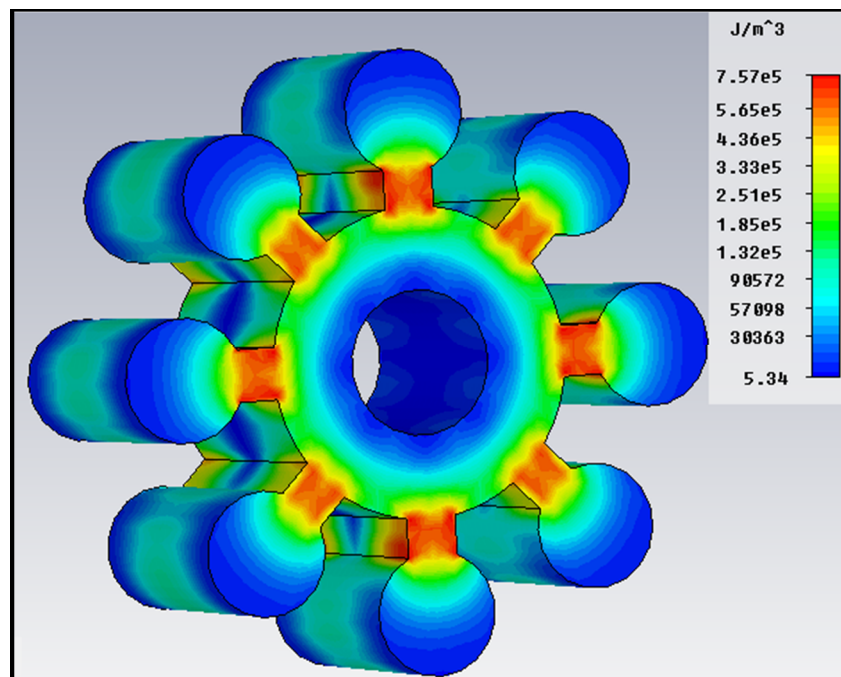Figure 3.23. 3D magnetic energy density pattern of mode 6 ($\pi - mode$) for a designed 8 cavity hole slot magnetron. The resonant frequency is 10.188 GHz

After this simulation, the field and current distribution are acquired as expected in Figure 2.14. The phase differences between adjacent resonators are π. When JDM solver method is used to verify AKS method, the results are obtained as the same with previous ones. Hence, the eigenmode part is finished by determining the electromagnetic field patterns. Although there exists a small difference in calculated frequency and simulation result frequency, it can be ignored at this level. Because, there will be also made some changes and optimized the structure in the following steps.

3.2.2. Particle Tracking Solver Section

Second step of modeling and simulation is particle tracking part. The purpose of this part is determining the required potential difference between anode and cathode blocks, and magnetic field to apply. To obtain these results, the electron motion in the interaction space under the influence of orthogonal electric and magnetic fields are investigated and observed using the CST Particle Studio, particle tracking solver. The desired situation is that the electrons should travel around the cathode neither go through the anode and strike the anode plate immediately nor go back to the cathode and do not emitted again. The trajectory of an electron should be completed to couple the energy of an electron to the RF field. The electron trajectories for different electromagnetic fields are represented in Figure 2.10. The analytic and discrete equations used by tracking solver are given in [56]. Contrary to eigenmode solver, PEC blocks do not removed and the boundary condition at the end of the magnetron is defined as $H_t = 0$ to prevent the magnetic field to escape from the interaction space. Fixed emission type is chosen for electron emission from cathode. The trajectory of an electron in one period is shown in Figure 3.24.

Figure 3.24. The trajectory of an electron under the influence of electromagnetic field, $V_{app} = 48\text{kV}, B_{app} = 0.21$ T

According to this simulation result, the magnetic field value must be increased to prevent the electron strikes to the anode plate. For this reason, new simulation is performed and the results are shown in Figure 3.25 to Figure 3.27.
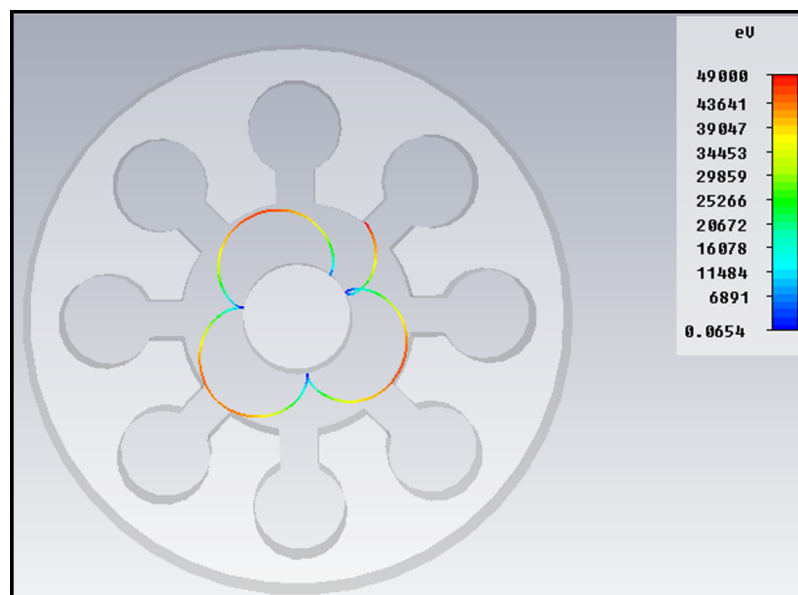
Figure 3.25. The trajectory of an electron under the influence of electromagnetic field, $V_{app} = 48\text{kV}, B_{app} = 0.22$ T
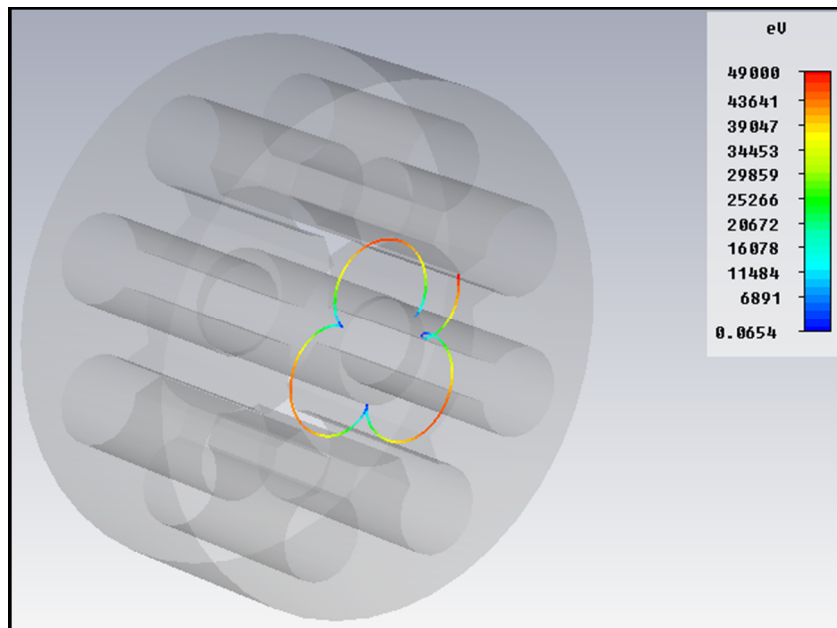
Figure 3.26. The trajectory of an electron under the influence of electromagnetic field in different view, $V_{app} = 48\text{kV}$, $B_{app} = 0.22\text{T}$

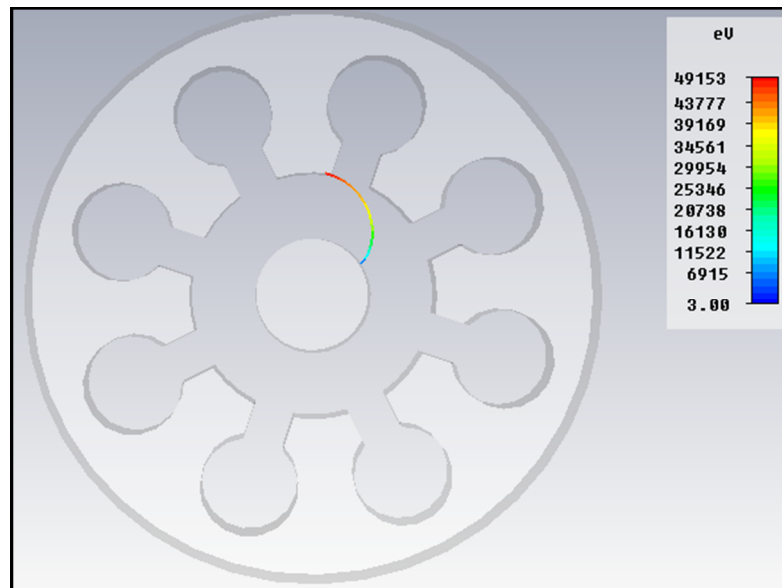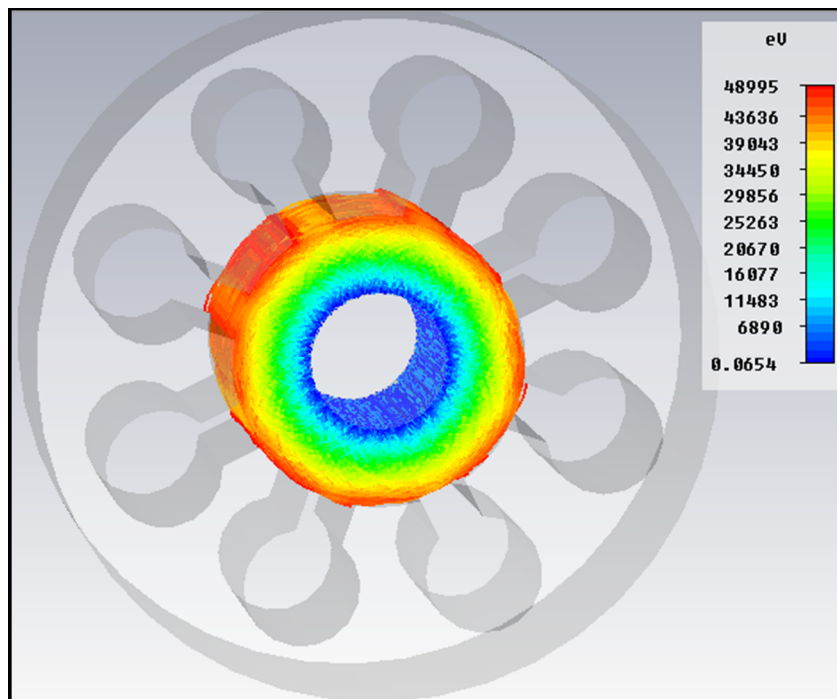Figure 3.27. The trajectory of all electrons emitted from the cathode under the influence of electromagnetic field. The number of total electrons is 1830. $V_{app} = 48 \text{ kV}$, $B_{app} = 0.22 \text{ T}$

As it is seen, the electron can rotate around the cathode plate. On the other hand, it should be known that this trajectory also depends on position where the electron emits. Therefore, it is not true to decide the required magnetic field and anode – cathode voltage difference only looking a one simulation. This can just provide useful insight to start and continue a design. The last parameters should be determined after PIC simulations.

After this step, the anode voltage and magnetic field values are determined approximately. The magnetic field value is changed from 0.21 T to 0.22 T. These values may also be optimized to get desired results during PIC simulations. Until the last simulation part called PIC simulation, the dimensions and the required electromagnetic field values are determined using eigenmode and particle tracking solver steps respectively. Now, in this step, using the probes, the electric field of the magnetron is monitored versus time and frequency at the specific point.

3.2.3. PIC Solver Section

PIC solver part is used to simulate charged particles emitted from arbitrary surfaces under the influence of the electromagnetic fields. The calculation method is explained in [57]. Using determined values of dimension and electromagnetic fields from the previous steps, the first PIC solver simulation is performed. For this simulation, explosive emission model with 1830 number of emission points for emitted electrons is chosen. Rise time and kinetic value of energy are taken as 1ns and 3eV respectively. Two probes are used and they are located at the beginning and end of the slot as in Figure 3.28.
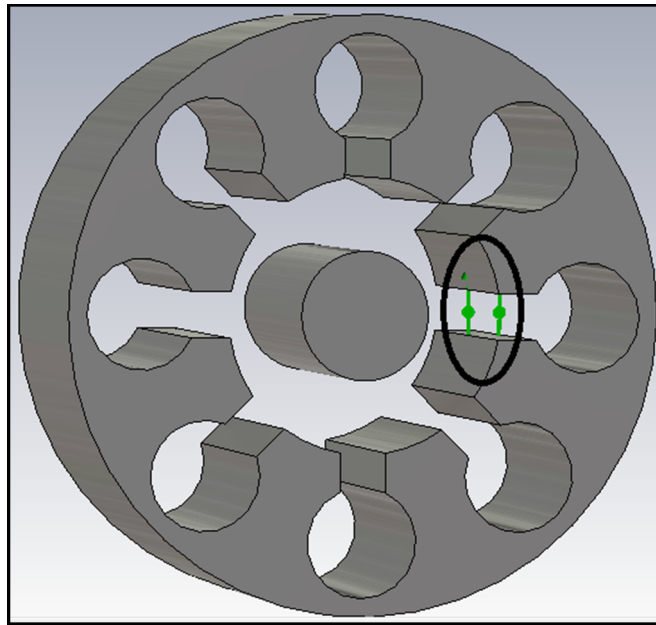
Figure 3.28. The location of probes in magnetron structure

The electric field signal (V/m) measured by the probes are given in the following figures
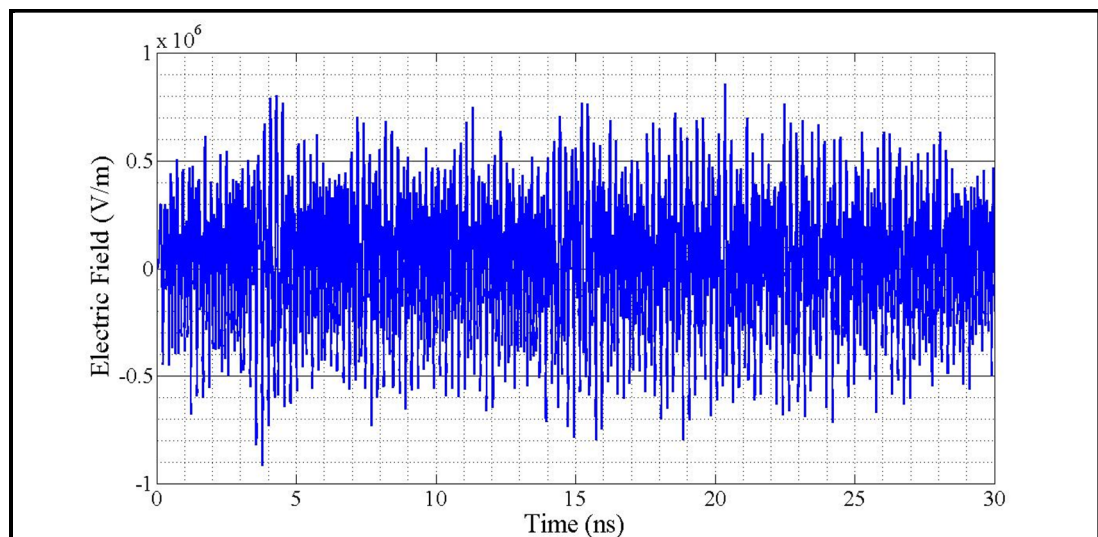
Figure 3.29. Measured electric field as a function of time by the probe located at the end of the interaction space (at beginning of the slot part)
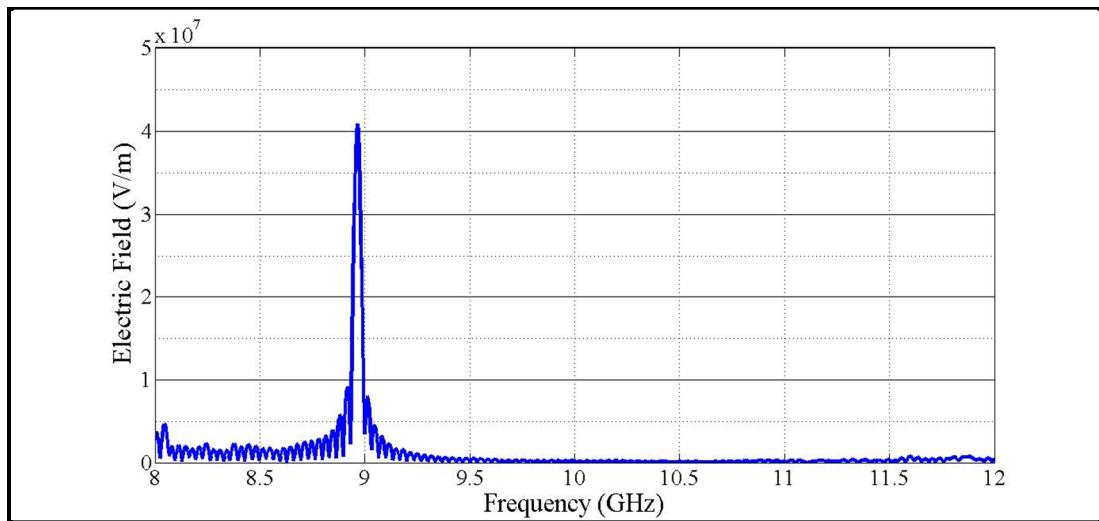
Figure 3.30. The frequency spectrum of measured electric field by the probe located at the end of the interaction space
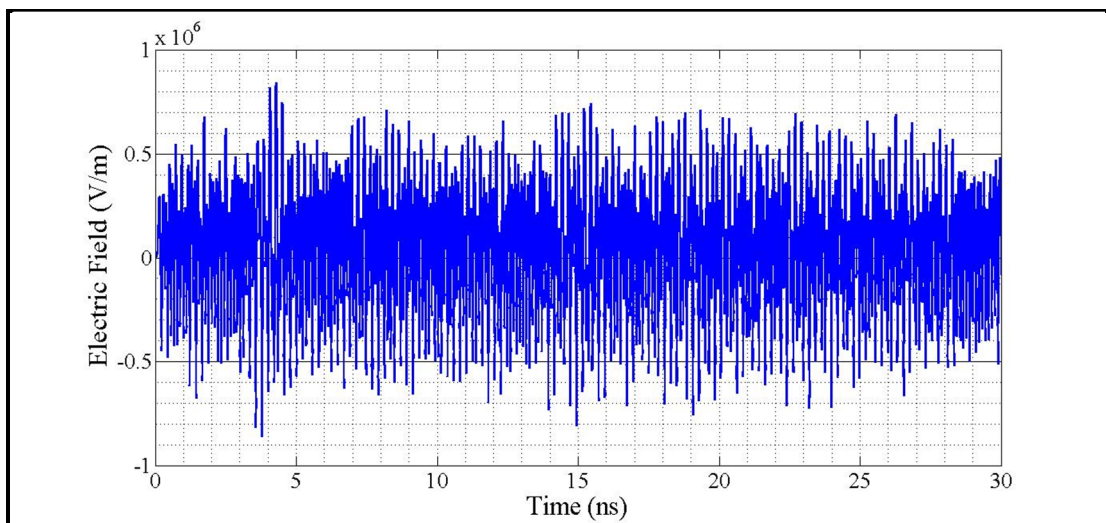
Figure 3.31. Measured electric field as a function of time by the probe located at the end of the slot part
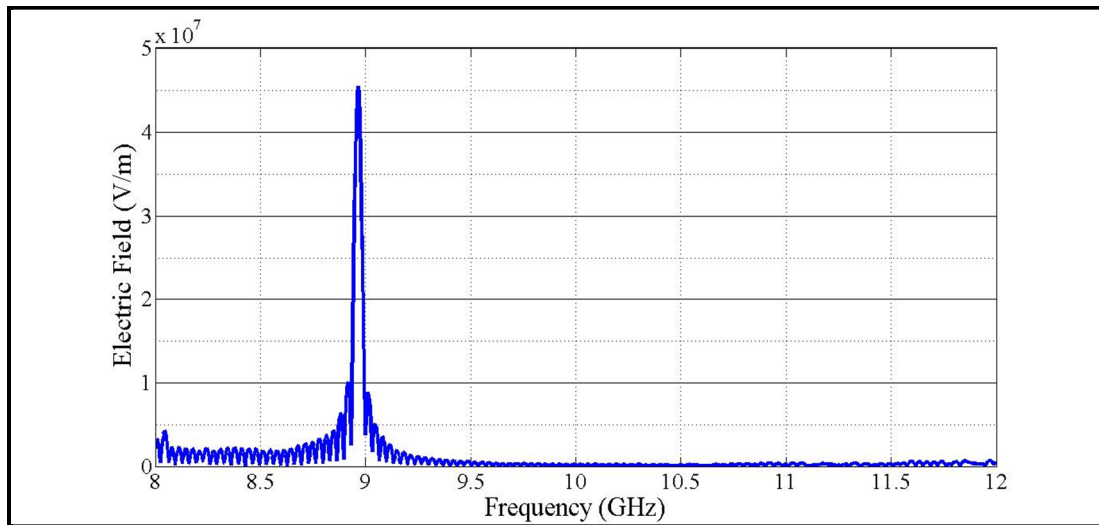
Figure 3.32. The frequency spectrum of measured electric field by the probe located at the end of the slot part
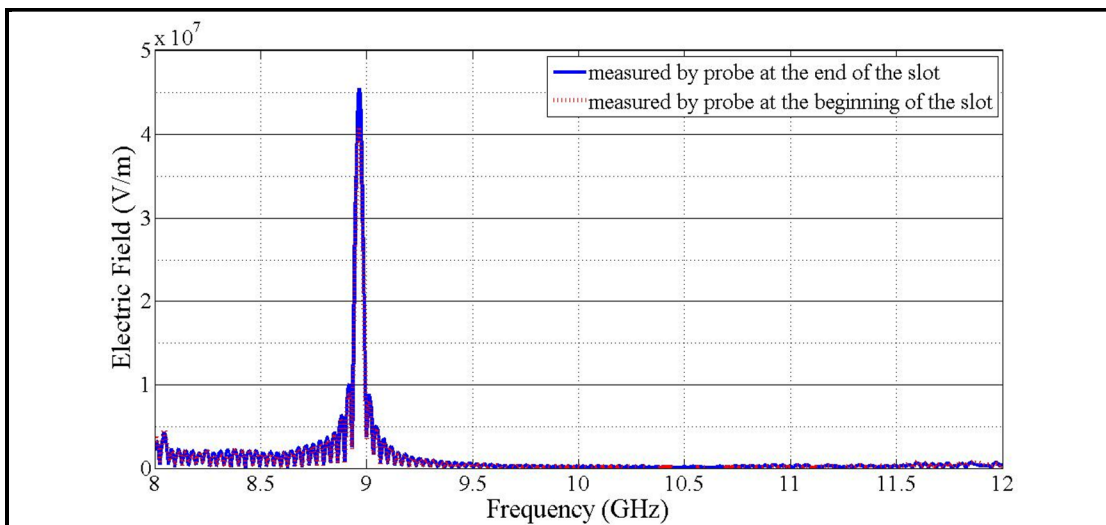
Figure 3.33. The comparison of the frequency spectrum of electric fields (V/m) monitored by probes located in different places
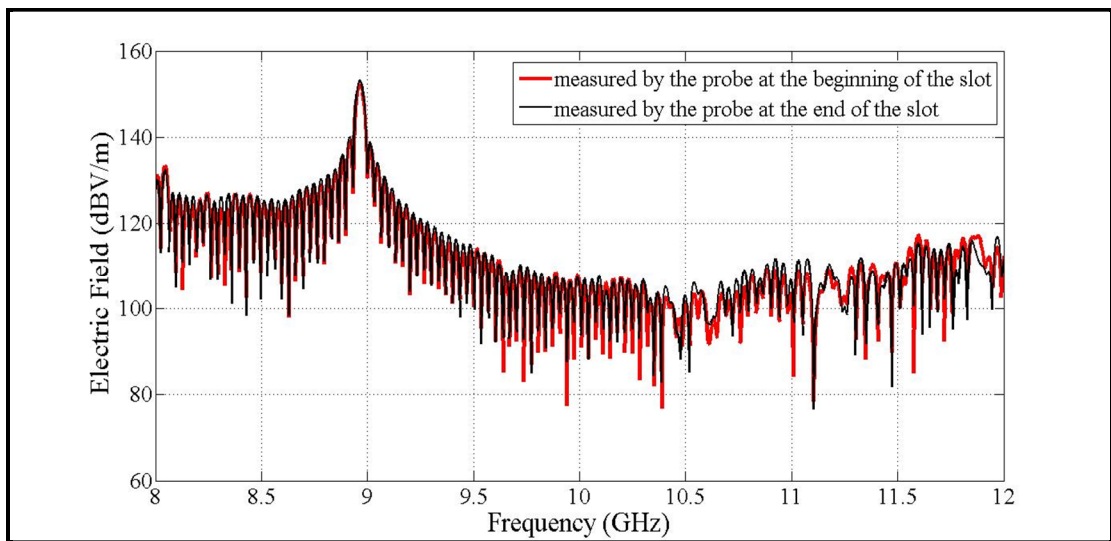
Figure 3.34. The comparison of the frequency spectrum of electric fields (dBV/m) monitored by probes located in different places
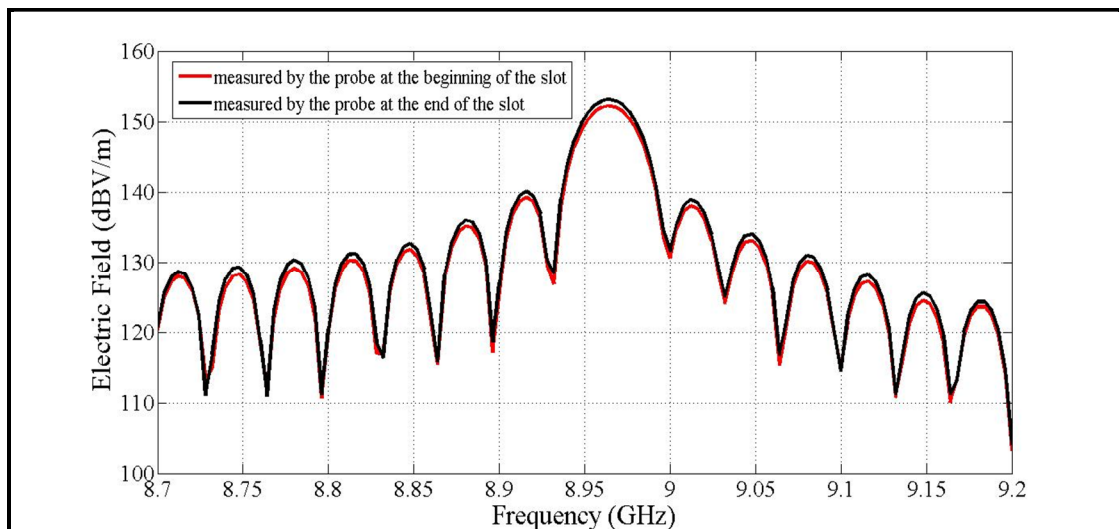
Figure 3.35. Detailed view of the comparison of the frequency spectrum of electric fields (dBV/m) monitored by probes located in different places

As it is seen from the comparison Figures 3.33, 3.34 and 3.35, there is no variation in resonant frequency and only appears a little difference in magnitudes between the measured values of electric fields according to probe location. Therefore, only one probe is used for simplicity after this part. In CST simulation, hexahedral mesh is used and the lines per wavelength are chosen 20. There exists total 51240 mesh cells and the simulation takes

approximately three hours. The number of emission points and the mesh cells are the critical parameters to determine the simulation time. By the PIC solver, it is seen that the desired solution is obtained that there is only one resonant frequency in overall, 8 GHz – 12 GHz, X band. Also, there exists an important point that the initial parameters are calculated for the resonance frequency f = 10 GHz, but, frequency shift is occurred and the resonance frequency is moved to f = 8.965 GHz. On the other hand, this change can be, since the analytical equations are derived for simplicity, these equations and formulas do not give exact results.
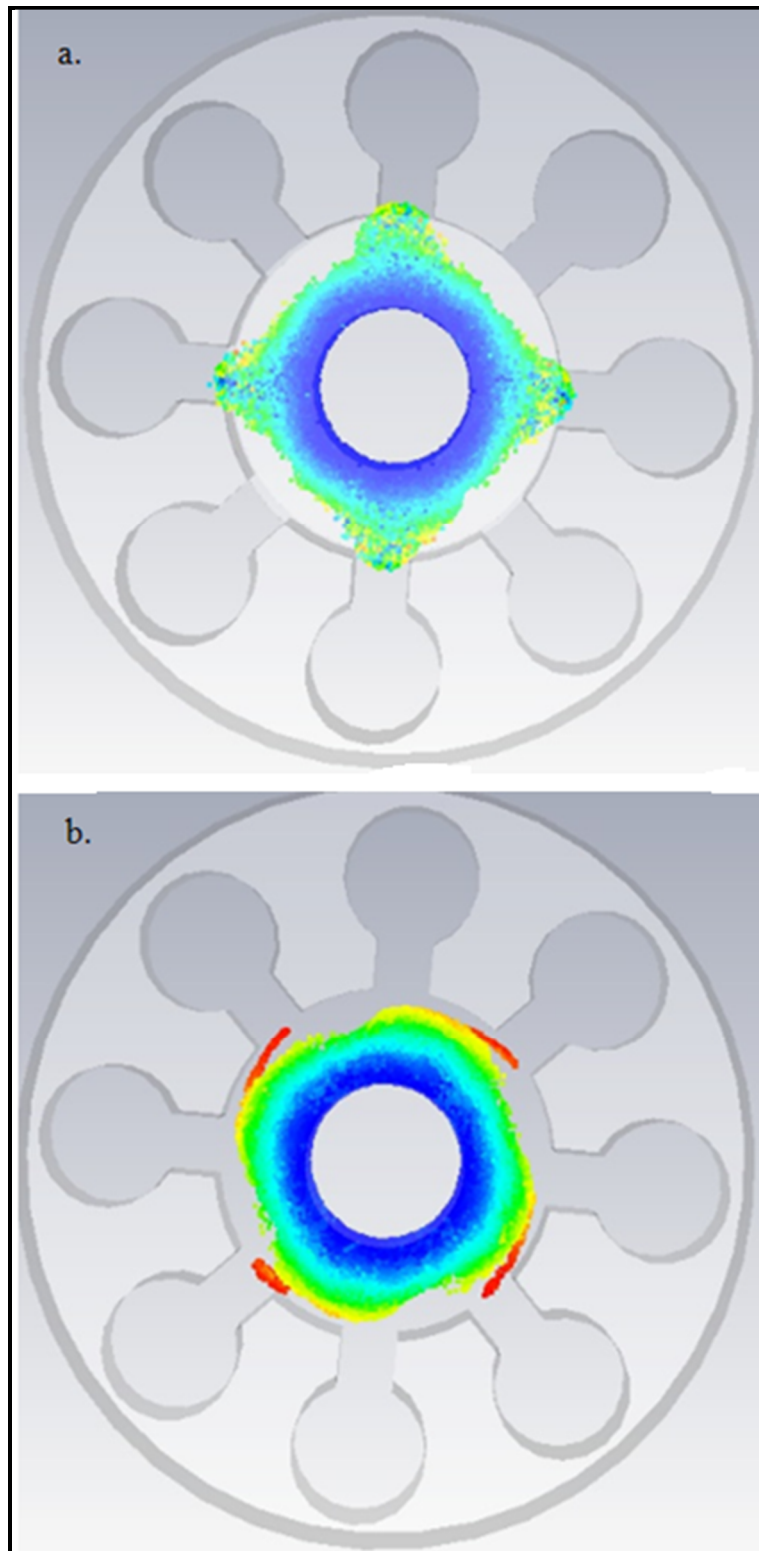
Figure 3.36. The particle previews of emitted electrons in a PIC simulation at different times

The next step is determining the optimum values of parameters about the number of emission points, mesh accuracy and PIC solver time to obtain the best results without changing the characteristics of structure. These obtained parameters are used anymore to develop the design. The first investigated parameter is PIC solver time. Although the length of time is dependent on the rate that the magnetron model simulations would settle down, this is chosen arbitrarily. It should be considered the optimum level between the stability and simulation time, neither very long time to achieve settling down nor very short PIC solver time to perform the simulation in a short time.
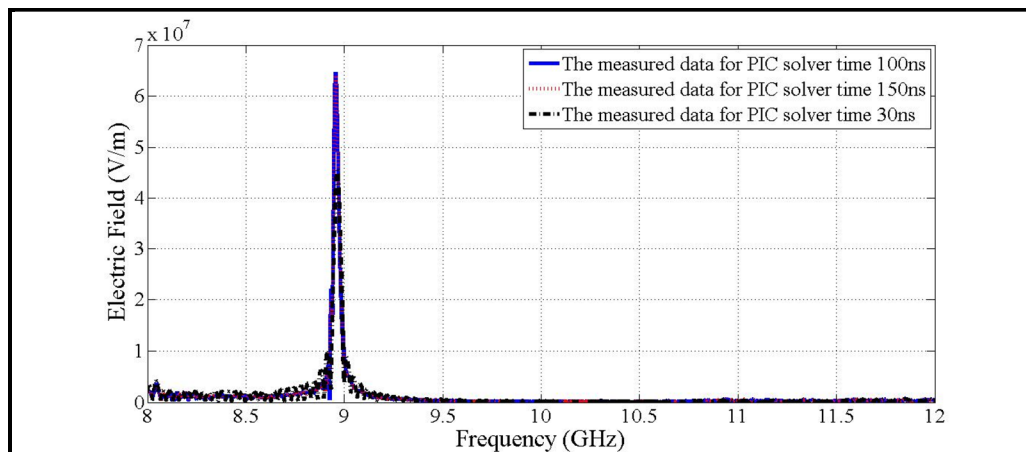
Figure 3.37. The comparison of the frequency spectrum of measured electric fields (V/m) for different PIC solver times
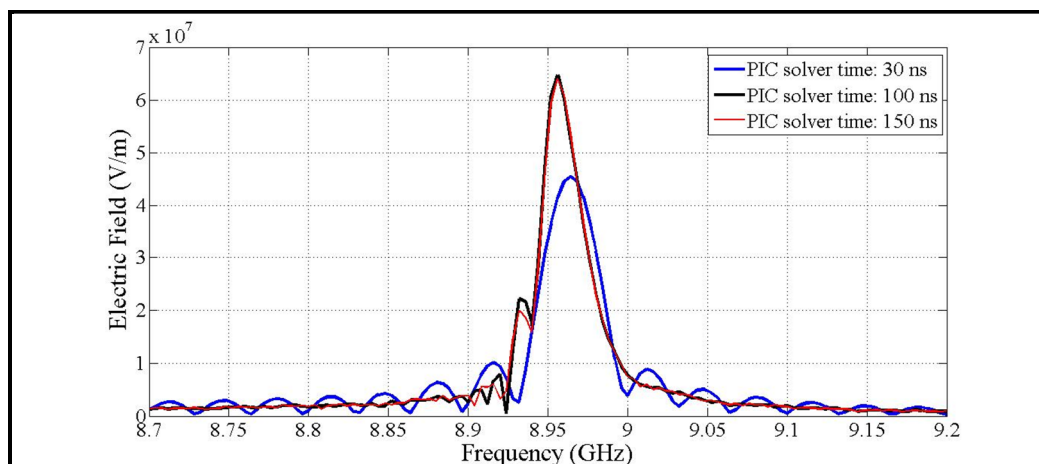
Figure 3.38. Detailed view of the comparison of the frequency spectrum of measured electric fields (V/m) for different PIC solver times
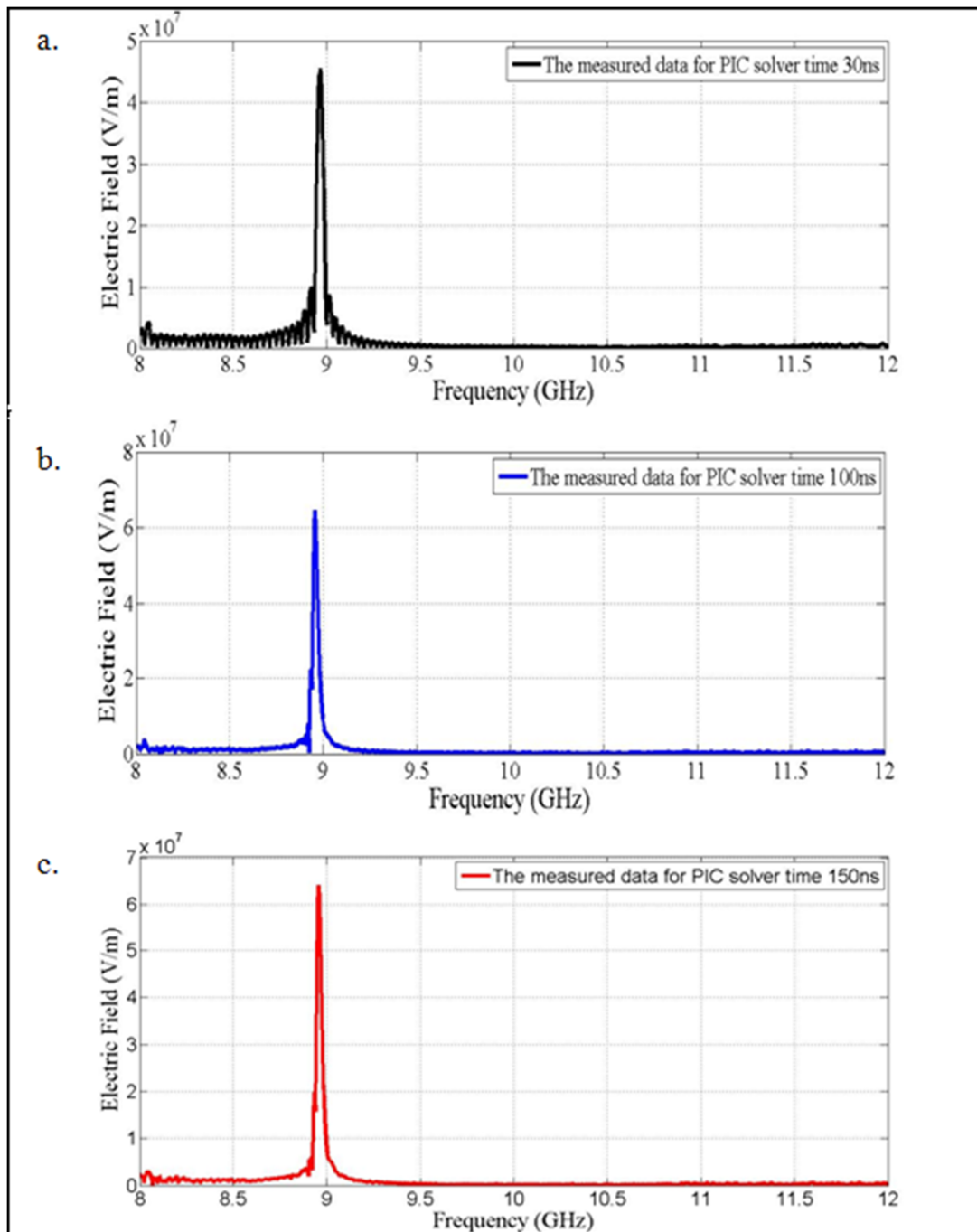
Figure 3.39. a., b., c. The monitored values of electric field for 3 different PIC solver time 30 ns, 100 ns and 150 ns respectively. The parameters used in CST except PIC solver time are hold same for all simulations

As it is seen from the figure, PIC solver time affects the spectral characteristics and simulation result accuracy. But, these changes are tolerable. On the other hand, the simulation time also increases, i.e. for 100 ns PIC solver time simulation, it continues 7

hours and for 150 ns PIC solver time, the simulation is completed in 13 hours. Since the required simulation times are get longer when PIC solver time is increased, and the resonance frequency does not affected from this change, for simulations to get quick results, generally PIC solver time is chosen 30 ns. After desired solutions, a new long time simulation is performed to get final more accurate result using previously obtained parameters.

The effects of number of emission points and number of mesh cells are investigated in the following simulations and presented in the Figures 3.40, 3.41, 3.42, 3.43. From the figure, the simulation results show that the mesh number affects the resonance frequency and it causes the frequency shift. But, there is no very important change when the simulation time is considered as the mesh number is increased. If the lines per wavelength are chosen 25, the total mesh cells number become 94608, and for 15, the same number is 23040. The RAM requirement of computer also increases by increasing the number of the lines per wavelength parameter. For the lines per wavelength: 15, there exists a staircase mode presented in Figure 3.44, which can affect the accuracy, therefore, the optimum and convenient choice is the least "lines per wavelength" number for less total mesh cells that satisfies the required accuracy. For our simulation, this number is 20.
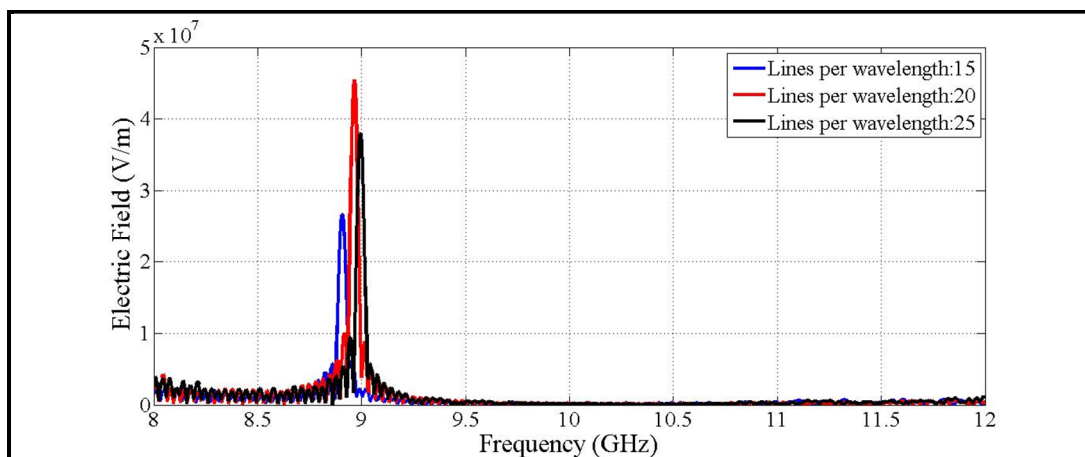
Figure 3.40. The comparison of measured electric field values (V/m) for different "lines per wavelength" parameter
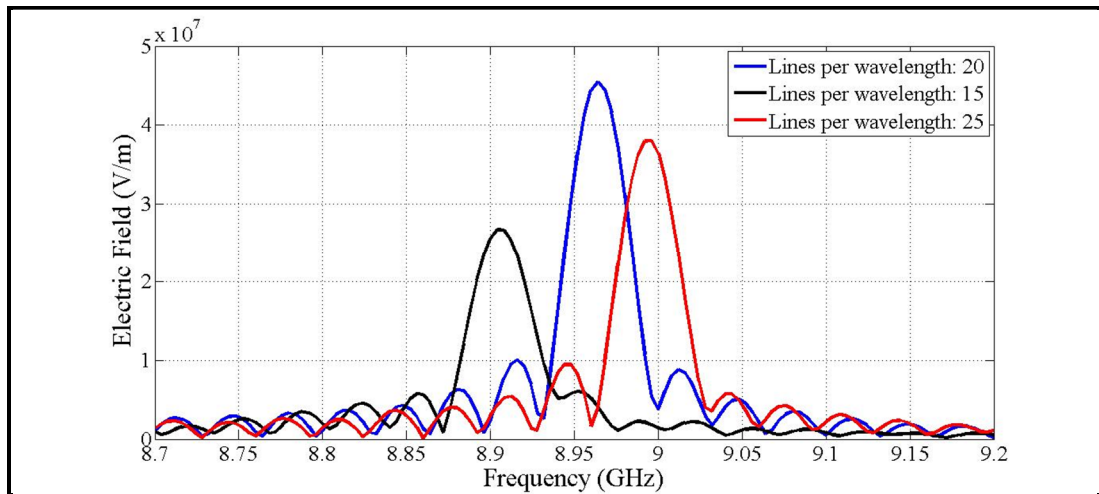
Figure 3.41. Detailed view of the comparison of measured electric field values (V/m) for different "lines per wavelength" parameter
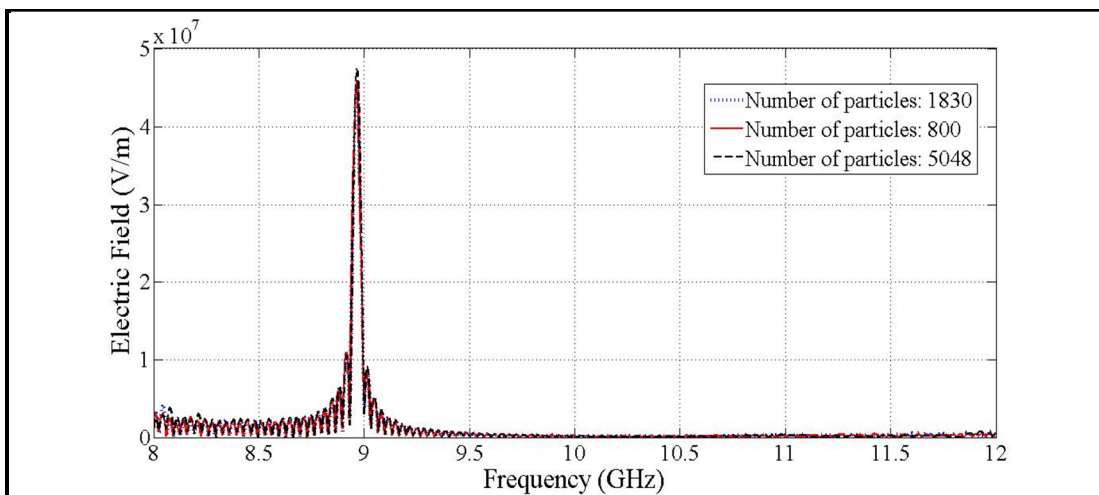
Figure 3.42. The comparison of measured electric field values (V/m) for different "number of particles" parameter
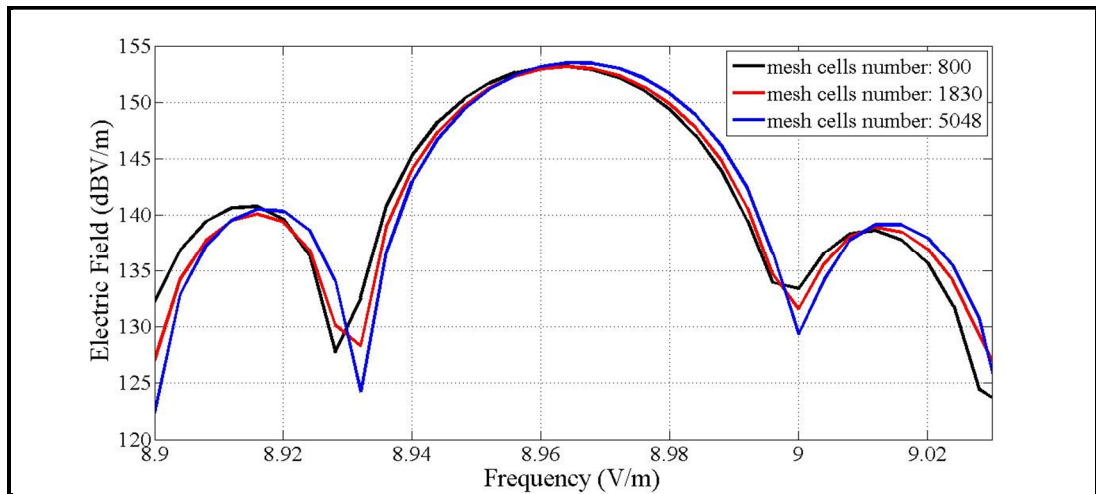
Figure 3.43. Detailed view of the comparison of measured electric field values (dBV/m) for different "number of particles" parameter

Although "the number of particles" parameter causes to increase in simulation time as the parameter increases, it does not affect the result. The other parameters for these 3 simulations are kept same and the simulation time increases from 1.5 hours to 7 hours. For this reason, number of particles is chosen 800 for the rest of the simulations.
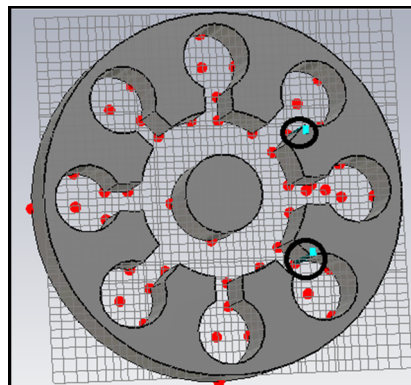
Figure 3.44. The cross section of magnetron structure modeling and the representation of mesh cells in staircase mode

CST parameters that will be used in general for the rest of the simulations are determined, these are 30ns for PIC solver time, lines per wavelength 20, and the last, number of

particles is 800. On the other hand, it should be specified that, there would be exceptional simulations using different values mentioned above to get more accurate results.

3.2.4. Impact of Design Parameters

Now, the impact of magnetron structure parameters such as the height of anode block, the radius of cathode, the radius of hole, slot length and width are investigated. The first examined parameter is the height of the cathode (and anode) block. Two more simulation is performed to compare the first model.
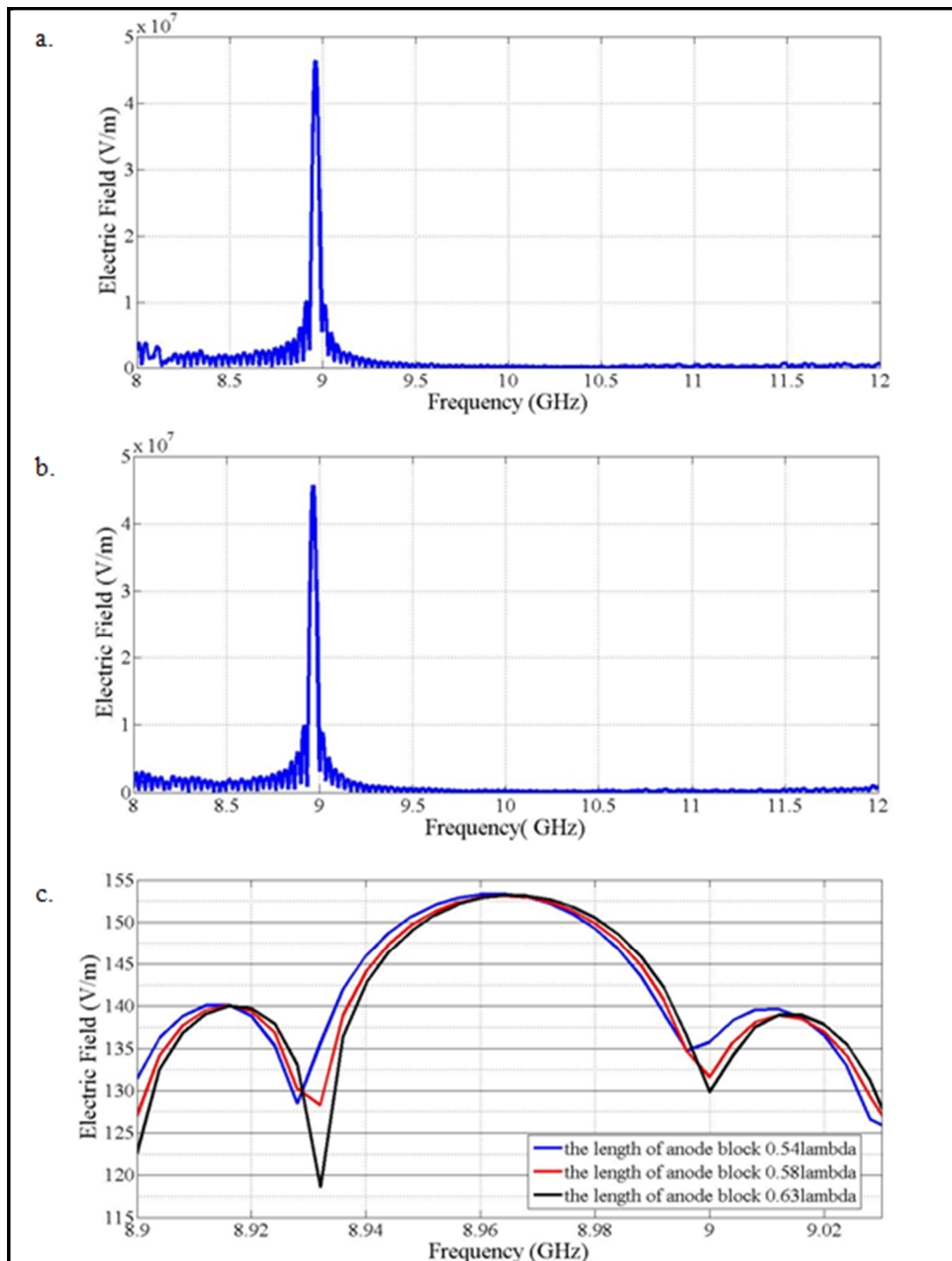
Figure 3.45. a. The frequency spectrum of the electric field result when anode block height is taken 0.54λ which is less than the first designed model, b. The frequency spectrum of the electric field when anode block height is taken 0.63λ which is bigger than the first designed model, c. The comparison of three magnetron model having different anode block heights

The length of the magnetron does not affect the resonance frequency, but the noise level varies according to this value. The most desired solution is obtained when the magnetron height is lengthened to 0.63λ. If this extension is continued to 0.68λ, the result gets worse compared to previous one as presented in Figure 3.46.
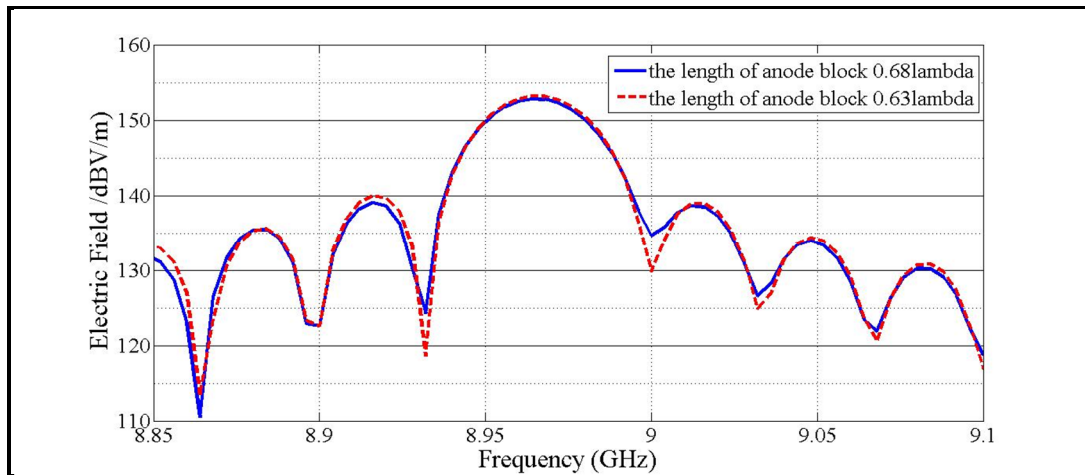
Figure 3.46. The comparison of three magnetron model having different anode block heights

From these simulations, the length of the magnetron structure is determined as 0.63λ. The effects of cathode radius and anode inner radius are shown in the following figures
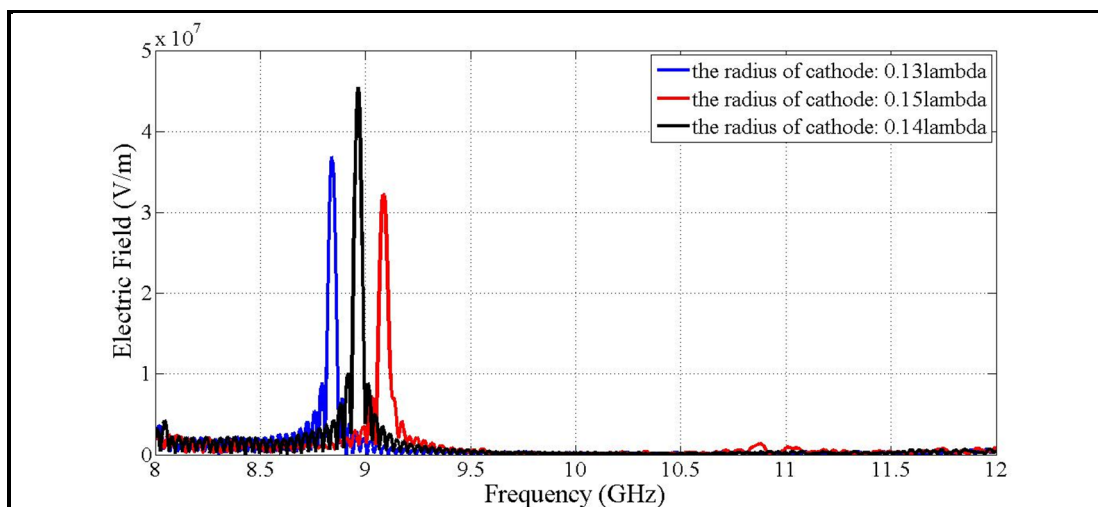
Figure 3.47. The comparison of electric field values of three magnetron models having different cathode radiuses for whole frequency band
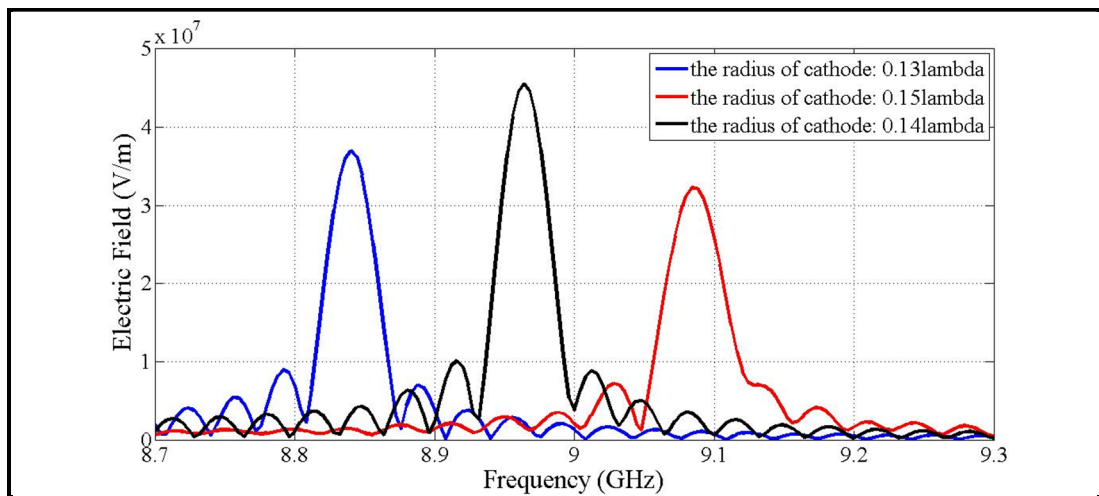
Figure 3.48. Detailed view of the electric field values of three magnetron models having different cathode radiuses
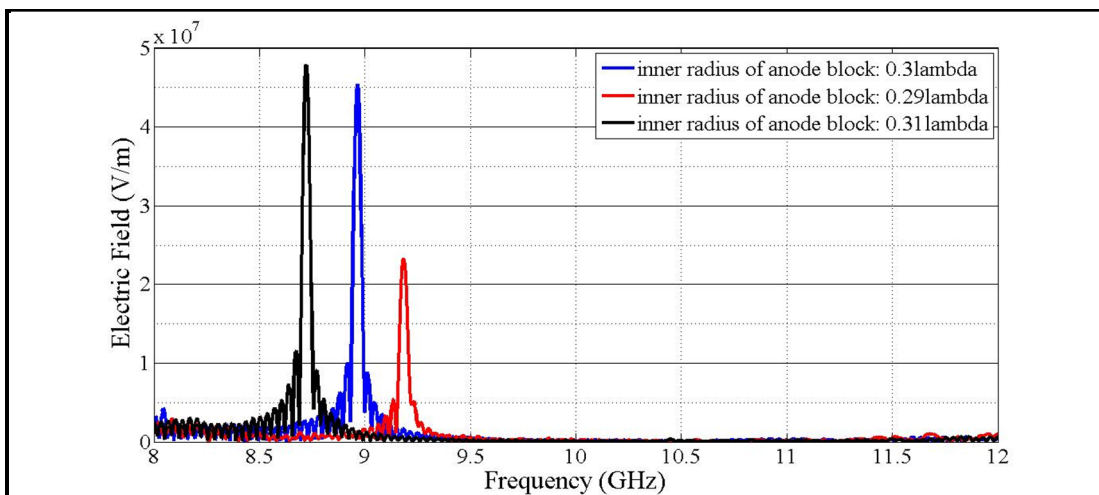
Figure 3.49. The comparison of the frequency spectrums of three magnetron models having different anode inner radiuses for whole frequency band
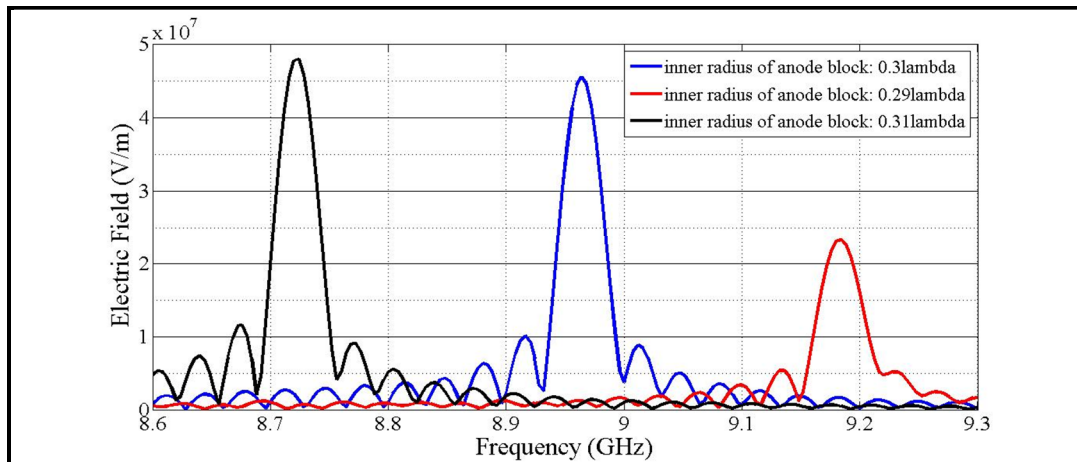
Figure 3.50. Detailed view of the frequency spectrums of three magnetron models having different anode inner radiuses

As it is seen from the Figure 3.39 and Figure 3.40, the cathode and anode inner radius do not only affects the signal and noise level, but also determines the resonance frequency. When these are altered, it should be known that the interaction space also changes which has directly impact on the frequency. If the interaction space region is extended, then the resonance frequency is decreased and vice versa. Therefore, the effects of cathode radius and anode radius dimensions are inversely. The following parameter is the slot length; this region is a connection of holes and the interaction space. The dimension of slots also plays a role on magnetron characteristics. The impact is shown in Figure 3.51 and Figure 3.52.
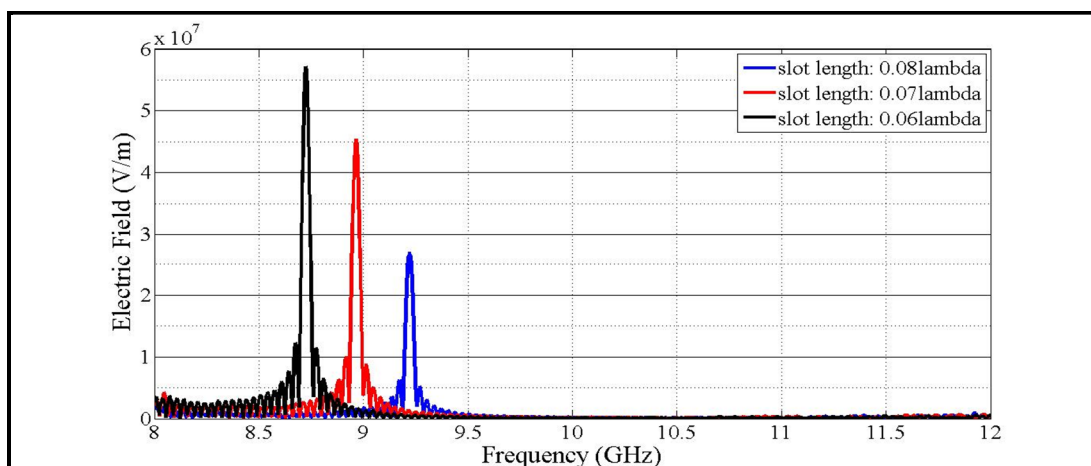
Figure 3.51. The comparison of the frequency spectrums of three magnetron models having different slot lengths for whole frequency band
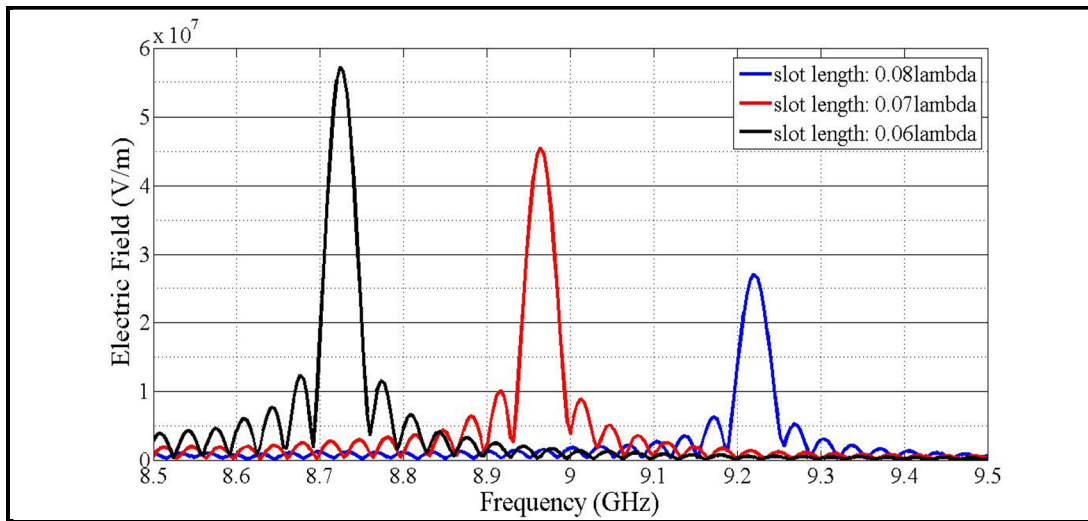
Figure 3.52. Detailed view of the frequency spectrums of three magnetron models having different slot lengths

The dimension of slot width and the resonance frequency are directly proportional. The resonance frequency decreases as the width of the slot region is decreased. This relation can be seen from the Figure 3.53 and Figure 3.54.
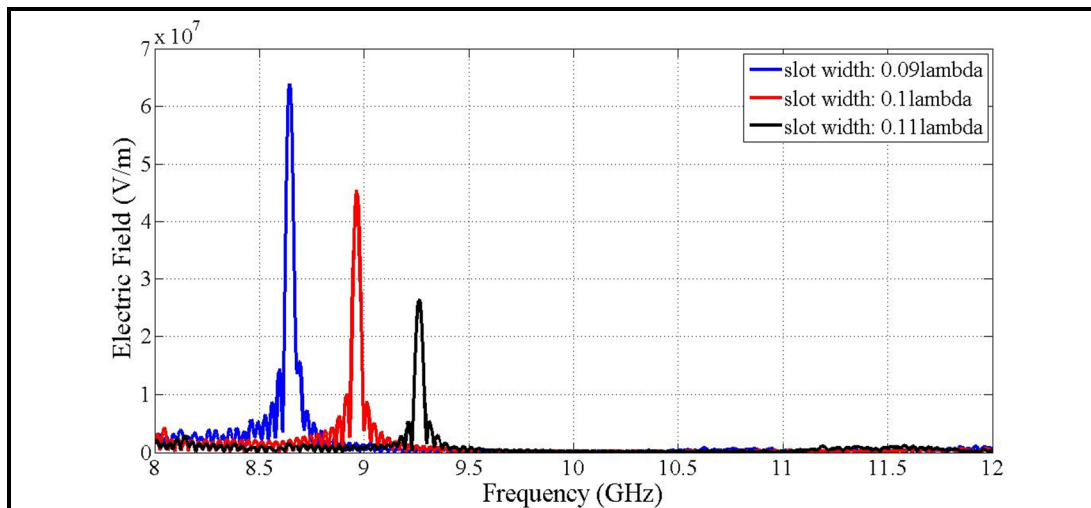
Figure 3.53. The comparison of electric field values of three magnetron models having different slot widths for whole frequency band
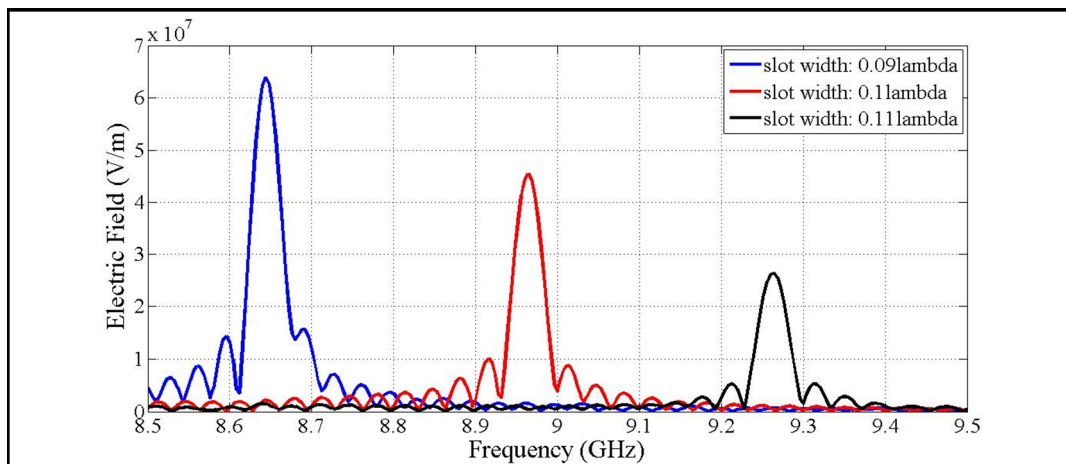
Figure 3.54. Detailed view of the frequency spectrum of electric fields of three magnetron models having different slot widths

Although it seems that if the dimensions mentioned above are changed alone, then the resonance can shifted to any frequency, the situation would not realized as it supposed. Since the signal and noise levels are also varied according to magnetron structure, the model should be designed by considering all parameters together. The hole radius effect is shown in Figure 3.55 and Figure 3.56. As expected, the resonance frequency is increased when hole radius dimension is decreased. The sideband noise levels are also affected from these changes. On the other hand, for all simulations, the magnetron has only one resonance in whole frequency band as desired.
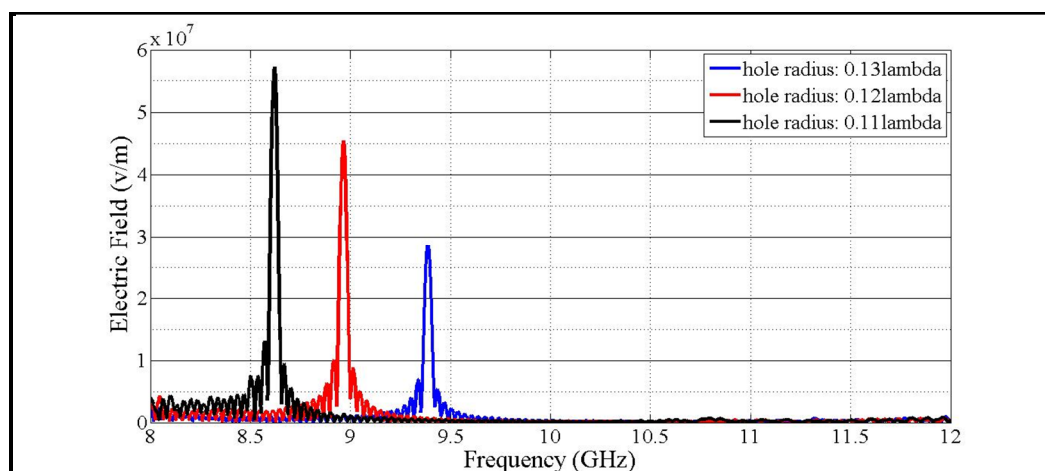
Figure 3.55. The frequency spectrum of electric fields related with three magnetron models having different hole radius dimensions for whole frequency band
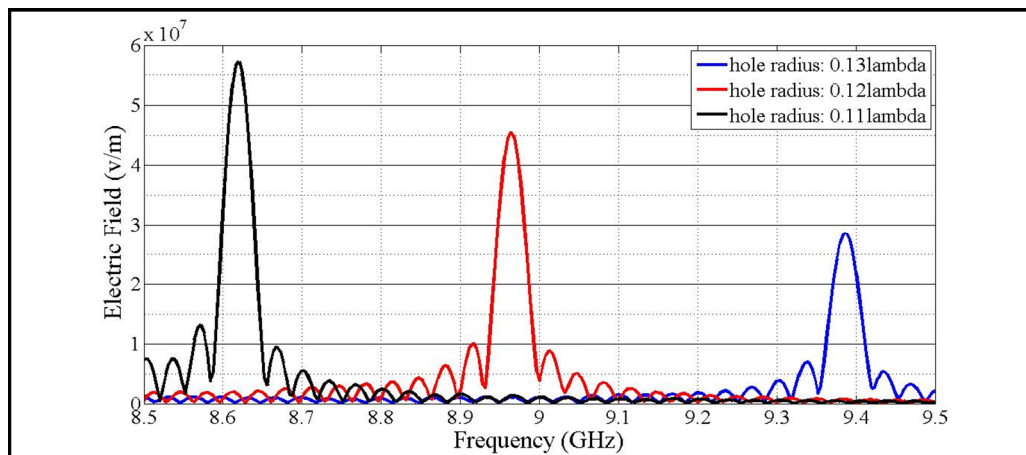
Figure 3.56. Detailed view of electric fields related with three magnetron models having different hole radius dimensions

After the investigation of impact of structure parameters, the effects of applied electromagnetic fields are examined by keeping the dimensions constant. Applied anode voltage and magnetic field comparisons are made and the results are shown in Figures 3.57, 3.58, 3.59 and 3.60. It is important that obtained electric field from the magnetron increases without any change in resonance frequency as applied voltage is increased. Meanwhile, the noise levels vary for three different models. Applied magnetic field levels do not affect the result like anode voltages and there exists just small variations in electric field values.
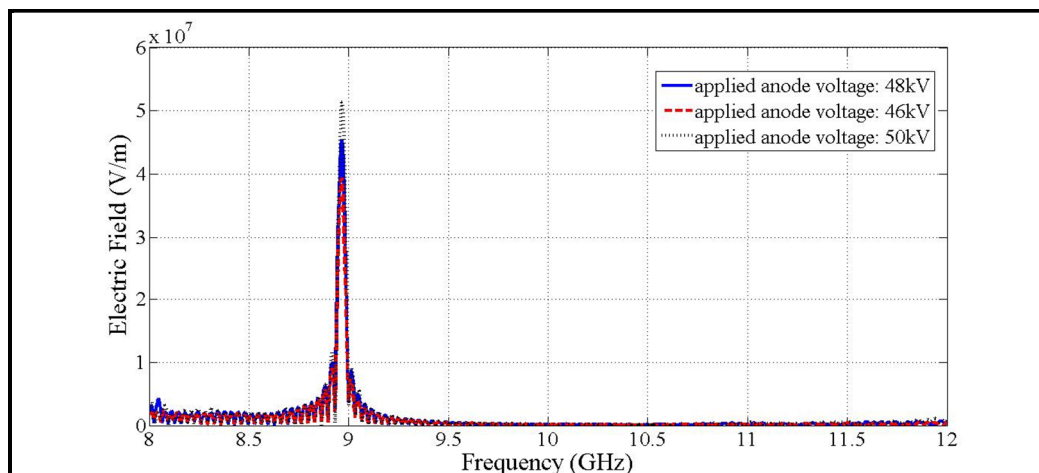
Figure 3.57. The comparison of electric field values of three magnetron models when applied anode voltages are different
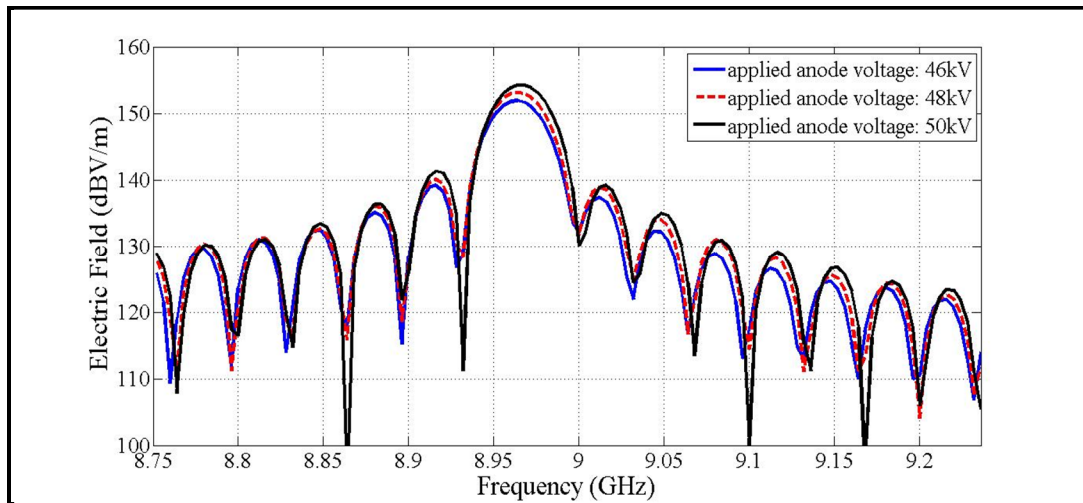
Figure 3.58. The comparison of noise levels about the resonance frequency for three different applied anode voltages
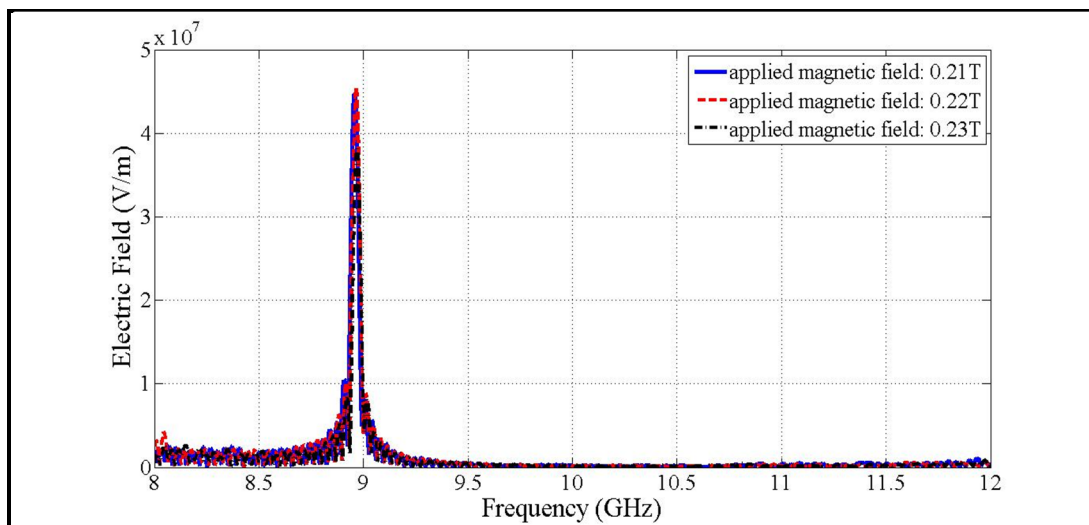
Figure 3.59. The comparison of electric field values of three magnetron models for whole frequency band when applied magnetic fields are different
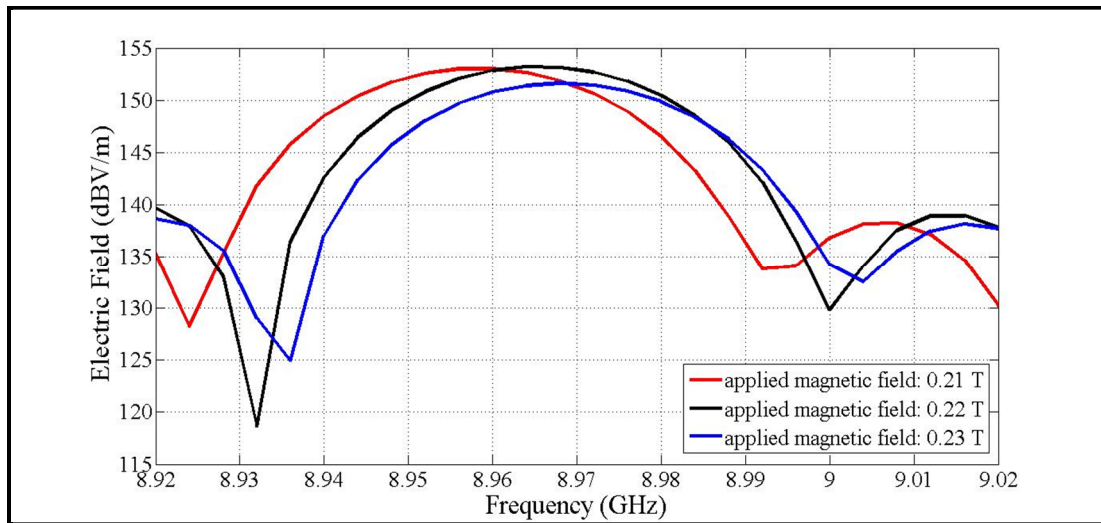
Figure 3.60. Detailed view of the frequency spectrum for three magnetron models when applied magnetic fields are different

3.2.5. Magnetron Output Design

The interaction of emitted electrons and the electromagnetic field causes RF field in the interaction space. The RF field is converted microwave energy at the output and this field coupled out of the tube using coaxial and/or waveguide outputs. The wavelength and the tube power level determine the output whether coaxial or waveguide output. In some cases, two of them are used together by using the coaxial to waveguide transitions. The RF field is coupled to output waveguide by coaxial line used as a loop coupling. In this work, since the frequency and the power level is appropriate, the output is designed using both loop coupling and rectangular X band, WR 90, waveguide. The model of structure and the simulation results are presented in the following figures.
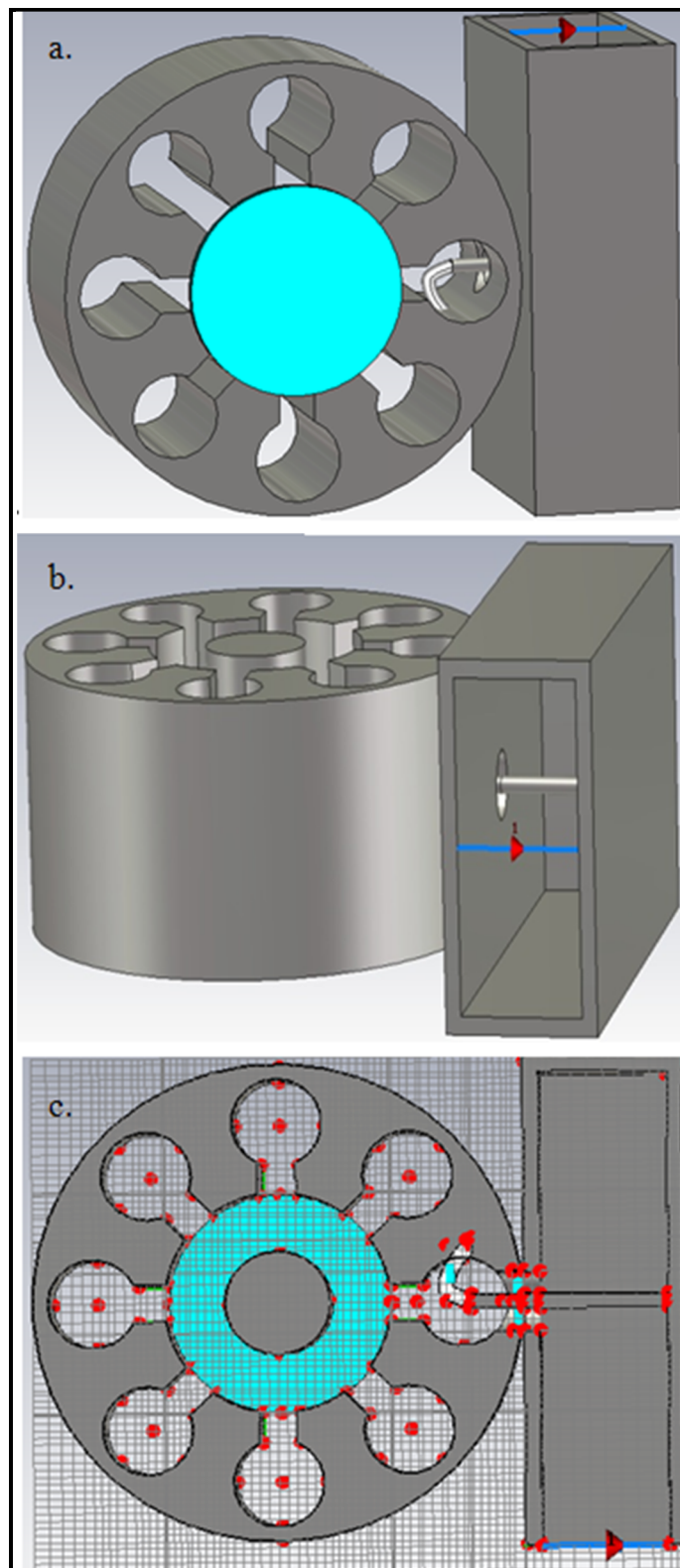
Figure 3.61. a. The top view of magnetron model, b. The side view of magnetron model, c. The cross section of magnetron model

The magnetic field is defined using a magnet instead of analytic source field as in previous simulations. The reason of change is that as seen from the model, the output waveguide width is larger than the height of the magnetron which prevents defining the required boundary conditions at the ends of the interaction space. Therefore, to solve this problem the magnet is used. The magnets will also be used in the following noise section and will be described in detail. Discrete port is defined at the end of the output waveguide to monitor the voltages and currents. The resonant frequency shifts by adding the output section. Since the resonance is actualized at one frequency in whole frequency band, it is not necessary to adjusted to 10 GHz again.
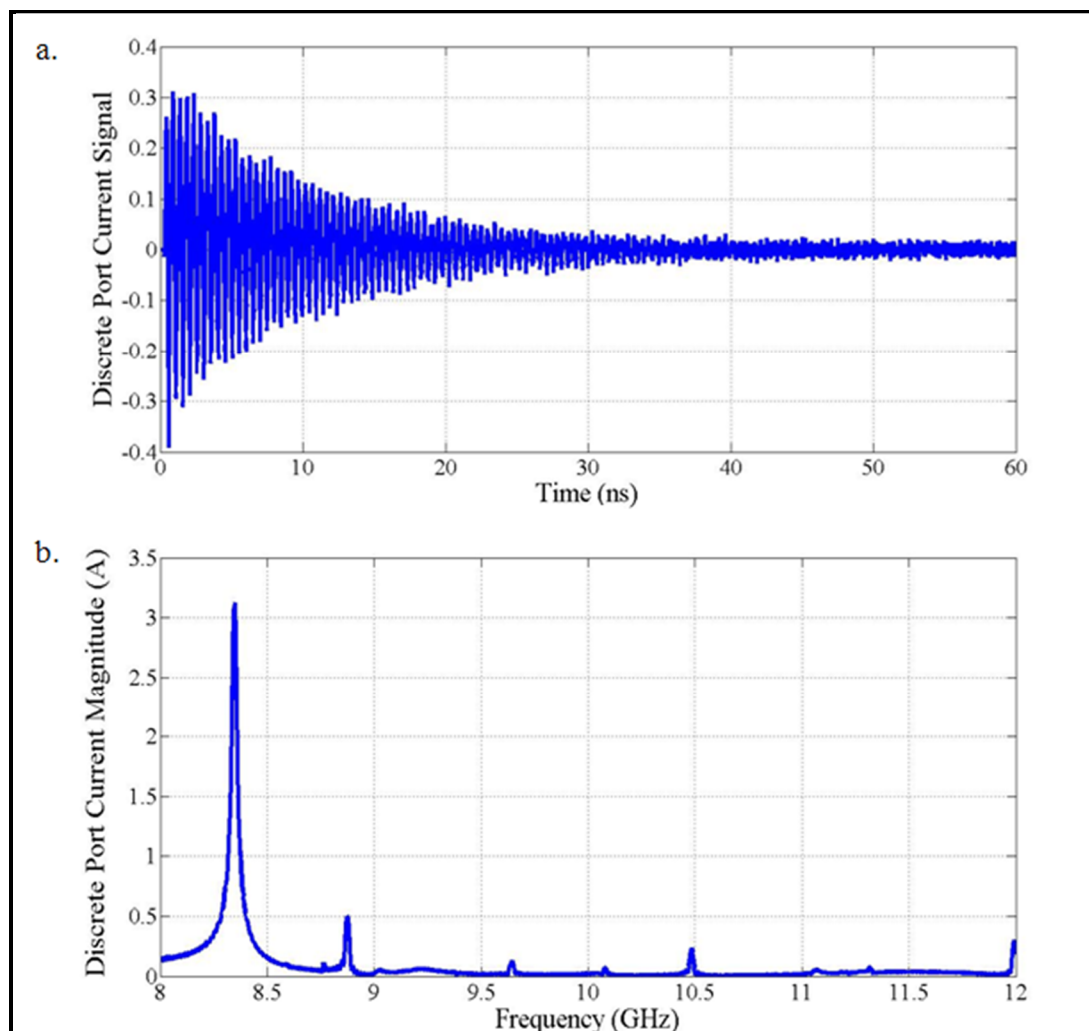
Figure 3.62. a. The current signal as a function of time response monitored by the discrete port at the output waveguide, b. The current signal variation according to frequency monitored by the discrete port at the output waveguide
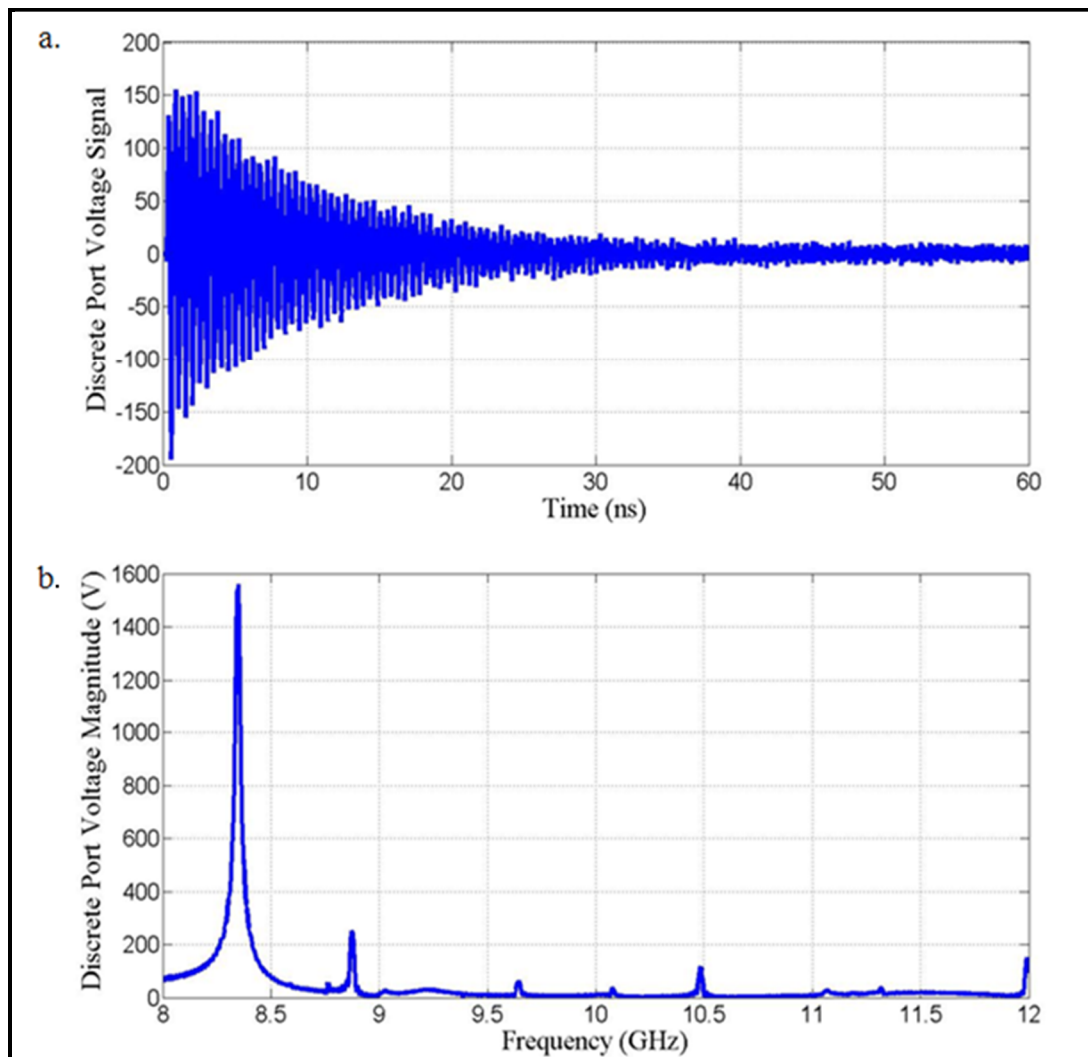
Figure 3.63. a. The voltage signal as a function of time response monitored by the discrete port at the output waveguide, b. The voltage signal variation according to frequency monitored by the discrete port at the output waveguide

The length of the waveguide is very important to adjust the resonance and matching. The output power is calculated approximately five kW using the voltage and current values at the resonant frequency. Since the output section is also used as a matching part from the resonant system to the output load, the noise performance of magnetrons with output section is better than the previous ones which the electric fields monitored by probes. The output voltages and currents are obtained almost free of noise in operating frequency.

4. MAGNETRON NOISE AND THE REDUCTION TECHNIQUES

The cross field amplifiers, especially magnetrons are high noise devices due to the common instability of electron clouds. Although the noise generation mechanisms have not well understood until now, in order to prevent the interference from other communication systems occupying the same region of the microwave spectrum, various techniques are developed. In this chapter, the source of noise is explained. The noise reduction techniques are also investigated and compared to each other. The performance of these techniques is examined.

4.1. THE ORIGIN OF NOISE IN MAGNETRON

The magnetrons are the most widely used vacuum microwave devices spite of their low noise performance. As mentioned in chapter 2, the motion of electron in the interaction space causes RF signal as a noise and since the oscillation appears from this signal, the noise cannot be eliminated completely from the magnetron. The existing particles in the interaction space, ions and electrons move in different velocities and this difference causes the ions to produce momentary variations in the electron current, thus, the noise appears [8]. Hence, the noise is considered as an inherent part of the operating structure of a device. Since the analytical model of magnetron operation cannot be constructed easily, most of the investigations about the magnetron noise are based on the experiments and measurements.

The reasons of noise are varied in magnetron operation. One is about the circulating motion of electron stream in the interaction space [58], which is associated with the wide-band noise generation [59]. The applied voltage and the magnetic field values are very important for stable oscillation. In general, the noise level rises as an anode voltage increases [60]. Correct value and the direction of magnetic field can help to prevent back bombardment of emitted electrons which causes excess noise and provides better signal to noise ratio. The other is related to the cathode heating source. Back bombardment and cathode heating conditions which are related to cathode structure have primarily effects on the noise levels of microwave magnetrons [59, 61]. In order to improve the noise

performance, the cathode heater current of a magnetron should be turned off during the oscillation after startup [62, 63]. It prevents the excess current emission which is over required for the operation. By this change, sideband noises are suppressed and noise close to the operating frequency is reduced [64]. The cathode temperature also affects the noise. According to measurements, the increase in cathode temperature causes to rise the noise level [60, 62]. The kind of cathode is another important parameter that influence the noise, i.e. for the conventional oxide-coated cathodes, the residual gas had no influence on the noise, on the other hand, the pressure of neon in tungsten cathodes causes noise [8]. The existence of more than one mode which is called pairs of degenerate modes, doublets, also produces the noise. Except $\pi - mode$, two components of doublets have nearly same frequencies, but not exactly same and these prevents the desired mode-frequency separation which causes the sideband noises. The starting time of oscillation is another noise generating phenomenon in magnetron [64].

4.2. NOISE REDUCTION TECHNIQUES

In order to increase performance, various methods are developed to suppress generated noise in magnetron operation. Although the noise generating mechanism is very complicated and it is not understood completely, since the measurements show the source of a noise in magnetron operation is based on the motion of particles in anode-cathode space, all methods intend to form the electron flow in the interaction space. These methods are

- Cathode priming
- Cathode shielding
- Electric priming
- Magnetic priming
- Strapped system

4.2.1. Cathode Priming

As mentioned in the previous part, rapid startup and mode locking are critical challenges for low noise levels. In cathode priming method, the electron emission from the cathode is

divided into N/2 parts to accomplish $\pi - mode$ operation. This division is actualized in two ways. On is that the single cathode is fabricated with N/2 emitting region. This operation can be made by laser micromachining of aluminum metal by projection ablation lithography (PAL) [65]. The other way is using N/2 separate cathode. Cathode priming simulations are performed by CST Particle Studio, the schematics and the result are shown in the following figures. In Figure 4.2, it is shown that using cathode causes the frequency shift, since the electron emissions also exist between the cathodes, and this leads the interaction space. The total simulation continues approximately five hours, when PIC solver time is chosen 30 ns.
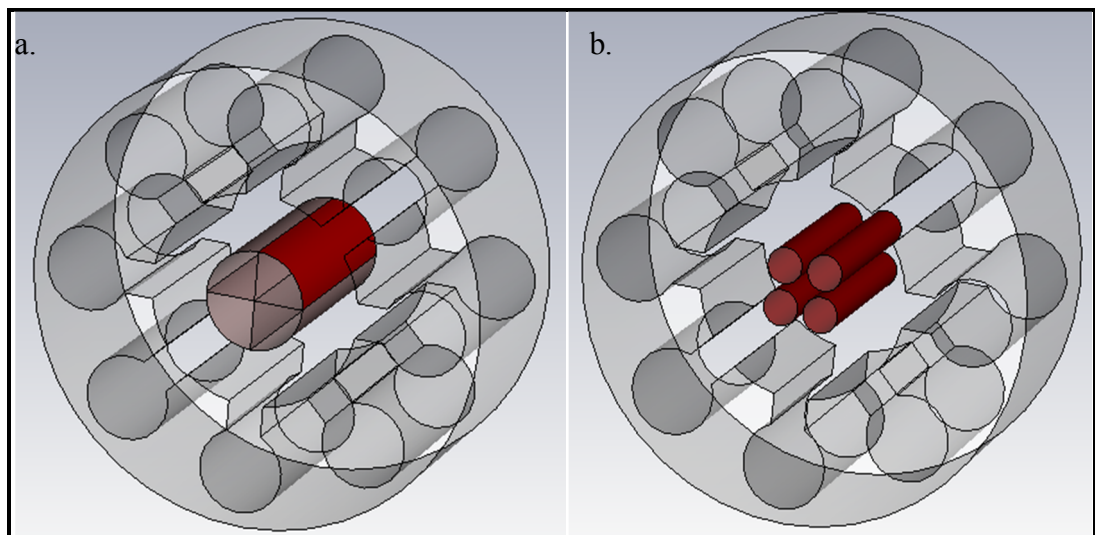
Figure 4.1. Basic configurations of cathode priming by CST Particle Studio, a. Single cathode with (N/2) four electron emission regions, b. (N/2) four separate cathode
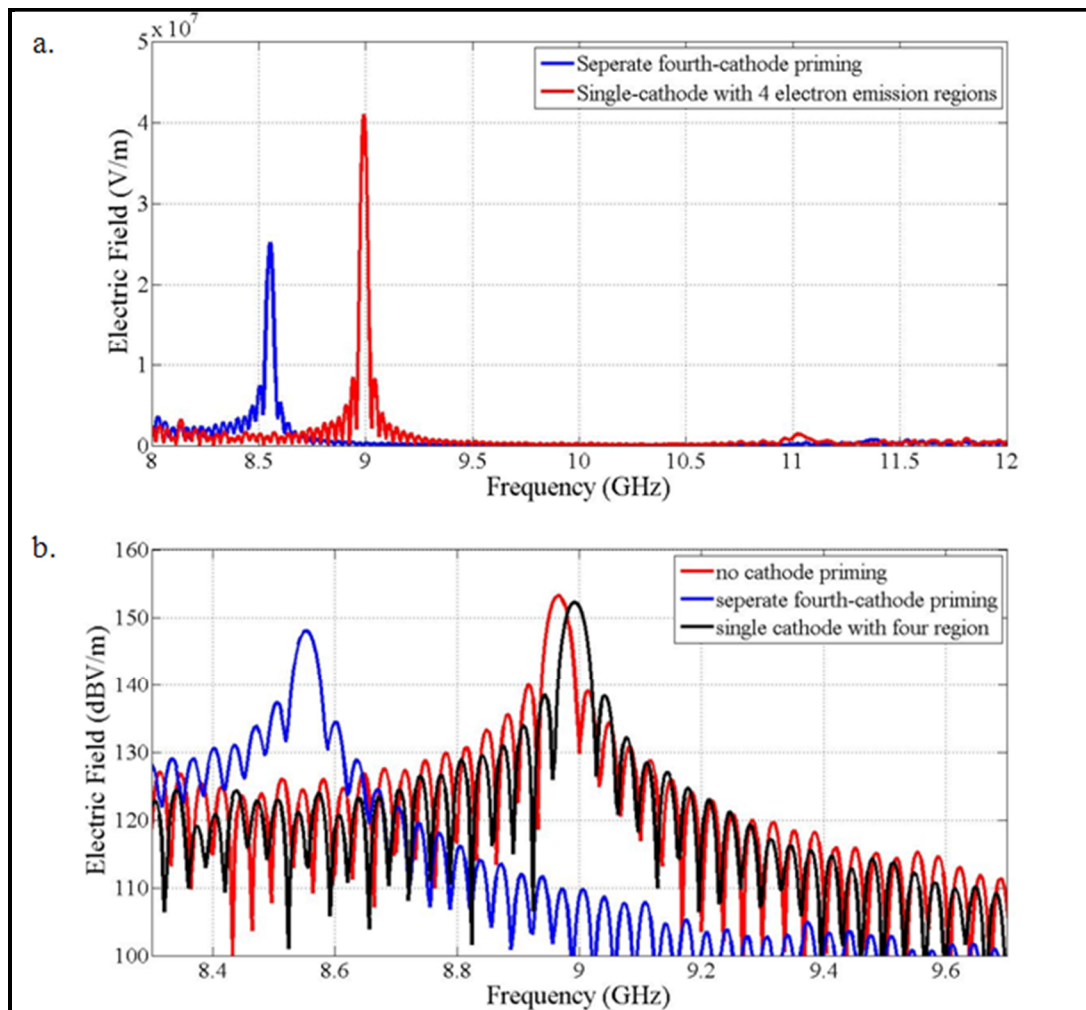
Figure 4.2. a. b. The comparison of cathode priming methods. Measured data from the CST Particle Studio simulations

4.2.2. Cathode Shielding

Another technique to suppress the noise in the magnetron is shielding the cathode ends by metals. The cathode shielding can be applied to both sides of the cathode [66], or just one side [67]. The schematics of magnetron cathodes are shown in Figure 4.3.
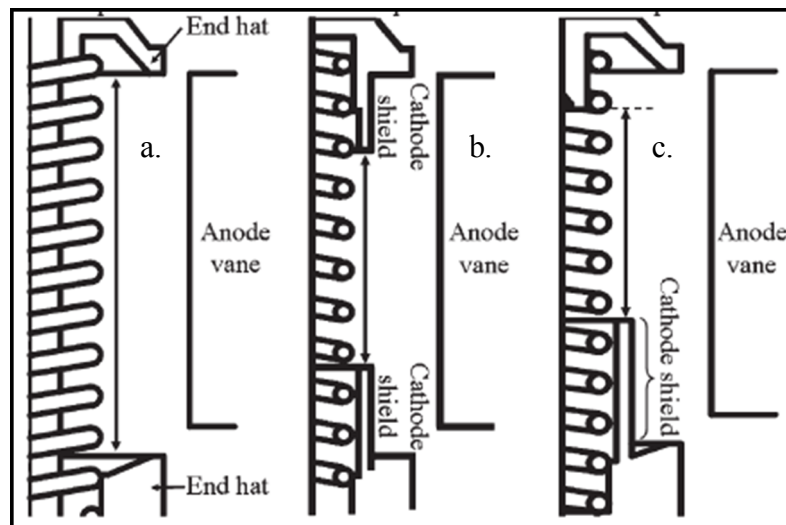
Figure 4.3. The inside schematics of a. Conventional magnetron, b. Cathode shields on both sides of the cathode, c. Cathode shield on one side [67]

This noise reduction technique is used to prevent the electron emission from the end portions of the cathode and it causes to reduce the spurious noise. The simulations verify the results in [67] unlike in [66]. The axially asymmetric configuration works better than axially symmetric configuration. Here, the important phenomenon is that, this "axially asymmetric" situation is also valid for other noise reduction techniques such as strapping and magnetic priming which will be shown in the following parts.

In our CST Particle Studio simulations, since the cathode structure is not formed from filaments as in Figure 4.3, the cathode shield part is built distinctly. The schematic is presented in Figure 4.4.
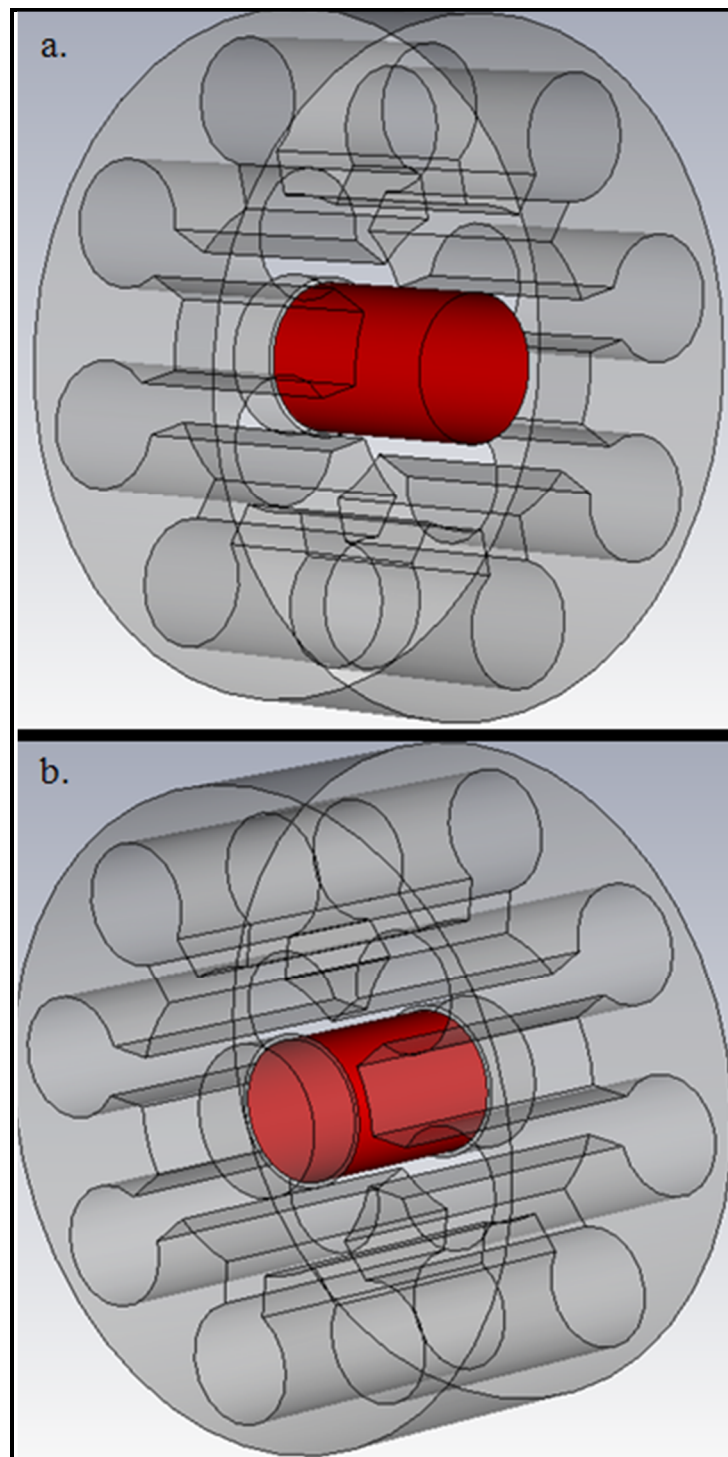
Figure 4.4. a. The schematic of magnetron with a cathode shield on one side, b. The schematic of magnetron with a cathode shield on both sides. The red parts specify the emitted regions of cathode

The most important parameters in this configuration are the height and the thickness of the cathode shield. The desired values are determined by numbers of simulations. The measured probe electric field magnitude is given in Figure 4.5.
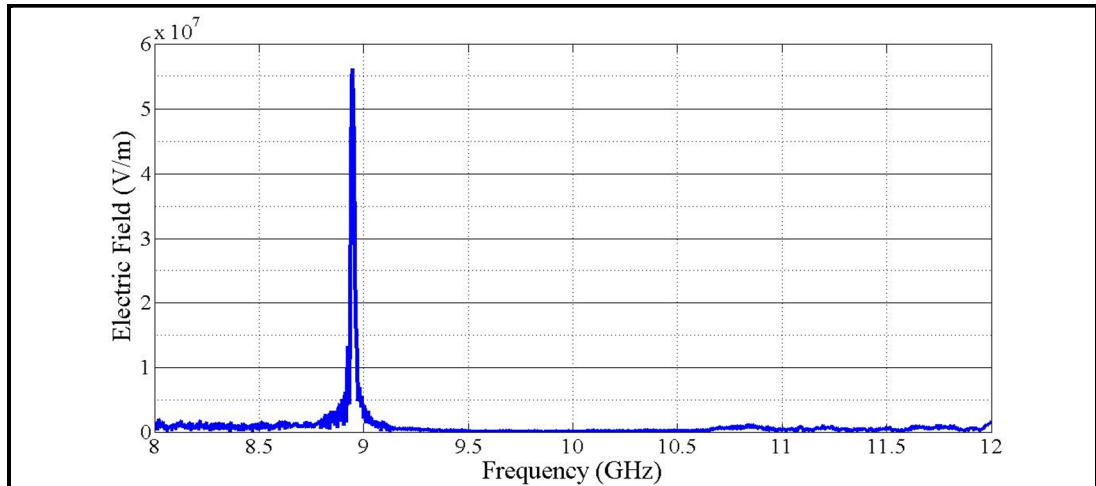
Figure 4.5. The electric field variation for whole frequency band in magnetron operation using cathode shielding noise reduction technique. PIC solver time is adjusted to 80 ns

When axially symmetric configuration of cathode shield is used as in Figure 4.4.b., the comparative results are shown in Figure 4.6.and Figure 4.7. The electrons are emitted in the middle section of the cathode.
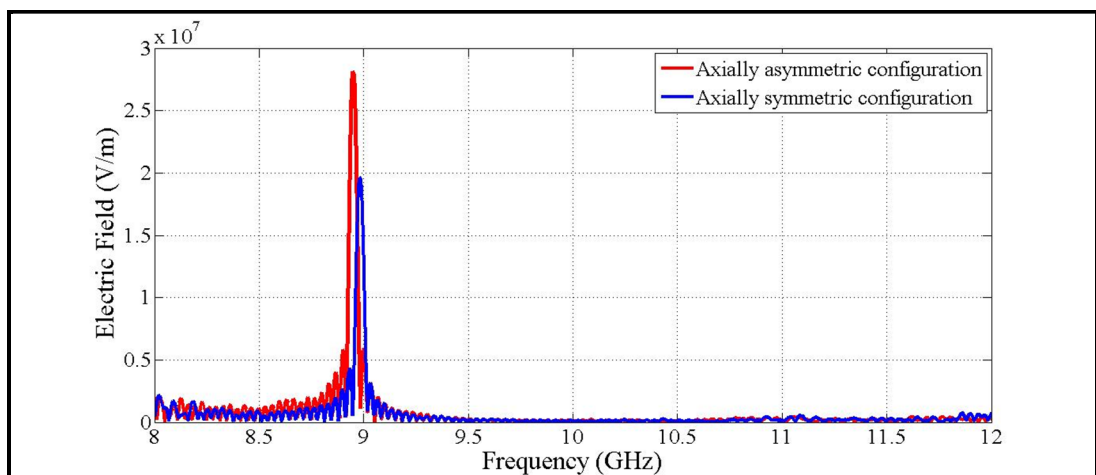
Figure 4.6. The electric field values for two different cathode shield configuration. PIC solver time is chosen 30 ns for simulation process
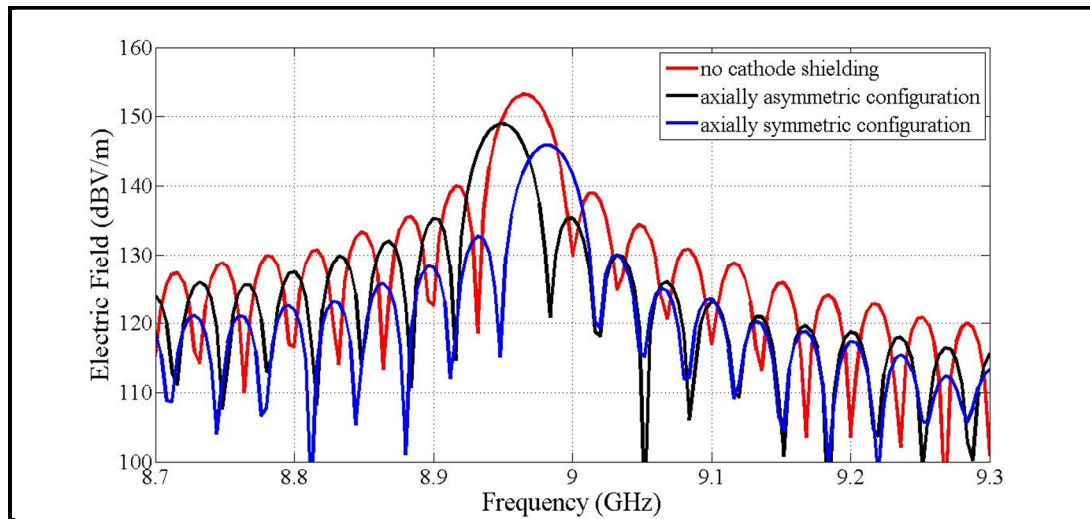
Figure 4.7. The comparison of cathode shielded magnetrons with conventional one. Detail view of the frequency spectrum of three types structure; red curve represents a magnetron that is not used any type of noise reduction method, black curve is used for a cathode shielded structure with axially asymmetric configuration, and blue one is used for a cathode shielded magnetron with axially symmetric configuration

4.2.3. Electric Priming

This method is based on the electron prebunching into the $\pi - mode$ using the anode shape modification, hence, the noise is planned to reduce. The electric priming experiment was performed in strapped magnetron and the noise suppression appeared in [68]. Various modifications are made in anode structure and the schematics are shown in the following figures
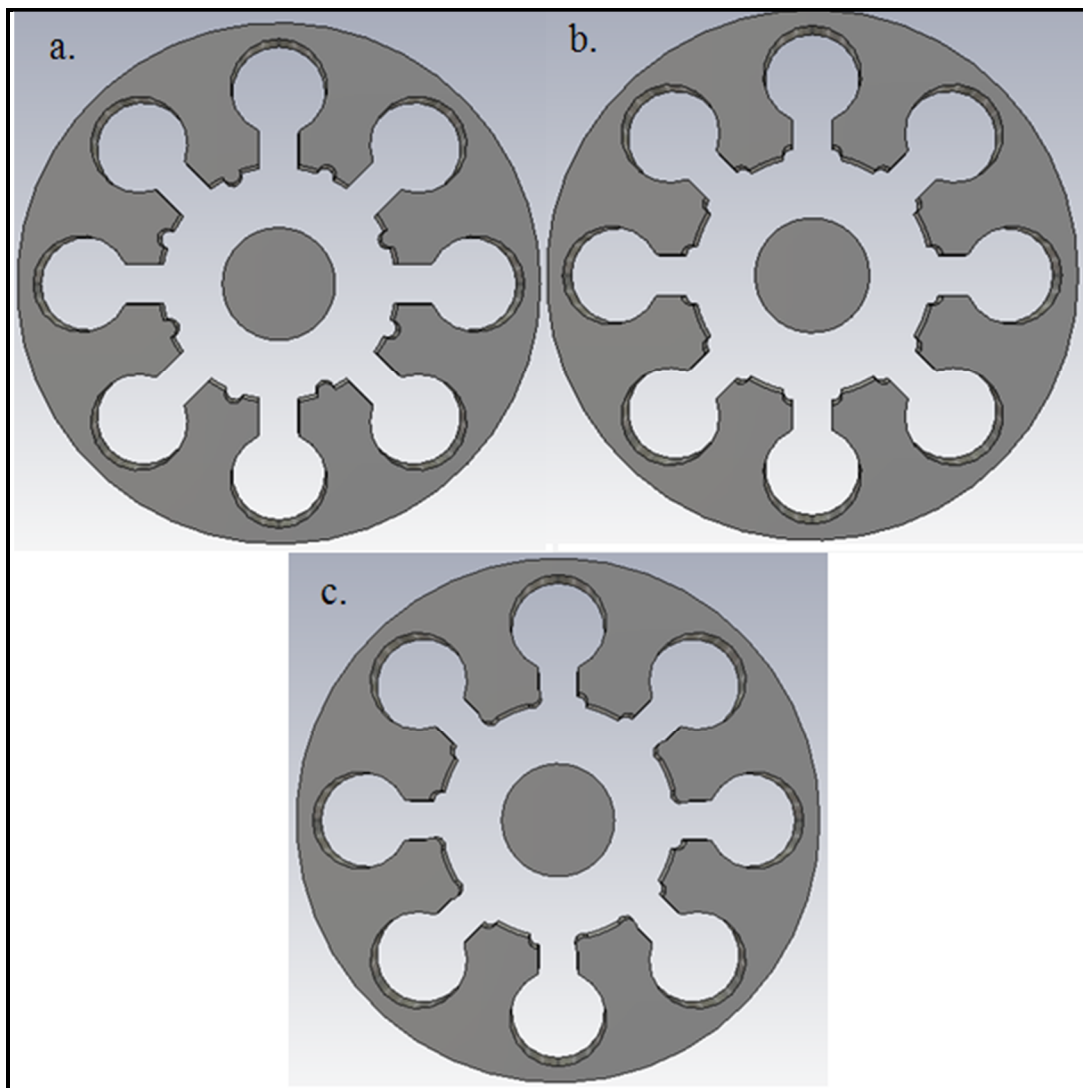
Figure 4.8. The schematics of eight cavity magnetron with three different anode modifications, a. The middle of the anode structure between the slots are perturbed, b. Two edges are cut, c. One edge is cut, the other edge is expanded. All cuts are cylindrical for both three models

For all types, the purpose is to create a perturbed electric field along the azimuthal direction using periodic shape modifications. The resonant frequency is also affected from these modifications. The related results with different anode modified magnetrons are presenting as
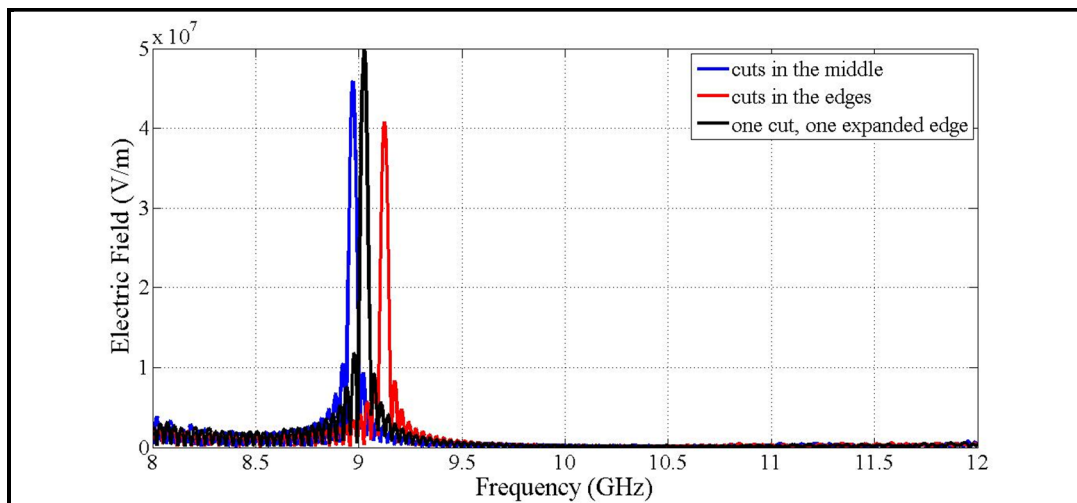
Figure 4.9. The electric field simulation results of three different anode modified magnetrons
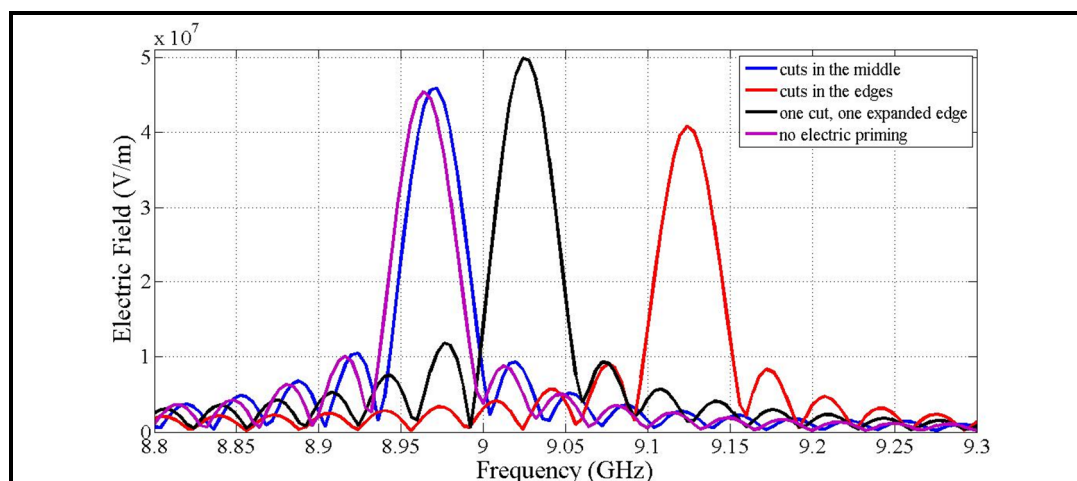
Figure 4.10. The comparison of applied electric priming magnetrons with conventional one. Detail view of the frequency spectrum of four types structure; pink curve represents a magnetron that is not used any type of noise reduction method, black curve represents a structure as in Figure 4.8.c., blue one is used for a model represented in Figure 4.8.a., red curve is used for a structure modeled in Figure 4.8.b.

The size of the variations in anode shape also affects the result; this can be seen in the following figure,
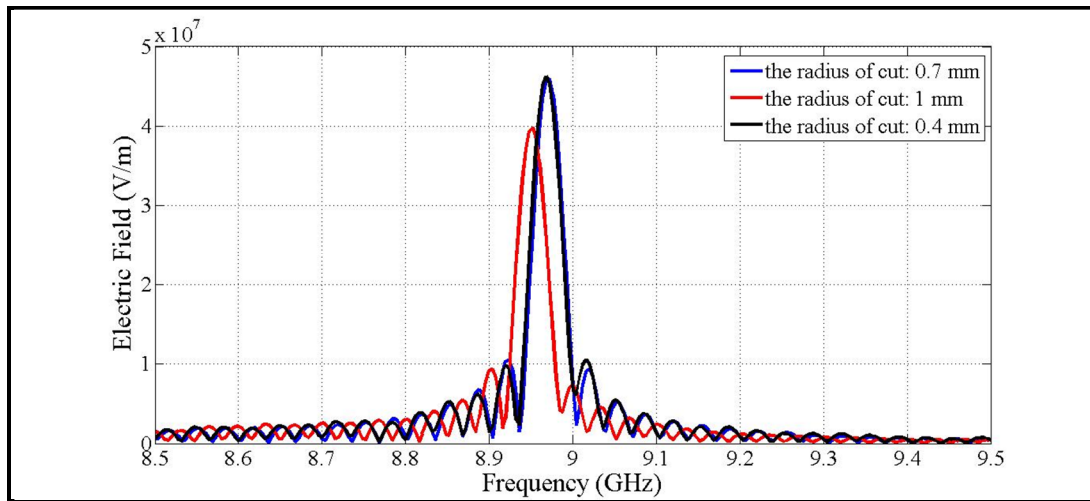
Figure 4.11. Obtained electric field values of three different models. The modification type is same for all simulated magnetrons, the radiuses of cuts are different in structures

4.2.4. Magnetic Priming

Magnetic priming method is based on generating an azimuthally varying non-uniform magnetic field. In this case the magnetic field is intended to perturb instead of electric field being in electric priming technique. This is one of the most investigated and applied method in noise reduction techniques [61, 64, 69, 70]. Azimuthally varying non-uniform magnetic field enable the more electrons emitted and enhance the startup performance of $\pi - mode$ oscillation which causes noise reduction and improves the frequency spectrum [71]. Since it is not necessary to make big changes in the structure and redesign the anode block, applying magnetic priming is relatively easy compared to other methods.

For an N-cavity magnetron, N/2 magnetic field perturbations are imposed in the azimuthal direction by added N/2 magnets on the perimeter of the existing magnet to operate the magnetron in $\pi - mode$. The perturbing magnets should have the same polarity. This technique can be applied axially symmetric or asymmetric as in cathode shielding method.
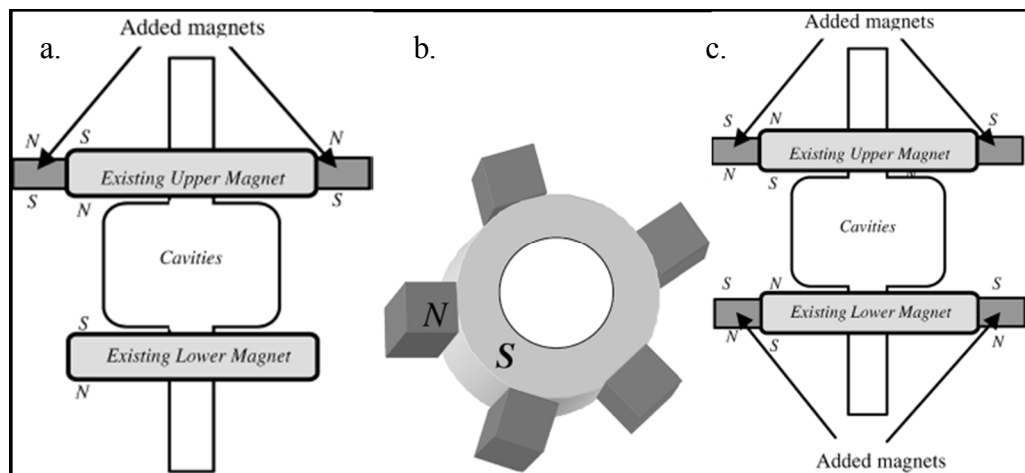
Figure 4.12. a. Side view of axially asymmetric magnetic priming configuration, b. 3D view of magnetic priming configuration with added 5 perturbing magnets for 10-cavity magnetron, c. Side view of axially symmetric magnetic priming configuration [64]

In our simulations, magnetic field has been applied by defining analytical source field until now, but azimuthally varying magnetic field cannot be applied by this way. Therefore, the magnets are used to provide the essential and perturbing magnetic field. The schematic is shown in Figure 4.13,
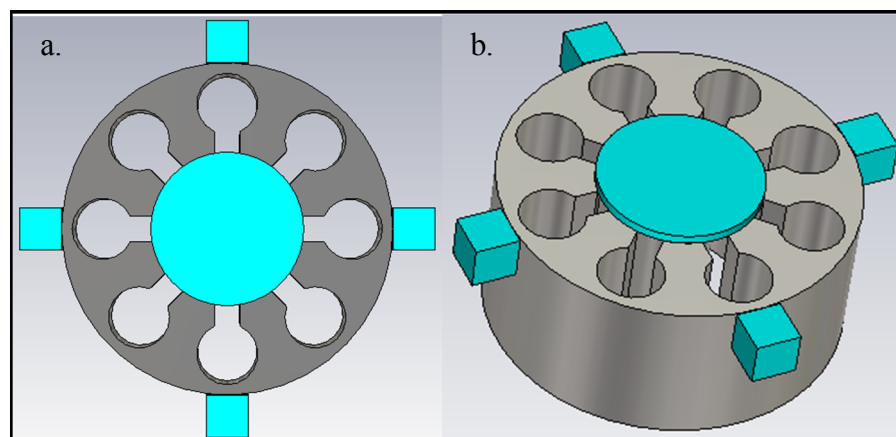
Figure 4.13. The 3D schematics of the magnetic priming magnetron in CST Particle Studio with four (N/2) square perturbing magnets added on the perimeter of the anode structure, a. Top view, b. Side view

The magnetic field values of perturbing magnets and essential magnet are 0.11and 0.22 Tesla, respectively and the polarities are inverse. The correct values of parameters are found by the optimization process. The frequency spectrum of this model appears as
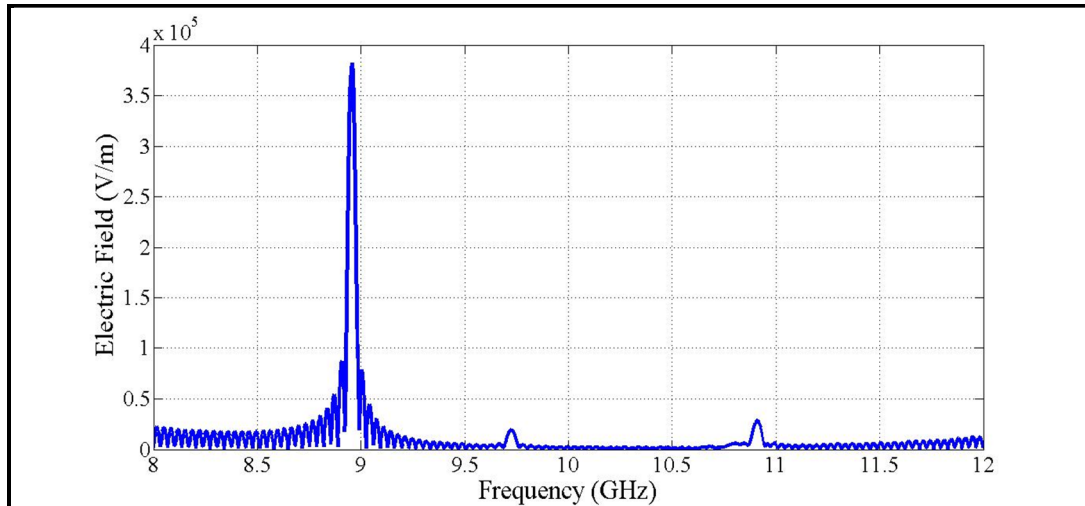
Figure 4.14. The frequency spectrum of the magnetron with perturbed magnetic field
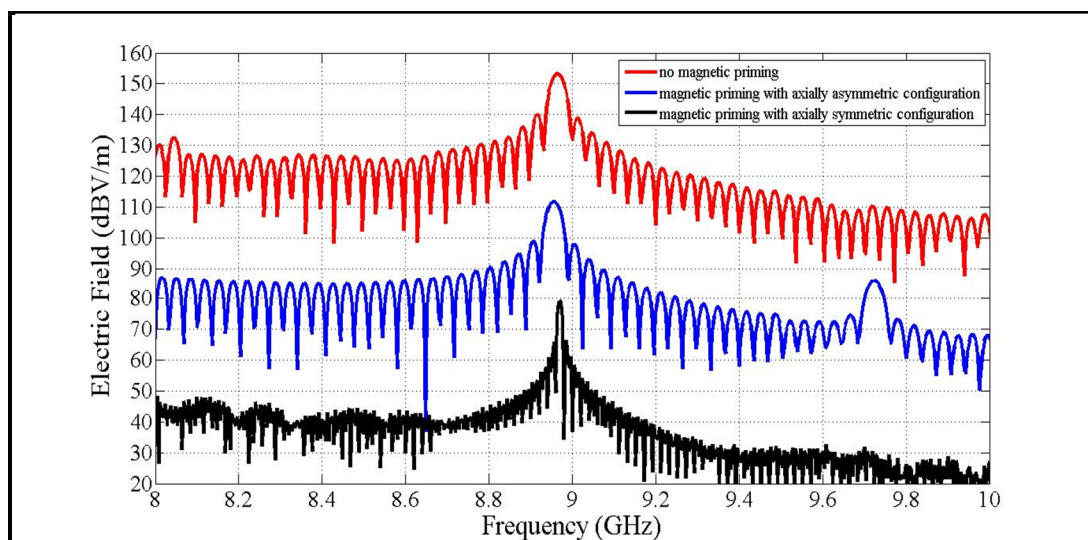
Figure 4.15. The comparison of frequency spectrums for three different magnetrons. Red curve indicates microwave spectrum with unperturbed magnetic field, blue curve is used for axially asymmetric configured magnetron, and black curve represents axially symmetric configured magnetron. PIC solver time is fixed as 30 ns for simulation process

4.2.5. The Strapped System

Strap is a conductor connected to alternate segments of the magnetron to make the phase difference between them zero. It is first used in 1941 by Randall and Sayers at Birmingham as a name "mode locking system". It is shown that the operating frequency was increased to about 50 percent [8]. The strap may be continuous or broken at one point above a segment to which is not brazed. Strapping can be made in two general form; ring strapping and echelon strapping. Ring strapping is also divided into groups such that single ring and double ring. These mentioned types are illustrated in Figure 4.16 and Figure 4.17. In double ring design, an individual segment is connected to only one of straps.
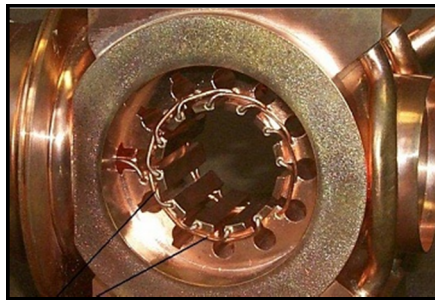
Figure 4.15. The echelon strapping [4]
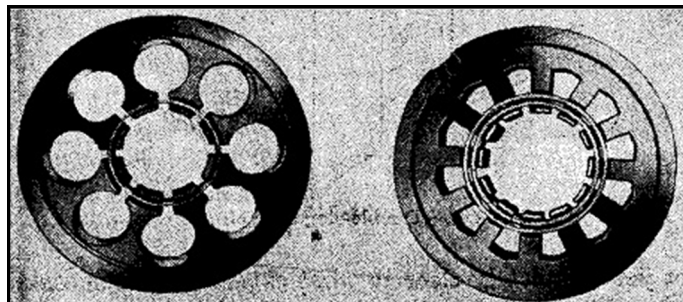
Figure 4.17. Single and double ring strapping of magnetrons [8]

Adding strap affects the capacitance and inductance of the individual cavities that adjust the resonant frequency of the magnetron as shown in equivalent circuits in Figure 4.18.
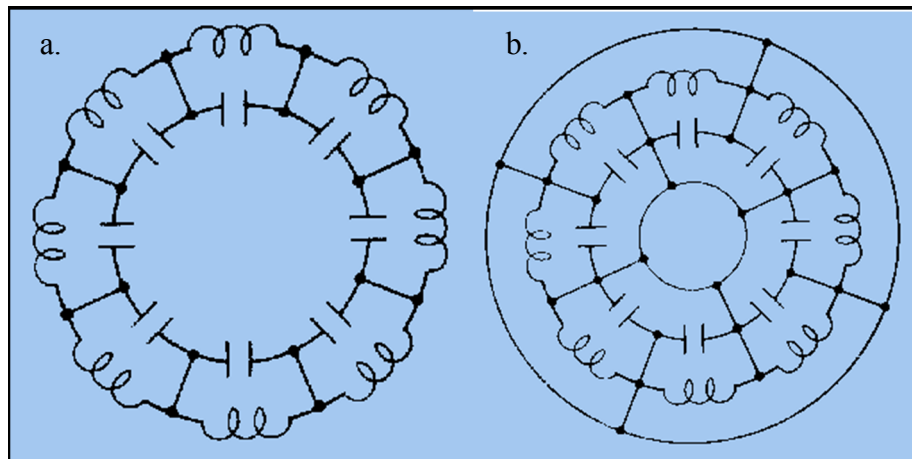
Figure 4.18. The electrical equivalent model of a. Unstrapped and b. Strapped magnetrons [72]

When the magnetron operates in a $\pi - mode$, all connected segments by straps, are at the same potential, thus there exists no current flowing through the straps, but the adjacent segment which is connected with other set of strap, the adjacent anode blocks have more different potentials as it is compared with unstrapped case, thus there will be increase in effective capacitance that is in parallel with the resonator capacitance. This causes a decrease in frequency of $\pi - mode$. For any other mode, this potential difference between the adjacent segments is not as large as the potential difference in $\pi - mode$. As a similar approach, except $\pi - mode$, there exists a current flowing along the straps, this causes an inductance in parallel with the effective resonant inductance, leads to an increase in resonant frequency of other modes. Hence, the effect of strapping can be summarized that the resonant frequency of $\pi - mode$ is decreased, whereas the frequencies of other modes are increased. In this way, the mode separation can be provided. This effect can also be seen in Figure 4.19.
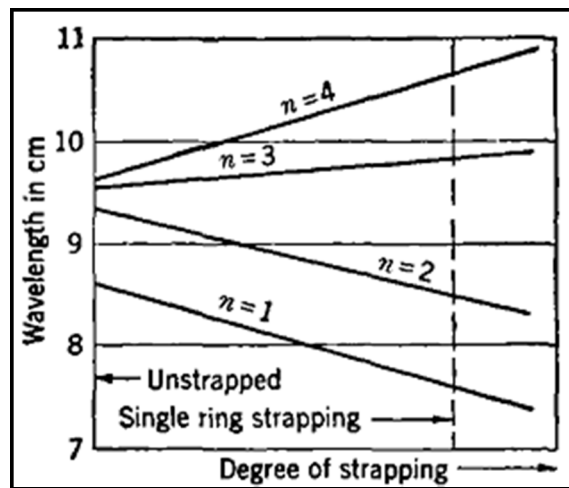
Figure 4.19. The effect of strapping on mode separation in an eight cavity magnetron [8]

CST Particle Studio schematics and the simulation results are presented in the following figures,
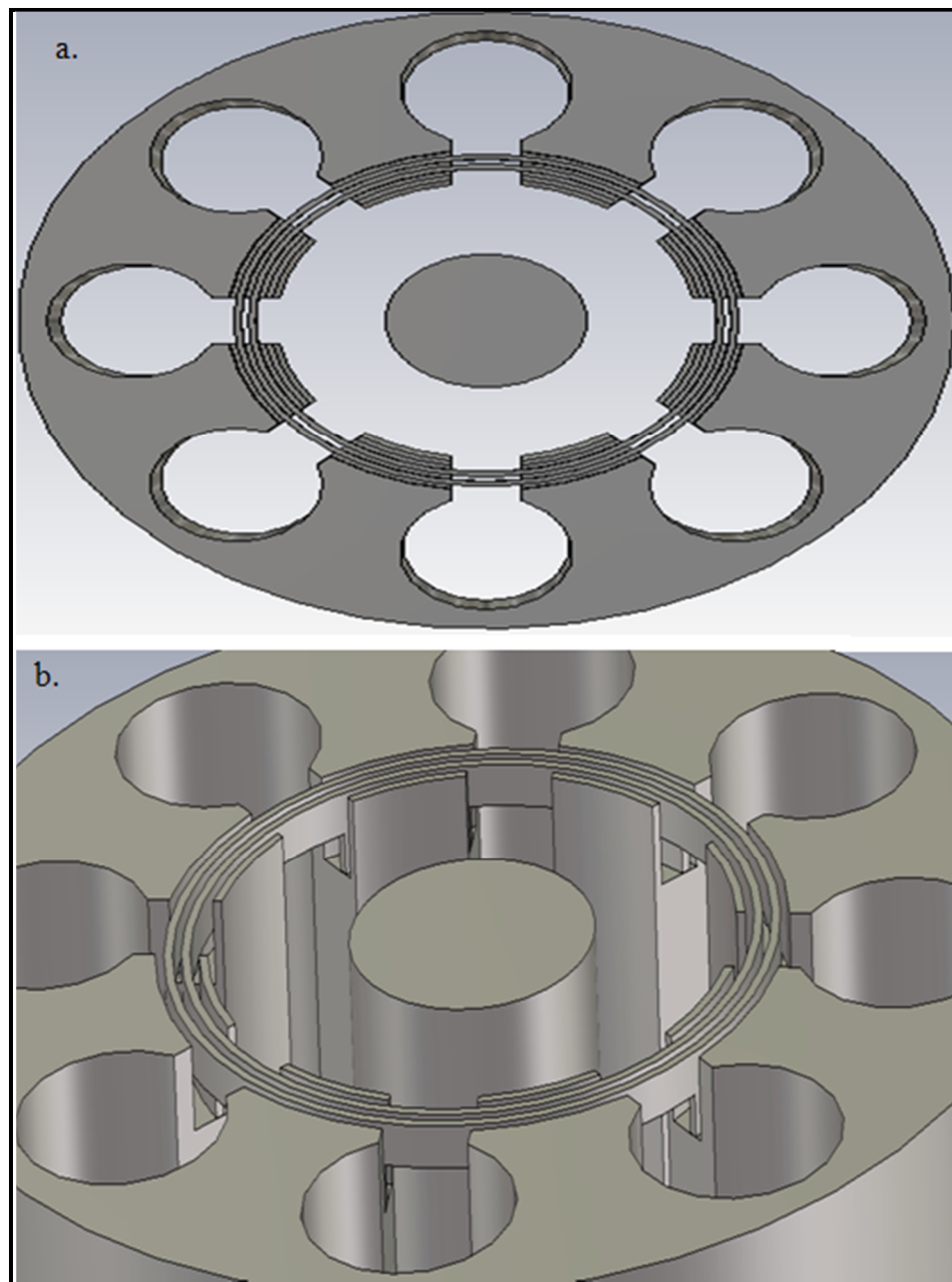
Figure 4.20. Different 3D views of strapped magnetron model. The strap is used on one side of the anode block
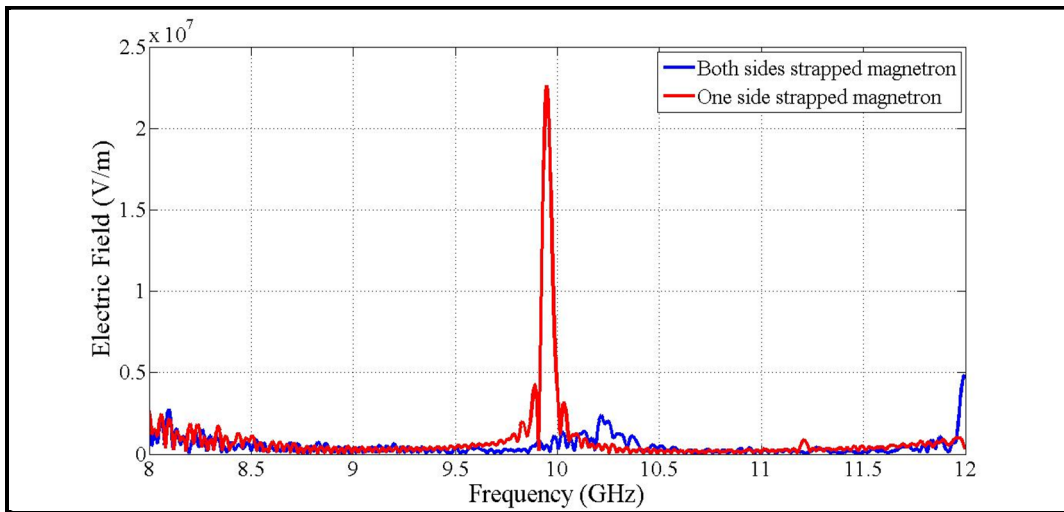
Figure 4.21. The frequency spectrum of designed strapped magnetrons. The structure dimensions are same
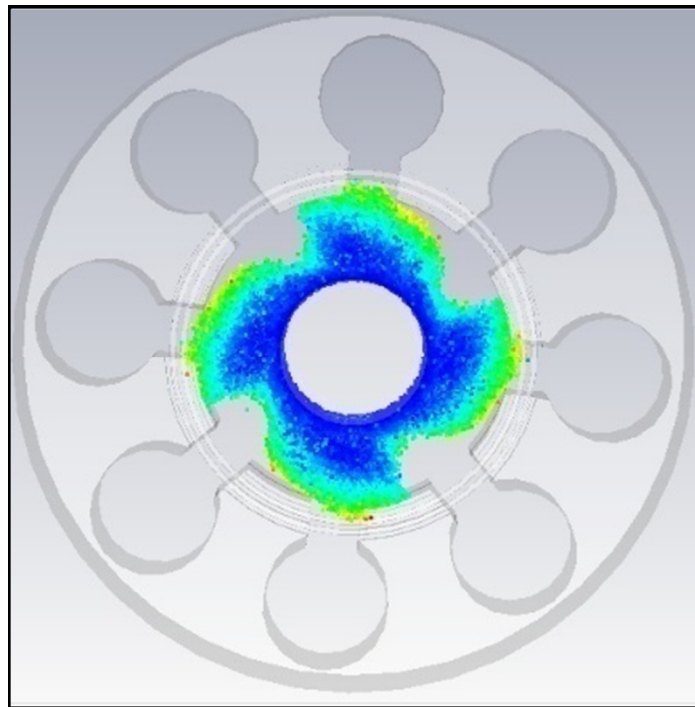
Figure 4.22. The image of electron beam of one side strapped magnetron. The shape was formed as desired in $\pi-mode$ operation. There exist four beams which is expected for 8-cavity magnetron

The other technique to make the frequency difference as it is desired is the change of a magnetron anode block structure. This type of magnetron is called rising sun type magnetron which was explained in detail in section 2.2.3.3.

The last but not the least important parameter for stable operation is selected PIC time, in other words operation time. As in mentioned in chapter 3, although the simulation time also increases too much and the simulations cannot be finished in a few hours, PIC solver time should be chosen as much as possible. Its significant effect can be seen in the following figures
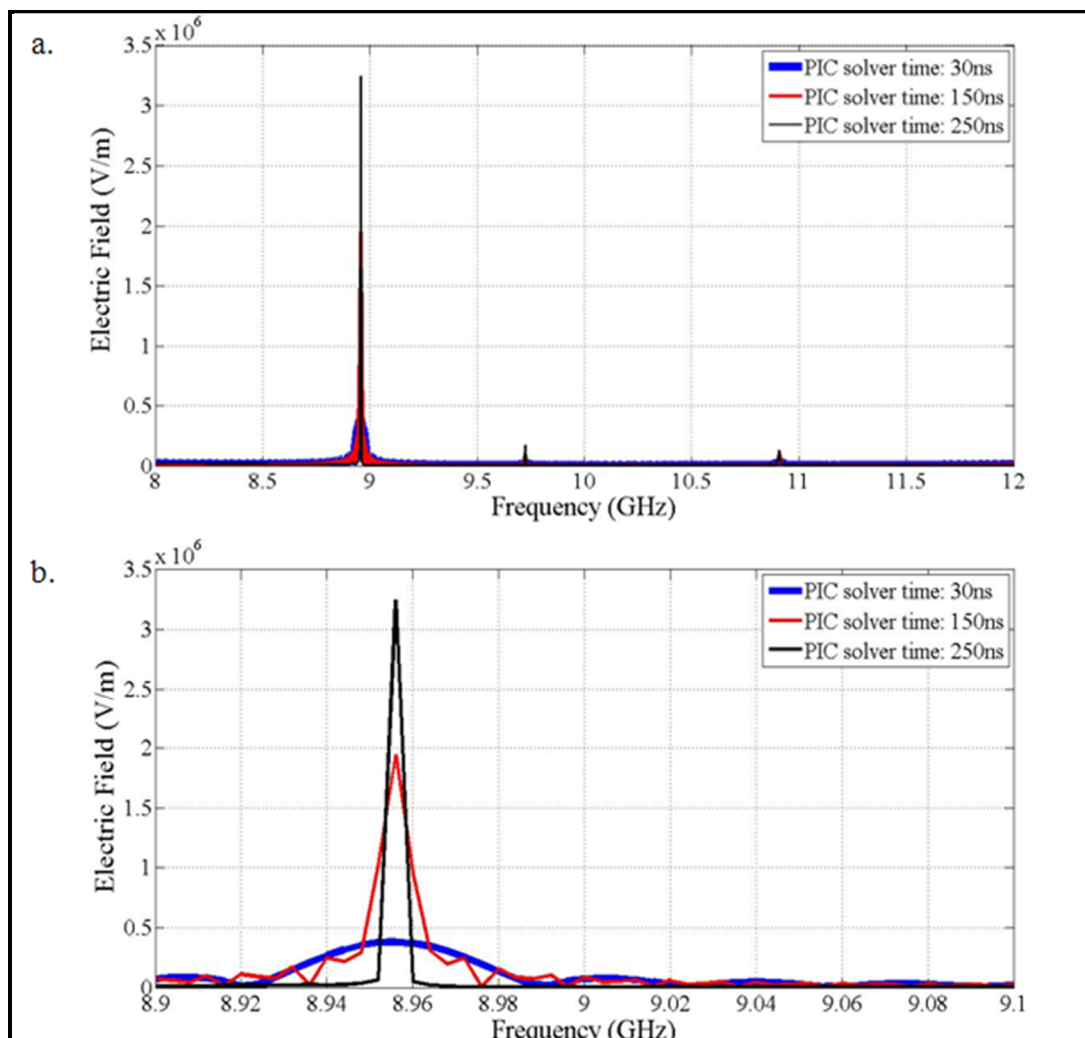
Figure 4.23. a. The frequency spectrum of magnetic priming magnetrons having three different PIC solver times, b. Detailed view of Figure 4.21.a
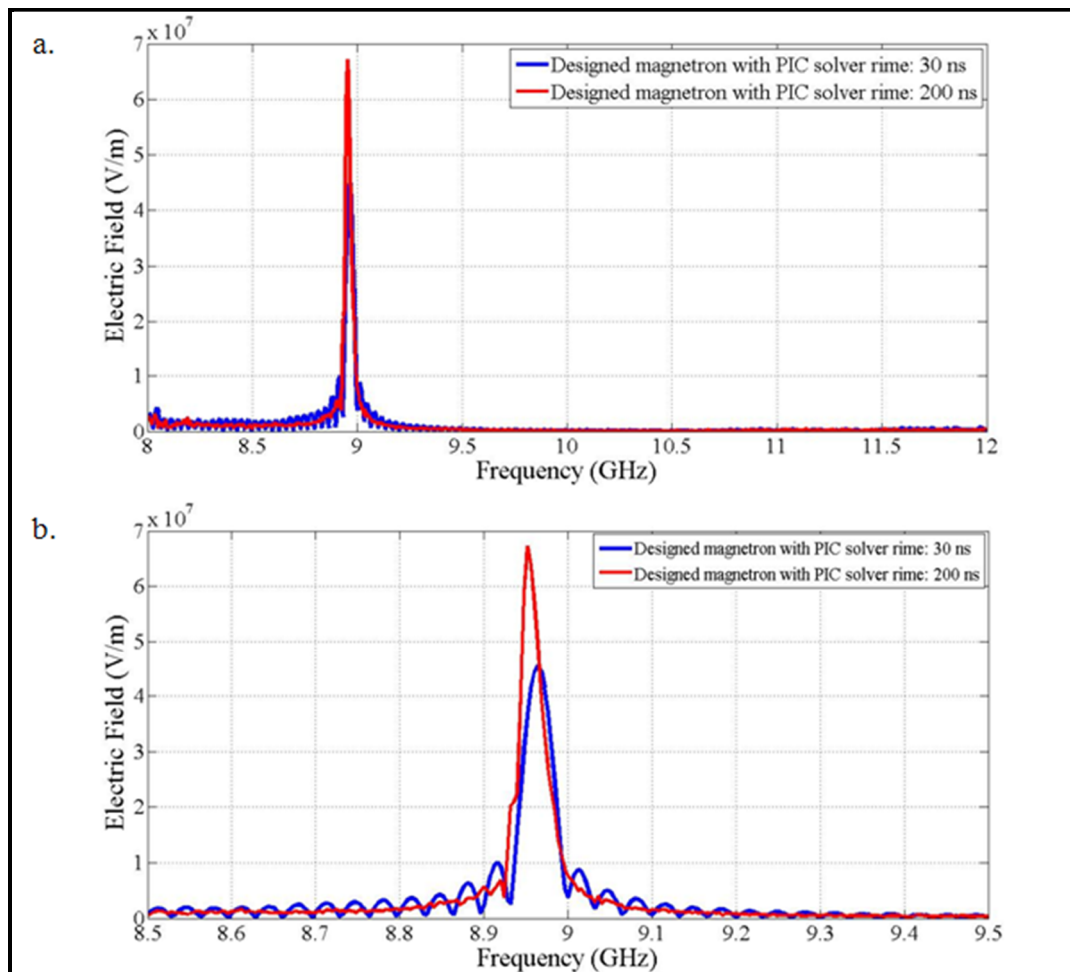
Figure 4.24. a. The frequency spectrum of magnetrons having two different PIC solver times. 15 dB sideband noise level decrement is provided, b. Detailed view of Figure 4.24.a

These results show that PIC solver time should be long enough to interpret the behavior of the designed magnetron completely. There is not specific unique simulation time, it is determined by controlling the behavior of the magnetron is either stable or not. 15-30 dB sideband noise level decrements are provided by true PIC solver time. Therefore, before arriving a final magnetron design, the structure should be simulated at long PIC solver times to see the real performance.

5. CONCLUSIONS

In this thesis, comprehensive magnetron history, theory and design are presented. Conventional cavity magnetron device is investigated in different perspectives. Following the history and the importance of cavity magnetrons, a design procedure for hole-slot type cavity magnetron is derived.

The electron motion in an electromagnetic field inside a cylindrical diode, the theory and operating principles of magnetron are explained in Chapter 2. The principles of design and required expressions about a design strategy are derived in Chapter 3. According to these equations, an X band 8 cavity hole – slot type magnetron is designed. Using CST Particle Studio, designed magnetron performance is controlled by various parameters. The validity of CST Particle Studio which has not been used as a magnetron design up until now is examined. During these simulations, the effects of the program parameters such as mesh number, solver types and numbers of emission points in cathode block are investigated. The impact of design parameters on the performance of an X-band magnetron are studied in detail. It is verified that the derived expressions and the proposed design method for a conventional hole–slot type magnetrons are in good agreement. We believe we presented a simple and accurate way to design this type of magnetrons. This design procedure consists of four steps. However, one should remember that these expressions give initial parameters that they should be optimized by the particle simulator used for the design. The time required for the designed magnetron model simulations is based on the program parameters such as mesh size, PIC solver time and the number of emission points. In general, this time varies from approximately three hours to 60 hours on a three GHz CPU, six GB RAM computer.

The magnetron noise and the reduction techniques are also investigated. The noise performance is analyzed on the X band hole – slot type eight cavity magnetron. The most important result about the noise is that axially asymmetric structures are more successful compared to those of symmetric ones. Another important observation is that the simulation time is a very critical parameter and it should be long enough to make magnetron simulation settle down for noise characterization.

REFERENCES

1. Symons, R. S., "Modern Microwave Power Sources", *IEEE Aerospace and Electronic Systems Magazine*, Vol. 17, pp. 19-26, 2002.

2. Collin, R. E., *Foundations for Microwave Engineering*, Second Edition, The IEEE Press Series on Electromagnetic Wave Theory, Wiley-Interscience, 2001.

3. Liao, S. Y., *Microwave Devices and Circuits*, Third Edition, Prentice Hall, Englewood Cliffs, New Jersey.

4. Ma, L., *3D Computer Modeling of Magnetrons*, PhD Thesis, The University of London, 2004.

5. Gilmour, A. S. Jr., *Principles of Travelling Wave Tubes*, Artech House, 1994.

6. Benford, J., "History and Future of the Relativistic Magnetron", *IEEE International Conference on the Origins and Evolution of the Cavity Magnetron*, Bournemouth, 19-20 April 2010, pp. 40-45, 2010.

7. Redhead, P. A., "The Invention of the Cavity Magnetron and Its Introduction into Canada and the U.S.A.", *Article De Fond*, La Physique Au Canada, Novembre/Decembre 2001.

8. Collins, G. B, *Microwave Magnetrons*, MIT Radiation Laboratory Series, McGraw-Hill Book Company, Inc. 1948.

9. Andreev, A. D., K. J. Hendricks, "First Multi-cavity Magnetrons were built in NII-9, Leningrad, during the Spring of 1937", *IEEE International Conference on the Origins and Evolution of the Cavity Magnetron*, Bournemouth, 19-20 April 2010, pp. 71-75, 2010.

10. Bekefi, G., and T.Orzechowski, "Giant microwave bursts emitted from a field-emission, relativistic-electron-beam magnetron", *Phys. Rev. Lett.*, Vol. 37, p. 379, 1976.

11. Pengvanich, P., *Theory of Injection Locking and Rapid Start-up of Magnetrons, and Effects of Manufacturing Errors in Terahertz Travelling Wave Tubes*, PhD Thesis, The University of Michigan, 2007.

12. Pozar, D. M., *Microwave Engineering*, Third Edition, John Wiley & Sons, Inc. 2005.

13. Boot, H. A. H., J. T. Randall, "Historical Notes on the Cavity Magnetron", *IEEE Transactions on Electron Devices*, Vol. 23, pp. 724-729, 1976.

14. Electrical Engineering Training Series, "Negative Resistance Magnetron", http://www.tpub.com/neets/book11/45g.htm [retrieved 10 January 2011].

15. Boumeester, H. G., *Entwicklung und Herstellung der modernen Sende - Röhren*, Philips Technische Rundschau, April 1937.

16. Boulding, R.S.H., *The Resonant Cavity Magnetron*, The Whitepriars Press Ltd., 1952.

17. Boot, H. A. H., J.T. Randall, *The Cavity Magnetron*, F.R.S., July 1946.

18. CPI Company, *Magnetron Theory of Operation*, Beverly Microwave Division Report.

19. Tsimring, S. E., *Electron Beams and Microwave Vacuum Electronics*, John Wiley & Sons, Inc 2007.

20. Christian Wolf, http://www.radartutorial.eu/08.transmitters/tx08.en.html [retrieved 12 January 2011].

22. Goerth, J., "Early Magnetron Development especially in Germany", *IEEE International Conference on the Origins and Evolution of the Cavity Magnetron*, Bournemouth, 19-20 April 2010, pp. 17-22, 2010.

23. Electrical Engineering Training Series, "Velocity Modulation", http://www.tpub.com/neets/book11/45a.htm [retrieved 18 January 2011].

24. Das, A., Sisir K. Das, *Microwave Engineering*, Tata McGraw-Hill Publishing Company Limited, 2000.

25. Treado, T. A., W. O. Doggett, G. E. Thomas, R. S. Smith III, J. J.-Ford, D. J. Jenkins, "Operating Modes of Relativistic Rising-Sun and A6 Magnetrons", *IEEE Transactions on Plasma Science*, Vol. 16, pp. 237-248, April 1988.

26. A. Palevsky, and G. Bekefi, "Microwave emission from pulsed, relativistic e-beam diodes II: The multi resonator magnetron", *Phys. Fluids*, 22, 986, 1979

27. Saveliev, Y. M., B. A. Kerr, M. I. Harbour, S. C. Douglas, W. Sibbett, "Operation of a Relativistic Rising-Sun Magnetron with Cathodes of Various Diameters", *IEEE Transactions on Plasma Science*, Vol. 30, pp. 938-946, April 2002

28. Fuks, M. and E. Schamiloglu, "Rapid Start of Oscillations in a Magnetron with a 'Transparent' Cathode", *Phys. Rev. Lett.*, 95, 205101, 2005.

29. Julian Robinson, "High Average Power C & X - band magnetrons", *IEEE International Vacuum Electronics Conference*, 28-30 April 2009, pp. 548-549, 2009.

30. Jules Needle, *A developmental voltage - tunable microwave magnetron*, Tech. Report No. 11, Electron Tube Laboratory, Dept. of Elect. Eng., University of Michigan, August 1951.

31. Willshaw, W. E., L. Rushforth, A. G. Stainsby, R. Latham, A. W. Balls, a. H. King, "The High-Power Pulsed Magnetron. Development and Design for Radar Applications", *Radio Section Paper*, Vol. 93, part IIIA, 30 April 1946.

32. Kroll, N. M., W. E. Lamb, "The Resonant Modes of the Rising Sun and Other Unstrapped Magnetron Anode Blocks", *Journal of Applied Physics*, Vol. 19, February 1948.

33. Brady, M., M. Edwards, "Developments in Marine Radar Magnetrons", *International Conference on the Origins and Evolution of the Cavity Magnetron (CAVMAG)*, 19-20 April 2010, pp. 58-63, 2010.

34. Cripps, A. M., P. A. Jerram, "X band linear accelerator magnetrons", *19th European Microwave Conference*,4-7 Sept. 1989, pp. 1086-1090, 1989.

35. Vaughan, J. R. M., "Magnetron anode erosion in the presence of cathodes containing oxides", *IEEE Transactions on Electron Devices*, Vol. 17, Issue 4, pp. 377, Apr 1970.

36. Zhang, E. Q., "On the magnetron cathode", *IEEE Transactions on Electron Devices*,Vol. 33, Issue 9, pp. 1383-1384, Sep. 1986.

37. Pomerantz, M. A., "Magnetron cathodes", *IRE Proceedings*, Vol. 34, Issue 11, pp. 903-910, Nov. 1946.

38. Gilmour, A. S. Jr., *Magnetron Calculation Example*, 4 May 2010.

39. Weatherall, J. C., "Numerical Simulations of a Relativistic Magnetron", *IEEE Transactions on Plasma Science*, Vol. 18, no.3, pp. 603-610, June 1990.

40. Dombrowski, G. E., "Computer Simulation Study of Primary and Secondary Anode Loading in Magnetrons", *IEEE Transactions on Electron Devices*, Vol. 38, no. 10, pp. 2234-2238, October 1991.

41. Chen, X., M. Esterson, P. A. Lindsay, "3D simulation of microwave magnetrons", *IEE Colloquium on High Frequency Simulation: Part Two*, Nov. 1997.

42. Chen, X., M. Esterson, P. A. Lindsay, "Computer Simulation of a High - Power Magnetron and the Possible Implications for the RF Pulse Shortening", *IEEE Transactions on Plasma Science*, Vol. 26, no.3, pp. 726-732, June 1998.

43. McDowell, H. L., "Magnetron Simulations Using a Moving Wavelength Computer code", *IEEE Transactions on Plasma Science*, Vol. 26, no.3, pp. 980-983, June 1998.

44. Wang, Z., X. Chen, M. Esterson, P. A. Lindsay, "Characterization of Resonance Modes of a Magnetron Cavity", *27th IEEE International Conference on Plasma Science*, 2000.

45. Kim, J., J.-H. Won, H.-J. Ha, J.-C. Shon, G.-S. Park, "Three-Dimensional Particle-in-Cell Simulation of 10-Vane Strapped Magnetron Oscillator", *IEEE Transactions on Plasma Science*, Oct 2004, Vol. 32, no.5, pp. 2099-2104, 2004.

46. Balk, M. C. "3D Magnetron Simulation with CST Studio Suite", *IEEE International Vacuum Electronics Conference (IVEC)*, 21-24 Feb. 2011, pp. 443-444, 2011.

47. Arter, W., J. W. Eastwood, "Characterization of Relativistic Magnetron Behavior by 3-D PIC Simulation", *IEEE Transactions on Plasma Science*, Vol. 26, no.3, pp. 714-725, June 1998.

48. Kim, H. J., J. U. Shin, J. J. Choi, "Particle in Cell Code Simulations on a Rising Sun Magnetron Oscillator", *IEEE Transactions on Plasma Science*, Vol. 30, no.3, pp. 956-961, June 2002.

49. Balk, M. C., *3D Magnetron Simulation with CST Studio Suite*, CST AG, Germany.

50. CST Particle Studio User Guide, *Solvers and Applications*, Mar-2009.

51. Birdsdall, C.K., "Particle-in-Cell Charged-Particle Simulations, Plus Monte Carlo Collisions with Neutral Atoms, PIC-MCC", *IEEE Transactions on Plasma Science*, Vol. 19, no. 2, pp. 65-85, April 1991.

52. CST Particle Studio User Guide, Particle Studio Emission Model Interview.

53. CST Particle Studio User Guide, CST Particle Studio, "Which Solver to Use" section.

54. CST Particle Studio User Guide, CST Particle Studio, "Eigenmode Solver Overview" section.

55. CST Particle Studio User Guide, CST Particle Studio, "Special Mesh Properties – Discretizer" section.

56. CST Particle Studio User Guide, CST Particle Studio, "Tracking Solver Overview" section.

57. CST Particle Studio User Guide, CST Particle Studio, "PIC solver overview" section.

58. Monossov, H. G., "Theoretical Studies of Magnetron Noise by Means of Two-dimensional Simulation" *4th IEEE International Conference on Vacuum Electronics*, 28-30 May 2003, pp. 370-371, 2003.

59. Yamamoto, K., H. Kuronuma, T. Koinuma and N. Tashiro, "A Study on Magnetron Noise", *IEEE Transactions on Electron Devices*, Vol. 34, no. 5, pp. 1223-1226, 1987.

60. Glass, R. C., G. D. Sims and A. G. Stainsby, "Noise in Cut-off Nagnetrons", *Journal of the Institution of Electrical Engineers*, Vol. 1, no. 2 , 1955.

61. Neculaes, V. B., R. M. Gilgenbach, Y. Y. Lau, M. C. Jones and W. M. White, "Low-Noise Microwave Oven Magnetrons with Fast Start-Oscillation by Azimuthally Varying Axial Magnetic Fields", *IEEE Transactions on Plasma Science*, Vol. 32, no. 1, pp.1152-1159, 2004.

62. Mitani, T., N. Shinohara, H. Matsumoto, M. Aiga and N. Kuwahara, "Experimental Research on Noise Reduction of Magnetrons for Solar Power Station/Satellite", *Proceedings of Radio Science Conference*, pp. 603-606, 2004.

63. Tahir, I., A. Dexter and R. Carter, "Noise Performance of Frequency and Phase-Locked CW Magnetrons Operated as Current-Controlled Oscillators", *IEEE Transactions on Electron Devices*, Vol. 52, no. 9, pp. 2096-2103, 2005.

64. Neculaes, V. B., M. C. Jones, R. M. Gilgenbach, Y. Y. Lau, J. W. Luginsland, B. W. Hoff, W. M. White, N. M. Jordan, P. Pengvanich, Y. Hidaka and H. L. Bosman, "Magnetic Priming Effects on Noise, Startup and Mode competition in magnetrons", *IEEE Transactions on Plasma Science*, Vol. 33, no. 1, pp. 94-102, 2005.

65. Gilgenbach, R. M., M. C. Jones, V. B. Neculaes, Y. Y. Lau, W. M. White, N. M. Jordan, B. W. Hoff, R. C. Edgar, P. Pengvanich and Y. Hidaka, "Cathode Priming of Magnetrons for Rapid Startup and Mode-Locking", *The Joint International Conference on Infrared and Milimeter Waves and 13th International Conference on Terahertz Electronics*, Vol. 2, pp. 535-536, 2005.

66. Kohsaka, A., H. Saitoh, and T. Kawaguchi, "Low Profile and Clean Spectrum Magnetron", *J. Microwave Power Electromagnetic Energy*, Vol. 24, no. 1, pp. 3-13, 1989.

67. Mitani, T., N. Shinohara, H. Matsumoto, M. Aiga, N. Kuwahara and T. Ishii, "Noise-Reduction Effects of Oven Magnetron with Cathode Shield on High-Voltage Input Side", *IEEE Transactions on Electron Devices*, Vol. 53, no. 8, pp. 1929-1936, 2006.

68. Kim, J. I., J. H. Won, G. S. Park, H. J. Ha and J. C. Shon, "Reduction of Noise in Strapped Magnetron by Electric Priming Using Anode Shape Modification", *Applied Physics Letters*, Vol. 88, no. 22, pp. 221501-221501-3, 2006.

69. Neculaes, V., R. M. Gilgenbach, Y. Y. Lau, M. C. Jones, J. Luginsland, W. White, P. Pengvanich, N. M. Jordan, Y. Hidaka and H. Bosman, "Magnetron Microwave Noise Reduction and Magnetic Priming by Azimuthally Varying Axial Magnetic Fields", *5th IEEE International Conference on Vacuum Electronics*, 27-29 April 2004, pp. 158-159, 2004.

70. Gilgenbach, R. M., V. B. Neculaes, M. C. Jones, Y. Y. Lau, W. White, J. W. Luginsland, N. Jordan, P. Pengvanich, Y. Hidaka and B. W. Hoff, "Low-Noise Operation and Magnetic-Priming of Magnetrons by Azimuthally-Varying Axial Magnetic Fields", *29th International Conference on Infrared and Millimeter Waves and 12th International Conference on Terahertz Electronics*, pp. 531-532, 2004.

71. Zhang, I., X. Chen, M. Esterson, P. Burleigh and D. Wilson, "Impact of Non-Uniform Magnetic Field on the Operation of Magnetrons", *IEEE 34th International Conference on Plasma Science*, 17-22 June 2007, p. 670, 2007.

72. Electrical Engineering Training Series, "Electrical Equivalent", http://www.tpub.com/neets/book11/45h.htm [retrieved 4 March 2011].